



TRANSPORTATION
INSTITUTE

PAVEMENT DAMAGE DUE TO DIFFERENT TIRES AND VEHICLE CONFIGURATIONS

FINAL REPORT

SUBMITTED TO:

**MICHELIN AMERICAS RESEARCH AND DEVELOPMENT
CORPORATION
515 MICHELIN ROAD
PO Box 1987
GREENVILLE, SC 29602-1987**

I.L. Al-Qadi, Principal Investigator

Charles E. Via, Jr. Professor of Civil and Environmental Engineering
Leader of the Roadway Infrastructure Group
Virginia Tech Transportation Institute

M. Elseifi, Investigator

Senior Research Associate
Virginia Tech Transportation Institute

P.J. Yoo, Investigator

Graduate Research Assistant
Virginia Tech Transportation Institute

THE ROADWAY INFRASTRUCTURE GROUP
VIRGINIA TECH TRANSPORTATION INSTITUTE
3500 TRANSPORTATION RESEARCH PLAZA
BLACKSBURG, VA 24060

MAY 2004

Table of Contents

1. EXECUTIVE SUMMARY	1
2. INTRODUCTION	4
2.1. PAVEMENT DAMAGE	5
2.2. OBJECTIVES AND SCOPE	5
3. BACKGROUND.....	7
3.1. LITERATURE REVIEW.....	8
4. EXPERIMENTAL PROGRAM AT THE VIRGINIA SMART ROAD.....	25
4.1. THE VIRGINIA SMART ROAD	25
4.2. PAVEMENT INSTRUMENTATION	28
4.3. EXPERIMENTAL PROGRAM.....	29
4.4. DATA COLLECTION.....	31
4.5. RESULTS AND DATA ANALYSIS	40
5. FINITE ELEMENT FORMULATION AND VALIDATION	47
5.1. MODEL DIMENSIONS AND GEOMETRY	48
5.2. ELEMENT DIMENSIONS: SENSITIVITY ANALYSIS	48
5.3. LOADING AREA AND MODEL	51
5.4. BOUNDARY AND CONTACT MODELING	59
5.5. MATERIAL CHARACTERIZATION.....	60
5.6. MODEL RESPONSE	68
5.7. MODEL VALIDATION	71
6. RESULTS AND ANALYSIS	79
6.1. FAILURE MECHANISMS	79
6.2. DAMAGE RATIO	85
6.3. RESULTS AND ANALYSIS	86
7. THE LAVAL STUDY	97
7.1. THE LAVAL TEST SITE	97
7.2. FINITE ELEMENT ANALYSIS OF THE LAVAL TEST SITE	101
7.3. SUMMARY.....	106
8. CONCLUSIONS.....	108
8.1. RECOMMENDATIONS.....	110
9. REFERENCES	111

1. EXECUTIVE SUMMARY

In response to the recent introduction of a new generation of wide-base tires (445/50R22.5), the Roadway Infrastructure Group (RIG) at Virginia Tech measured pavement responses to different tire configurations at the heavily instrumented Virginia Smart Road. The investigated new single wide-base tire has a wider tread and a greater load-carrying capacity than does the conventional wide-base tire. In addition, the contact patch is less sensitive and is especially designed to operate at 690kPa inflation pressure and 121km/hr speed for full load of 151kN tandem axle.

The experimental program included two load levels (L1=19kN and L2=38kN per dual tires assembly), four speeds (8, 24, 40, and 72km/h), and three tire pressures (715, 620 and 415, 620 and 205kPa), two of them being cases of differential pressures between the dual tires. While stresses and strains measured at the bottom of the hot-mix asphalt (HMA) layers were used to quantify the effects of different tire configurations on fatigue damage, measured vertical stress on top of the subgrade was used as an indicator of the rutting damage induced by different tire assemblies. Results of the experimental program indicated that the steering axle was the most damaging of all the tested axles. In addition, measured stresses and strains under the HMA BM-25.0 layer suggested that the new generation wide-base tire induced greater fatigue damage than the dual configuration. On top of the subgrade, vertical compressive stresses induced from the dual tires were approximately equal to those induced by the new generation wide-base tire. This study recommended the adoption of a calibrated theoretical-approach to accurately quantify pavement damage due to different axle configurations and to expand the considered failure mechanisms to other pavement distresses such as HMA rutting, and top-down surface-initiated cracking.

In response to this need, the primary objective of this study was to quantify pavement damage caused by dual tires and the newly developed class of wide-base tires using three-dimensional FE analysis. Since the completion of the experimental program at the Virginia Smart Road, a second size new generation of wide-base tire was introduced in October 2002: the 455/55R22.5. The 455/55R22.5 tire (second size new generation) is wider than the 445/50R22.5 tire (first new generation); hence, it may reduce the contact stress at the pavement surface under the same nominal tire pressure. The new generations of wide-base tire, 445/50R22.5 and 455/55R22.5, were evaluated in this study.

The developed FE models simulated two test sites: a typical section at the Virginia Smart Road (Section B), and the pavement design at the Laval test site in Canada. As a base of comparison, the same pavement designs were also simulated using the multi-layer elastic theory, the most popular method for pavement analysis. The developed FE models were unique in different ways. First, geometry and dimensions of the developed theoretical models were selected to accurately simulate the axle configurations typically used in North America. Second, actual tread sizes and applicable contact pressure for each tread were considered in the models. Third, these models made use of laboratory-measured pavement material properties. Finally, the developed FE models were calibrated and properly validated using actual stress and strain measurements obtained from the experimental program. Four main failure mechanisms

were considered to quantify pavement damage due to tire loading: fatigue cracking, hot-mix asphalt rutting (primary rutting), subgrade rutting (secondary rutting), and top-down cracking. Pavement damage was calculated at three pavement temperatures (5, 25, and 40°C) and at four vehicle speeds (8, 24, 72 and 105km/h).

Based on the results of the FE analysis, it was concluded that the first new generation of single wide-base tires would cause greater fatigue damage in the pavement system than would dual tires. The results also indicated that the first generation of wide-base tire would cause slightly greater primary and secondary rutting damage and less surface-initiated top-down cracking than would dual tires. The frequency of top-down cracking would be less when wide-base tires are used because top-down cracking would only initiate at the edges of the tire. Although tire aggressiveness was found to be a function of temperature, speed, and pavement structure, the increase in damage due to the first new generation of wide base tire at a speed of 8km/h ranged between 14 to 28%. At a vehicle speed of 105km/h, the increase in pavement damage was more significant; ranging from 18 to 57%. The new generation of wide-base tire has a lower radial stiffness, which reduces the dynamic impact of the tire. Therefore, the pavement damage at high speed will be reduced when the dynamic loading is considered in the analysis. The dynamic loading effect will be considered in future research but was not covered in this phase.

Similarly, results of the FE analysis were used to quantify pavement damage caused by the second generation of wide-base tire (455/55R22.5) under the same loading and operating conditions. It was found the tire would induce more damage than the conventional dual-tires assembly with respect to fatigue cracking. The results also suggested that the second generation would cause less primary and secondary rutting damage at slow speed; but slightly greater damage at high speed. In all cases, the tire would cause significantly less surface initiated top-down cracking. Overall, the use of the second generation of wide-base tire would reduce pavement damage between 18 to 32% at slow speed and may increase pavement damage between 5 to 23% at high speed. Given the viscoelastic nature of hot-mix asphalt, one should consider the criticality of pavement damage at high temperature and/or at low speed. Pavement damage is reduced as temperature decreases and/or vehicle speed increases.

Based on the calculated combined damage ratios, equivalent loads were determined to balance the damage induced by the new generation of wide-base tires when compared to the dual-tire assembly. Results of this analysis indicated that the recommended load reduction on an axle equipped with the first new generation of wide-base tire (445/50R22.5) should range between 4.0 to 6.0% at a speed of 8km/h and between 5.0 to 11.0% at a speed of 105km/h to maintain the same effects on flexible pavements as dual tires. For the second generation of wide-base tire (455/55R22.5), the load carried at slow speed may be increased by 5 to 10% depending on the pavement temperature without causing any increase in pavement damage. At high speed, a load reduction ranging between 2 to 5% is recommended to maintain the same level of pavement damage. If wide-base tires are used, the overall truck weight can be reduced by approximately 450kg. This should be considered in the calculation of the hauling weight; hence, the recommended load changes may differ from the limits shown in Tables 1-1 and 1-2. In summary, if the second generation of wide-base tire

(455/55R22.5) is used, it is reasonable to uphold the current load limits that are applied to dual-tire assembly at this point of research.

Table 1-1. Recommended Load Limits at a Speed of 8km/h

Temperature (°C)	Tire	Dual (kg)	Wide-Base Tire	
			445/50R22.5 (kg)	455/55R22.5 (kg)
5		9000	8700	9900
25		9000	8400	9500
40		9000	8600	9500

Table 1-2. Recommended Load Limits at a Speed of 105km/h

Temperature (°C)	Tire	Dual (kg)	Wide-Base Tire	
			445/50R22.5 (kg)	455/55R22.5 (kg)
5		9000	8600	8900
25		9000	8200	8900
40		9000	8000	8500

2. INTRODUCTION

Although traditional materials have performed satisfactorily on a wide range of roads in the past, roads have recently begun to fail at an accelerated rate. Some of the most important factors that contribute to rapid pavement deterioration are changes in truck loading, which include axle weight and configuration; tire type and pressure; and suspensions systems. The damage to the pavement is real and represents a serious challenge that manifests itself in surface deterioration. Such deterioration is hazardous and costly. The monetary cost and the disruption to daily life are astronomical: ASCE estimated that one third of the US pavement system infrastructure is in poor or mediocre condition, costing users approximately \$5.8 billion a year (ASCE 2001).

In recent years, innovative tire and suspension technologies have been strongly supported by the trucking and tire industries to improve the efficiency of the transportation network. One of these new technologies is the introduction of wide-base single tires to replace the conventional dual-tires system. Compared to conventional dual tires, wide-base tires offer the trucking industry potential economic advantages, such as improved fuel efficiency (savings of 1605 liters per year for a typical long-haul combination truck [Ang-Olson and Schroer 2002]), increased pay load, superior handling and braking and comfort, and reduced repair and tire costs.

Although wide-base tires were designed in accordance to current pavement regulation, such as “inch-width” laws, earlier studies on a previous generation of wide-base tires have caused many to conclude that using wide-base single tires would result in a significant increase in pavement damage compared to dual tires (Bonaquist 1992; Sebaaly 1992). This conclusion has led State and pavement agencies to penalize wide-base axle configurations to ensure that economic advantages to the trucking industry would not result in adverse consequences to the road infrastructure (pavement costs vs. non-pavement costs). After more than two decades of research powered by the tire industry and pavement agencies, a new generation of wide-base tire was recently introduced to reduce pavement damage and to offer other safety and cost-savings characteristics.

In spite of the benefits that the new generation of wide-base single tires offers to the trucking industry, optimum operational conditions should be identified to prevent economic advantages for trucking operations at the expenses of increasing road infrastructure damage. This first requires quantification of the pavement damage induced by different axle configurations, tire pressure, and tire types. Hence, feasible solutions may be suggested to optimize benefits to the trucking industry while minimizing damage to pavements and increasing driving safety. For example, COST 334 (2001) has suggested the use of wide-base single tires on the steering axles to balance the overall damage of the vehicle, while improving the efficiency of transportation operations.

2.1. PAVEMENT DAMAGE

Evaluation of pavement damage caused by different axle configurations may be based on either experimental or theoretical approaches, or on a combination of both. Each approach possesses its advantages and drawbacks. Experimental approaches consist of either accelerated testing or pavement responses to different truck loading using in-situ instrumentation. Accelerated pavement testing (APT) is a valid approach to relatively compare the damage induced by different configurations, tire pressures, and tire types. However, the relationship between field performance and APT results is still vague, at best. On the other hand, pavement instrumentation may provide a useful indication as to the damage induced by different loading configurations on the pavement system. Some variability is expected, however, because of variable environmental conditions during testing and the lateral offset of the tire from the instruments.

The use of theoretical approaches, on the other hand, may only be beneficial if accurate modeling of the problem is achieved. Although theoretical calculations using the layered theory are relatively inexpensive and easy, the reliability of the results is questionable due to the use of several assumptions. For example, uniform pressure distribution and circular contact area are assumptions that barely resemble reality, especially when the objective is to quantify the damage of different tire configurations. Therefore, a detailed modeling approach that may consider almost all controlling variables is essential to improve the accuracy of pavement damage prediction. An analysis technique, such as the finite element method (FEM), provides the needed versatility and flexibility to accurately simulate pavement loading. This method considers almost all controlling parameters such as dynamic loading, non-uniform pressure distribution, viscoelastic and nonlinear elastic behavior, infinite and stiff foundations, system damping, quasi-static analysis, and crack propagation. Although FEM is capable of accurately simulating dynamic loading, it was not considered in the phase of research, but will be evaluated in future research.

An optimum understanding of pavement damage caused by different axle configurations could be achieved by measuring the in-situ pavement responses complemented by advance modeling. In this case, experimental techniques are used to establish a benchmark for pavement responses that is then used to validate and calibrate the developed theoretical models based on actual field measurements. If successful, the developed model may then be expanded to different scenarios that were not tested in the field and to establish a parametric study that may be used to define different design and load regulation parameters, such as the pavement damage ratio between different axle configurations.

2.2. OBJECTIVES AND SCOPE

In 2000, the Roadway Infrastructure Group (RIG) at the Virginia Tech Transportation Institute (VTTI) measured pavement responses to both a new generation of single wide-base tire and dual tires at the heavily instrumented Virginia Smart Road. The investigated wide-base tire (MICHELIN 445/50R22.5) has a wider tread than the conventional wide-base tire. In addition, the contact patch is less sensitive and is

especially designed to operate at 690kPa inflation pressure and 121km/h speed for full load of 151kN tandem axle. The experimental program included two load levels, four speeds, and three tire pressures, two of them being cases of differential pressures between the dual tires. This array of measurements established the needed benchmark to calibrate and validate a realistic finite element (FE) model, which may then be used to quantify the potential damage of the wide-base tire as compared to the conventional dual tire configuration. A summary of the results has been presented elsewhere (Al-Qadi et al. 2002).

The main objective of this project was, therefore, to evaluate the mechanism of load distribution for dual and wide-base tires utilizing FEM. In addition to the two tire configurations tested at the Virginia Smart Road, the newly-developed wide-base tire (455/55R22.5) was also evaluated. This allowed the potential damage to pavement due to wide-base single tires as compared to conventional dual tires to be assessed and quantified. This research also investigated this finding and compared dual tires vs. single tires and their impact on different pavement damage mechanisms, such as top-down cracking, fatigue cracking, and pavement rutting. To achieve these objectives, the following tasks were conducted:

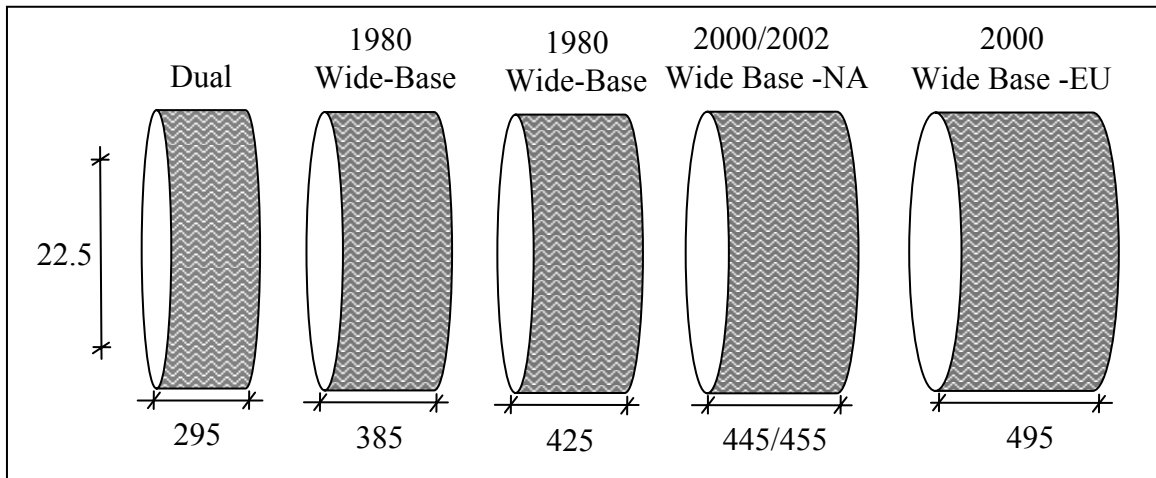
- Development of the necessary finite element models to simulate a typical section at the Virginia Smart Road.
- Simulation of tread patterns for dual and wide-base tire configurations to accurately transfer the dynamic vehicular loading to the pavement structure. Dynamic loading was not considered in this phase of research, but the analysis is planned for future research.
- Incorporation of a viscoelastic constitutive model into the FE problem to simulate the time dependent properties of HMA.
- Incorporation of a creep constitutive model into the FE problem to simulate the accumulation of permanent deformation due to repetitive loadings.
- Validation of the developed FE models as related to field measurements.
- Evaluation of pavement performance as related to a single passage of a dual and wide-base configuration; four speeds were considered.
- Evaluation of service life prediction of pavement based on different axle configurations.

3. BACKGROUND

Wide-base single tires have been used successfully on trucks in Europe and Canada since the early 1980s. In 1997, around 65% of trailers and semi-trailers tires in Germany used the wide-base single tire (COST 334 2001). Although current wide-base tires are wider than earlier models and are legalized in all 50 states of the United States for 5-axle, 80,000N gross-vehicle-weight (GVW) trucks, the market share of wide-base tires in the US does not exceed 5% of truck applications (Olson and Schroeer 2002). Moreover, most of the trucks using wide-base single tires in the United States were found to be carrying lightweight commodities or were traveling empty (Bell et al. 1996). Although the use of the wide-base tire is expected to increase in the future in the United States, some drivers are still concerned that the failure of a wide-base tire will prevent the truck from reaching the next service station (Bonaquist 1992, Olson and Schroeer 2002). Moreover, some drivers still think that the use of such tires is not legal. These beliefs may be easily addressed through proper guidance of the users and by conducting adequate testing to validate the claims that wide-base single tires would reduce tire cost, improve fuel consumption, handling, and braking, when compared to the conventional dual tire assembly.

A real problem associated with the use of wide-base tires is the potential increase in pavement damage compared to dual tires. Offering potential economic advantages to the trucking industry while increasing the cost of road repairs has long been a concern for pavement agencies. Therefore, it is important to balance the benefits to the trucking industry with the potential increased costs to the pavement agencies. This necessitates accurate quantification of the damage induced by wide-base tire and dual tire assemblies. This quantification could also help identify the needed information to establish differential load limits between different tire assemblies or tire pressure limits.

Historically, wide-base tires have evolved considerably since the introduction of the first generation in the early 1980s. Over the years, wide-base tires have become increasingly wider than their predecessors; see Figure 3-1, which shows the general trend in wide-base technology (different patterns of dual and wide-base tires exist and are not shown in this figure for simplicity). New generations of wide-base tires are 15 to 36% wider than the conventional ones (Al-Qadi et al. 2002). The increase of the tire footprint reduces the potential pavement damage compared to conventional wide-base tires. A major problem in the first generation of wide-base tires was the increase in contact stress at the pavement surface as compared to dual tire assemblies. Among different problems associated with this increase in contact stress is the acceleration of the top-down crack failure mechanism. This distress is usually attributed to the high tensile strains and stresses induced at the top of the pavement layer by the tire. In the new generation of wide-base tire, a better stress distribution was achieved while reducing the contact stresses. In summary, it appears that tire manufacturers are currently paying more attention to pavement damage than they did when the first generation of wide-base tire was introduced in the early 1980s. Since its introduction in the early 1980s, the wide-base tire has been the subject of several studies to investigate its potential pavement damage as compared to regular dual assemblies. The following section highlights and reviews some of the literature related to this subject.



NA: Designed for North America, EU: Designed for the European Union

Figure 3-1. Evolution of Wide Base Tires

3.1. LITERATURE REVIEW

3.1.1. Tire Designation Code

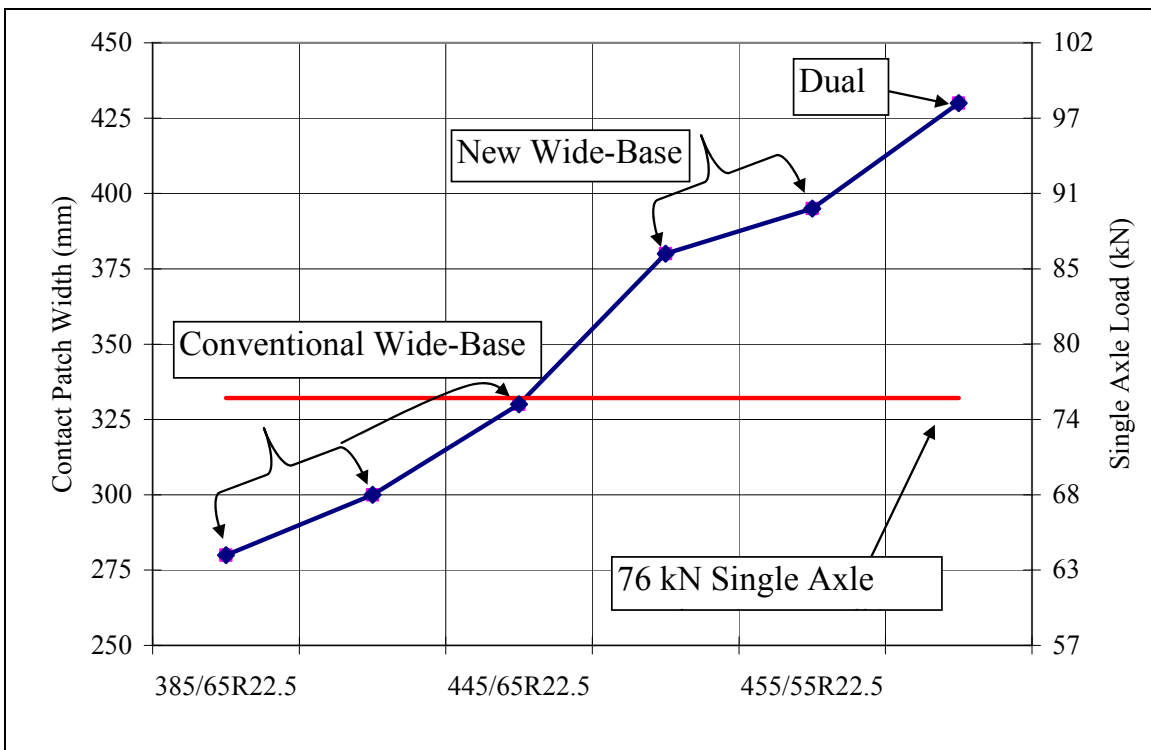
Tire designation codes are set to define the tire characteristics and dimensions. For example, 12-22.5, 12R22.5, and 275/80R22.5 are conventional dual tires, while the 425/65R22.5 is a wide-base tire. The first number in the designation code refers to the nominal section width. For example, the first number (e.g., 275 and 425) is the section width in mm. However, the first number (e.g., 12) in a dual tire designation is sometimes the section width code. The second number in the designation code (e.g., /80 and /65) is the tire aspect ratio in percent. The term “R” is a construction code indicating that the tire is a radial ply tire structure. Similarly, the term “-” indicates that the tire structure is bias. The decimal number in the tire designation code (e.g., 22.5) is the nominal rim diameter code.

3.1.2. The New Generation of Wide Base Tire

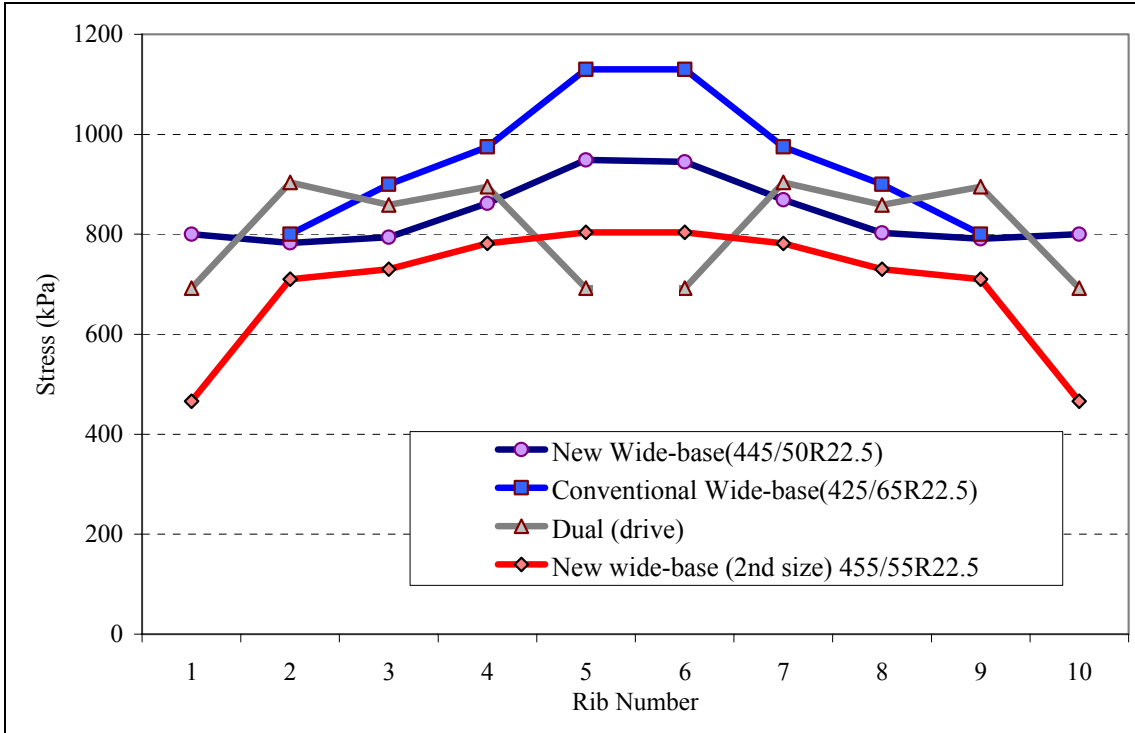
Recent advances in tire design and technology have led to the design of a wide-base tire that has a wider tread than the conventional wide-base tire. This tire was optimized for a tandem axle load of 151kN at 690kPa. This new design resulted in a wider and flatter transverse profile, which provides a uniform pressure distribution. Figure 3-2(a) shows the contact patch width and load-carrying capacity for conventional and new wide-base tires. The new generation of wide-base tire (445/50R22.5 and 455/55R22.5) is 15 to 18% wider than the conventional one, respectively. The load-carrying capacity is based on 11.6kg/mm of tire width, as recommended by Gillespie et al. (1993). Therefore, the new wide-base tire has greater load-carrying capacity than the conventional wide-base tire and is designed based on inch/width principle. This implies that the contact stress between

the tire and the pavement surface is less for the new wide-base tire compared with the conventional wide-base, as shown in Figure 3-2(b), where the new wide-base tire appears to provide a relatively uniform contact pressure, which is lower than the conventional wide-base tire and close to that of a dual tire. These data, plotted for each rib across the tire width, present the contact pressure resulting from a 151kN tandem axle load and 690kPa inflation pressure.

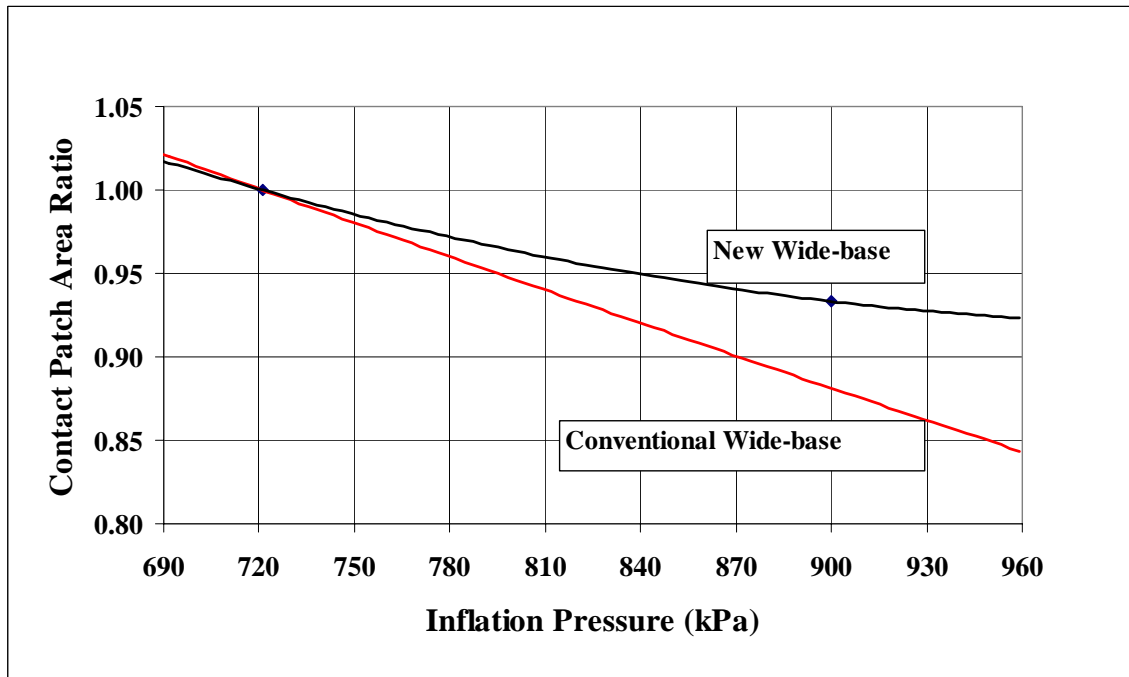
Because most tires are designed with a round profile, the greater the inflation pressure, the smaller the contact area between the tire and the pavement surface. This is generally preferred for casing endurance but significantly increases the contact stress on the pavement surface and causes more damage to the pavement. Most wide-base tires require a high inflation pressure, 790 to 890kPa, to carry a 151kN tandem axle load at 121km/h. The new wide-base tire was designed to carry the same load at a tire inflation pressure of 690kPa at 121km/h. This inflation pressure results in lower contact pressure with the pavement surface for the new wide-base tire versus the conventional wide-base tire. The new wide-base tire also appears to be less sensitive to the increase in tire pressure; see Figure 3-2(c); the referenced contact patch area is at 690kPa. In addition, the new wide-base tire reduces the truck weight by 450kg, which ultimately results in a reduction of up to 2.5% in truck loading repetition on pavements due to fewer trips to carry the same net load. As to the effect on pavements, preliminary results at the U.K. Transport Research Laboratory and the Laboratoire Central des Ponts et Chaussées showed that the newly developed wide-base tire causes the same rutting as the dual tires.



(a)



(b)



(c)

Figure 3-2. Difference between Conventional and Newly Developed Wide Base Tires: (a) Contact Patch Width and Load Carrying Capacity Based on 11.6kg/mm, (b) Contact Stress between the Tire and the Pavement Surface for Different Tire Size, (c) Contact Patch Area Sensitivity with Respect to Inflation Pressure (Markstaller et al. 2000)

3.1.3. Research in Pavement Damage Evaluation

In 1989, the Federal Highway Administration (FHWA) initiated a test program to assess the impact of wide-base tires on conventional flexible pavement damage (Bonaquist 1992). Using accelerated pavement testing (APT), pavement response and performance data were collected for comparable dual and wide-base single tires. The tires considered in this research were the dual 11R22.5 and the wide-base single 425/R65R22.5. The FHWA accelerated loading facility offers two modes of operation: one for response testing using pavement instrumentation, and the second for accelerated testing for performance evaluation. Since temperature fluctuations during testing resulted in different testing conditions, direct comparison of the dual and wide-base tires was not feasible. Therefore, response testing was conducted over a wide range of temperatures, and linear regression models were developed to compare the responses. The general form of the regression models was as follows:

$$R = b_0 + b_1(\text{temp}) + b_2(\text{load}) + b_3(\text{press}) \quad (3.1)$$

where,

R = predicted response;

temp = average pavement temperature (°C);

load = load (kN);

press = tire pressure (kPa); and

b₀, b₁, b₂, and b₃ = regression coefficients.

Despite the fact that the developed models provided a moderately good fit (coefficient of determination from 0.8 to 0.95), the author acknowledged that a better fit would have been obtained if the nonlinear nature of the response had been considered. Based on this analysis, it was concluded that wide-base tires induce significantly more damage than conventional dual tires. The damage was quantified assuming that the fatigue damage is related to the tensile strain at the bottom of the HMA layers rose to the fourth power, and that the relative rutting damage is related linearly to the compressive strain. Table 3-1 illustrates the results of this analysis.

Table 3-1. Relative Damage between Wide Base and Dual Tires (after Bonaquist 1992)

Damage	Relative Damage			
	89mm HMA (T = 14°C)		178mm HMA (T = 23°C)	
	Ratio	Damage	Ratio	Damage
HMA Rutting	1.23	1.23	1.31	1.31
Base Rutting	1.40	1.40	1.31	1.31
Subgrade Rutting	1.53	1.53	1.09	1.09
Fatigue	1.44	4.30	1.37	3.52

Results of the performance tests agreed reasonably well with the damage estimates from the pavement response experiment. Based on the results of accelerated loading testing, it was found that the fatigue life of the wide-base single tire section was only ¼ that of the dual-tire section. In addition, after 75,000 passes, the relative rutting damage between the wide-base tire section and the dual-tire section was 1.93. The distribution of permanent deformation between the different pavement layers was approximately equivalent for the two tire types.

In 1989, Sebaaly and Tabatabaee evaluated the effects of different tire types, tire pressures, loads, and axle configurations on the responses of flexible and rigid pavements using pavement instrumentation. While tensile strain at the bottom of the HMA layer and surface deflections were measured in the flexible pavement sections, surface strains and corner deflections were measured in the rigid pavement sections. Four tire types were considered in this research: the duals 11R22.5 and 245/75R22.5, and the wide-base singles 385/R65R22.5 and 425/65R22.5. The testing speed was 58km/h. Results of the rigid pavement study showed that tire type has no effect on the measured strains on top of the concrete slab. For flexible pavements, the authors defined relative damage between tested tires differently than the previous study. In this case, the following equations were used to calculate the number of cycles for 10 and 45% fatigue damage (Finn 1986):

$$\log N_f(10\%) = 15.947 - 3.291 \log(\epsilon) - 0.854 \log\left(\frac{E}{10^3}\right) \quad (3.2)$$

$$\log N_f(45\%) = 16.086 - 3.291 \log(\epsilon) - 0.854 \log\left(\frac{E}{10^3}\right) \quad (3.3)$$

where,

N_f = number of load applications to cause 10 or 45% fatigue cracking in the wheel path;

ϵ = tensile strain at the bottom of the HMA layers (microstrain); and

E = resilient modulus of the HMA material (psi).

The damage factor was then calculated as follows:

$$\text{Damage Factor (Fatigue)} = \frac{N_f(11R22.5)}{N_f(\text{any tire})} \quad (3.4)$$

Table 3-2 illustrates the results of this analysis at a load level of 78kN/axle. For comparison purposes, relative damage between wide-base and dual tires is also calculated using the fourth power law. Based on these results, it is interesting to notice that although the level of agreement between the two damage techniques is reasonable, the fourth power law is capable of differentiating between the different tires in terms of damage, while the damage method based on the 10 and 45% fatigue cracking is not. In addition, the relative fatigue damage between the wide-base and dual tires is considerably lower than the one reported by the FHWA study (see Table 3-1).

In 1986, Huhtala used pavement instrumentation to compare the effects of different axle configurations and tires commonly used in Finland. The tested tires included 12R22.5 and 265/70R19.5 for the dual tires, and 445/65R22.5, 385/65R22.5, and 355/75R22.5 for the wide-base tires. All the tested trucks were loaded at the maximum axle loads, and also 10 to 20% over and under load in order to assess the effect of the load. The legal load limit in Finland is 100kN for a single axle, 160kN for a tandem axle, and from 180 to 220kN for a tridem axle, depending on the spacing of the axles. The total weight limit for any truck is 470kN. The testing speed ranged from 72 to 76km/h. Similar to the research study conducted by Sebaaly and Tabatabaee (1989), damage was defined in terms of the ratio of the fatigue life of a standard axle to the axle under consideration. Fatigue curves used in the Shell Pavement Design Manual were implemented in this study.

Table 3-2. Relative Damage Factors between Different Tire Types (thick pavement)

Tire Type	Relative Damage				
	Microstrain (70°F)	Damage (10%)	Damage (45%)	Strain Ratio	Damage
11R22.5	145	1.00	1.00	1.00	1.00
245/75R22.5	156	1.30	1.30	1.07	1.34
425/65R22.5	159	1.50	1.50	1.09	1.44
385/65R22.5	164	1.50	1.50	1.13	1.64

Results of this study indicated that the steering (front) axle is the most detrimental of all axles. A tandem axle with wide-base tires was also found to be more damaging than a conventional tandem axle with dual tires. In order to quantify the potential damage of different axles, equivalent axle load weights were calculated with respect to the single dual-tire axle. A 100kN single axle with dual tires corresponds to a front (steering) axle of 75kN, a driving single axle of 90kN, a carrying tandem axle with dual tires of 185kN, and a tandem axle with wide-base tires of 130kN. Results have also shown that the wider the tires, the less damaging they are to the pavement. In addition, the detrimental effect of wide-base tires decreases with depth since the loading pattern and tire pressure have a negligible effect at greater depths.

In 2000, Al-Qadi et al. investigated pavement responses to dual and wide-base tires at the heavily instrumented Virginia Smart Road (Al-Qadi et al. 2000). The tested wide-base tire (MICHELIN 445/50R22.5 XONE XDA) has a wider tread than the conventional wide-base tire. In addition, the contact patch is less sensitive and is especially designed to operate at 690kPa inflation pressure and 121km/h for a full load of 151kN tandem axle. This newly developed wide-base tire has greater load-carrying capacity than the conventional wide-base tire. In addition, it provides a relatively uniform contact pressure, which is lower than the conventional wide-base tire and comparable to dual tire configurations. Markstaller et al. (2000) showed that this new generation of wide-base tire reduced fuel consumption by 4% and improved ride comfort by 12%. Moreover, the tested wide-base tire reduces the truck weight by 450kg, which would result in a reduction of 2.5% in truck loading repetitions on pavements because

fewer trips would be needed to carry the same net load. The experimental program was conducted in three different stages between May 2000 and July 2001. Instrument responses were used in this study to calibrate and validate the accuracy of the theoretical approach. A detailed description of this study and its results are presented in Chapter 4.

In 2003, Prophète investigated the relative pavement damage of four different tire assemblies using instrumentation (Prophète 2003). In this study, the pavement section at Laval University, Quebec was instrumented using a multi-depth deflectometer, thermocouples, strain gages at the bottom of the HMA, and an instrumented plate at a 25-mm depth. The investigated tires were the 11R22.5 and 12R22.5 dual tires, and the 385/65R22.5 and 455/55R22.5 wide-base tires. Five loading cases (3000, 4000, 5000, 6000, and 7000kg per semi-axle) and three tire pressures (560, 730, and 900kPa) were evaluated at one speed of 50km/h. Testing was conducted in two periods: one in the spring (temperature between 5 and 20°C) and one in the summer (temperature between 15 and 30°C with an average of 20°C). Three failure mechanisms were considered: fatigue of HMA, rutting of subgrade (secondary rutting), and rutting of HMA (primary rutting). Measured responses were corrected with respect to the temperature by developing correction factors through the measurements taken using a Benkelman vehicle. With respect to the considered failure mechanisms, experimental measurements indicated the following trend:

- **Secondary Rutting:** Vertical strain measurements using the multi-depth deflectometer were inconsistent in some instances (vertical deformations did not increase with depth during some of the runs). In addition, the measured deformations were very small, indicating that tire type, load, and pressure do not have a strong effect on the vertical strain on top of the subgrade. The measurements might also have been affected by a region of frost detected in the subgrade. By considering the total deflection of the pavement system under different tire assemblies, it appeared that dual tires are causing less total deformation than wide-base single tires.
- **Fatigue of HMA:** In the spring, the two dual tire assemblies resulted in less strain at the bottom of the HMA than the single tire assemblies. However, the extra wide-base tire (455/55R22.5) resulted in significantly less strain than the standard wide-base tire (385/65R22.5). In the summer, the new generation of wide-base tire resulted in approximately the same strain as the dual-tire assemblies. However, the standard single wide-base tire was still much more damaging than were the dual-tire assemblies, and the new generation of wide-base tire.
- **Primary Rutting:** Both the new generation of wide-base tire and the standard single tire resulted in less vertical strain at 25mm from the pavement surface. The difference between the different tire assemblies appeared to increase with the increase in tire pressure.

A detailed description of this study and its results are presented in Chapter 7. Further evaluation of these results was also conducted based on a detailed FE analysis.

3.1.4. The COST Action 334

The effects of wide-base tires as compared to a conventional dual-tire assembly was recently investigated by COST 334 (COST 334 2001). The main objective of this intensive study was to identify possible advantages and disadvantages of different tire assemblies with respect to road pavement damage, vehicle operating costs, vehicle safety and comfort, and environment, in order to establish load limit regulations for different axle configurations commonly used in Europe. Seventeen different tire types were considered in the study, eight of them dual, and nine of them wide-base tires. The work plans for that study included (1) contact stress, footprint, and load measurements; (2) full-scale accelerated pavement testing on selected tire types; (3) instrument responses to different axle configurations, (4) finite element simulation of primary rutting, and (5) development of regression models that may be used to determine the relative damage of different tires and axle configurations.

(1) Wheel load measurements were conducted to evaluate the influence of tire types on dynamic wheel loading and load distribution between inner and outer tires in a dual configuration. In general, there was a 4% difference in loading between the inner and outer tire of a dual assembly. This was mainly attributed to difference in tire wear in a dual assembly. A significant difference was also found between dynamic load transmissibility of the wide-base when compared to dual tires. At 10Hz, which corresponds to the fundamental vibration frequency of a typical truck, the load transmissibility of the wide-base tire was 35% less than that of dual tires. This indicates that the load transferred from the tire to the pavement will be less for the wide-base tire than it is for the dual tires.

(2) To evaluate the relative pavement damage of different tire types using accelerated pavement testing, three classes of pavement structures were considered: thin pavement (HMA less than 100mm), medium pavement (HMA around 200mm), and thick pavement (HMA greater than 300mm). Accelerated pavement testing was conducted at two different pavement test sites (British Pavement Testing Facility and Dutch Lintrack Heavy Traffic Simulator).

Testing at the British Pavement Testing Facility compared a conventional wide-base tire (385/45R22.5) at a load 44.1kN and a tire pressure of 1000kPa to a new generation of wide-base tire (495/45R22.5) at a load 44.1kN and a tire pressure of 800kPa. It is worth noting that the difference in pressure between the two tire types is due to the fact that conventional wide-base tires require the use of a high inflation pressure with the increase in load. The average rutting ratio between the conventional wide-base and the new wide-base was 1.7 for medium-thickness pavements and 1.5 for thin pavements.

Testing at the Dutch Lintrack Heavy Traffic Simulator compared the performance of four different tire assemblies. Two dual tire assemblies (295/60R22.5 at a load of 57.5kN and a tire pressure of 940kPa and 315/80R22.5 at a load of 57.5kN and tire pressure of 740kPa) and two wide-base assemblies (385/65R22.5 at a load of 45.0kN and a tire pressure of 940kPa and 495/45R22.5 at a load of 57.5kN and a tire pressure of 940kPa) were tested. The experimental program was divided into two stages, each consisting of four pavement sections with the same pavement design (thick pavement

with 270mm HMA layers) that were used to test the four tire assemblies concurrently. The difference between the two testing stages was in the top HMA layers, with the second stages using a harder binder. Pavement temperature was maintained at 40°C using infrared heaters. The testing schedule for the first stage consisted of applying an initial 1000 load repetitions of the 385/65R22.5 tire in all pavement sections to ensure proper densification of HMA mixtures. Each pavement section was then subjected to an additional 33,000 load repetitions of its own tire type. The rutting measurements after the initial 1000 load repetitions were considered as the reference level. In the second testing stage, the same initial loading was applied, followed by 36,000 load repetitions. Lateral wander was applied assuming a Laplace distribution around the centre position. A load correction factor was applied to the rutting measurements of the 385/65R22.5 tire since it was tested at a smaller load (45.0kN). The average rutting ratio between the conventional wide-base (385/65R22.5) and the conventional dual tire assembly (315/80R22.5) was 1.94 in the first testing stage and 2.28 in the second testing stage. In addition, the average rutting ratio between the new generation of wide-base tire and the conventional dual tire assemble was 1.32 in the first testing stage and 1.34 in the second testing stage. It is worth noting that the ranking of the four tire assemblies was different in the first and the second testing stages. This was attributed to a possible difference in rutting resistance of the four pavement sections although they were assumed comparable. This was addressed by correcting rutting measurements to account for the difference in material rutting resistance between the different test sections.

(3) Evaluation of the pavement damage caused by different tire assemblies using pavement instrumentation was conducted at two different pavement test sites (French Manège de Fatigue and the Virttaa test site in Finland).

Testing at the French Manège de Fatigue compared the rutting and fatigue performance of two dual-tire assemblies (315/80R22.5 and 295/60R22.5) and two wide-base tires (385/65R22.5 and 495/45R22.5) based on in-situ pavement instrumentation and theoretical modeling. The experimental program was conducted on a very stiff pavement structure consisting of 80mm wearing surface, on top of 400mm base mix, and 400mm granular base. Due to large temperature variations during testing and repetitive occurrences of heavy rain, raw measurements suffered from different drawbacks that did not allow a clear conclusion to be drawn. In addition, due to the large temperature fluctuations during testing, the measured strains were very low (between 10 and 20 μ m at the bottom of the HMA, and between 40 and 70 μ m on top of the granular base). To account for the large temperature variation during testing, the second phase followed a theoretical approach, in which the different tire configurations were modeled using a multilayer elastic software. After the model was successfully calibrated based on measured pavement responses, comparisons were established between the different tire configurations at a temperature of 15°C. The vertical and longitudinal strains induced by the conventional wide-base tire (385/65R22.5) were equivalent to the damage due to the new generation of wide-base tires (495/45R22.5). In addition, the 315/80R22.5 dual-tire assembly resulted in a strain 6.2% lower than the 295/60R22.5 dual-tire configuration. It is worth noting that the magnitude of the measured strains as well as the difference between the different tire assemblies was very small because the pavement structure was very stiff and the testing temperature was low.

Testing at the Virttaa test site in Finland compared pavement responses to two tire assemblies using pavement instrumentation. The tested tire assemblies were the dual 315/70R22.5 at 750kPa and the new generation of wide-base tire (495/45R22.5) at 900kPa. The selected tire pressures were based on the manufacturer's recommendation given the applied load. Testing was conducted at two different speeds of 45 and 80km/h on a pavement structure consisting of 150mm HMA, on top of 150mm crushed rock base, and 400mm granular subbase. Measurements of the vertical stress in the pavement layers indicated that the wide-base tire configuration produces about 21% greater stresses in the base layer, and 14% greater stresses in the subbase layer than the dual-tire configuration. Stresses in the subgrade were approximately equal. In addition, measurements of the longitudinal strains at the bottom of the HMA indicated that the wide-base tire configuration induced about 17% greater strain than the dual-tire configuration.

(4) Evaluation of the pavement damage of different tire configurations was conducted in Portugal utilizing a finite element (FE) approach. Only primary rutting was considered in this study using a Burgers' model to describe the viscoelastic behavior of HMA. Four pavement structures were modeled covering a wide range of pavement thicknesses. Loading was applied over a rectangular area with uniform pressure. Lateral wander of the load was also considered through a modified Laplace distribution. After the model was successfully calibrated based on experimental data of accelerated pavement testing, comparisons were established between different tire assemblies. Results of this parametric study indicated that wide-base tires are more damaging than dual tires with respect to primary rutting. For example, the primary rutting ratio between the conventional wide-base tire (385/65R22.5) at a pressure of 1000kPa and the dual tire (315/80R22.5) at a pressure of 800kPa was 1.47. This ratio was only 1.09 between the new generation of wide-base tires (495/45R22.5) at a pressure of 800kPa and the same dual tire, however.

(5) The final relevant factor investigated in COST 334 was the development of regression models that may be used to determine the influence of different tire parameters on pavement damage. The use of these models is mainly recommended for the common axle configurations in Europe and for the European primary and secondary road network. A major deficiency in the developed models is that the utilized data did not result from a single experimental program, but a compilation of the field evaluation data presented above. Therefore, inter-researcher variation may be expected since differences in testing methods and data collection procedure would certainly exist.

The process of deriving the regression models consisted of two major steps. In the first stage, basic formulae for estimating the pavement wear ratio (PWR) between a given and a reference tire assembly were developed assuming ideal loading conditions (i.e., equal load distribution in case of dual tire assemblies, a completely even road, and no dynamic effects). In the second stage, the developed regression models were modified to account for real operating conditions to result in the final formulae to estimate the tire configuration factors (TCF) for different tire assemblies.

Separate models were developed for each pavement distress (i.e., primary rutting, secondary rutting, and fatigue of HMA). In addition, the formulation differentiated between three different pavement structures: thin, medium, and thick pavements (HMA

thickness around 100mm, 200mm, and 330mm, respectively). The initial model for estimating the pavement wear ratio took the following form:

$$\begin{aligned} \ln \text{PWR} = & a \ln(\text{tire type}) + b \ln(\text{relative pressure}) + c \ln(\text{relative width}) + \\ & d \ln(\text{relative diameter}) + e \ln(\text{relative pressure ratio}) + f \ln(\text{rel. contact area}) \\ & + g \ln(\text{rel. total width}) + h \ln(\text{rel. length}) + \ln \text{error} \end{aligned} \quad (3.5)$$

where,

PWR = pavement wear ratio;

tire type = 1 for dual tires, and e for wide-base;

relative pressure = (pressure / pressure reference);

pressure = actual tire inflation pressure;

relative width = (width / width reference);

width = footprint width for wide-base singles, and twice the footprint width of the individual tires for dual tire assemblies.

relative diameter = (diameter / diameter reference);

relative pressure ratio = (pressure ratio / pressure ratio reference);

pressure ratio = factor indicating over or under-inflation of the tire relative to the recommended pressure at a given load level + 100kPa. The addition of 100kPa is to account for the fact that due to heat, pressure increases by about 100kPa from their cold value;

relative contact area = (contact area / contact area reference);

relative total width = (total width / total width reference);

total width = footprint width for wide-base singles, and twice the footprint width of the individual tires plus the spacing between the footprints for dual tires;

relative length = (length / length reference);

error = error term, including measurement errors in the data, and lack of fit of the model; and

a, b, c, d, e, f, g, and h = regression coefficients.

The data used for determining the regression coefficients for primary rutting were all based on accelerated pavement testing, incorporating lateral wander. Therefore, in this case, the pavement wear ratio represents the ratio of actually observed distress levels. However, almost all the primary rutting data (30 observations) are for thick pavements, with the exception of one case of medium pavement. In contrast, the data used for determining the regression coefficients for fatigue (67 observations) and secondary rutting (47 observations) were all based on instrument responses to different axle configurations. Therefore, in these cases, the pavement wear ratio was calculated by using well-recognized transfer functions. Furthermore, correction factors were applied to account for the effect of the lateral wander of traffic.

The regression analysis was performed by following a stepwise approach, which allows incorporating the most significant variable first, then, in successive steps, the next most significant factor is included when its significance is substantial, or excluded if its level of significance is too low. Based on this analysis, the recommended regression models are shown in Table 3-3. It is worth noting that if several models are provided for the same distress, application of the models is recommended in a descending order

depending on data availability. In addition, while the level of confidence in the primary rutting models is high, the level of confidence in the secondary rutting and fatigue cracking models is moderate.

To address the dynamic load effects, and the potential load imbalance between the tires of a dual tire assembly, the concept of tire configuration factor (TCF) was introduced. The tire configuration factor is “a factor describing the pavement wear attributable to different tire types and sizes, when compared with an arbitrarily selected reference tire, at equal load.” The selected reference tire with a TCF of 1.0 is the dual tire 295/80R22.5 under maximum recommended loading conditions. Characteristics of the reference tire under a 98.0kN axle load are illustrated in Table 3-4. In addition, based on the selected reference tire, Table 3-5 presents the final set of formulae for determining the TCF. Note that the correction factor for the steering axle is equal to one. Several models were developed for thick pavements depending on the availability of data.

Based on the presented prediction models, COST 334 developed guidelines for relative damage between different tire assemblies as defined by the tire configuration factor. For example, Table 3-6 presents the defined TCF values for towed axles. It is worth noting that all single tires shown in this table represent old generation of wide-base tires. As shown in this table, while it is assumed that the main failure mechanism for primary roads is primary rutting, the failure mechanism for secondary roads is a combination of primary rutting, secondary rutting, and fatigue cracking. For secondary roads, a weighted average, which assumes 20% primary rutting, 40% secondary rutting, and 40% fatigue cracking, is also provided.

Table 3-3. Recommended Models for Evaluating the Pavement Wear Ratio (after COST 334 2001)

Distress	Primary Rutting	Secondary Rutting	Fatigue Cracking
Pavement Type			
Thin Pavement	No data available	$\text{PWR} = (\text{rel. total width})^{-2.57} (\text{rel. pressure ratio})^{1.58}$	$\text{PWR} = (\text{rel. total width})^{-2.88} (\text{rel. length})^{-3.13}$ <p style="text-align: center;">or</p> $\text{PWR} = (\text{rel. total width})^{-2.44} (\text{rel. length})^{-2.47}$
Medium Pavement	Model for thick pavements recommended		$\text{PWR} = (\text{rel. total width})^{-1.36} (\text{rel. length})^{-1.40}$ <p style="text-align: center;">or</p> $\text{PWR} = (\text{rel. total width})^{-1.36} (\text{rel. length})^{-1.40}$
Thick Pavement	$\text{PWR} = (\text{rel. width})^{-1.68} (\text{rel. pressure ratio})^{0.81} (\text{rel. length})^{-0.85}$ <p style="text-align: center;">or</p> $\text{PWR} = (\text{rel. width})^{-1.65} (\text{rel. pressure ratio})^{1.42} (\text{rel. diameter})^{-1.12}$ <p style="text-align: center;">or</p> $\text{PWR} = (\text{rel. width})^{-1.66} (\text{rel. pressure ratio})^{1.50}$	$\text{PWR} \cong 1.0^*$	$\text{PWR} \cong 1.0^*$

* Based on measured data.

Table 3-4. Characteristics of the Dual Reference Tire (295/80R22.5) with a 98.0kN Total Axle Load

Parameters	Recommended Values
Width	2 x 235mm
Total Width	570mm
Diameter	1059mm
Length	198mm
Contact Area	2 x 46500mm ²
Pressure Ratio	1.0 (inflated as recommended)
Inflation Pressure	750kPa under operating conditions (650kPa cold)

Table 3-5. Final Set of Models for Evaluation of the TCF

Pavement Thickness	Formulae	Total Translation Factors from PWR to TCF		
		Dual tires	Wide base single tire	Single tire (steering)
Primary Rutting				
Medium	TCF = (width / 470) ^{-1.68} (length / 198) ^{-0.85} (pres. ratio) ^{0.81} TCF = (width / 470) ^{-1.68} (length / 198) ^{-0.85} (pres. ratio) ^{0.81}	1.01	0.97	1.0
Thick	TCF = (width / 470) ^{-1.68} (length / 198) ^{-0.85} (pres. ratio) ^{0.81} TCF = (width / 470) ^{-1.68} (length / 198) ^{-0.85} (pres. ratio) ^{0.81}	1.01	0.99	1.00
Secondary Rutting				
Thin	TCF = (total width / 570) ^{-2.57} (pres. ratio) ^{1.58}	0.97	0.97	1.00
Medium	TCF = (total width / 570) ^{-2.57} (pres. ratio) ^{1.58}	0.98	0.97	1.00
Thick	≅ 1.00			
Fatigue Cracking				
Thin	TCF = (total width / 570) ^{-2.88} (length / 198) ^{-3.13} TCF = (total width / 570) ^{-2.44} (diameter / 1059) ^{-2.47}	0.94	0.97	1.00
Medium	TCF = (total width / 570) ^{-1.36} (length / 198) ^{-1.40} TCF = (total width / 570) ^{-1.23} (diameter / 1059) ^{-1.14}	0.96	0.97	1.00
Thick	≅ 1.00			

Table 3-6. Tire Configuration Factor for Towed Axles (after COST 334 2001)

						Tire Configuration Factor				
						Primary Roads	Secondary Roads			
						PR	WA	PR	SR	F
Tire size	Type	TIW	CAW	TW	D					
mm	mm	mm	mm	mm	mm					
Ref. Tire	Dual	235	470	570	1059	1.00	1.00	1.00	1.00	1.00
205/65R17.5	Dual	175	350	450	711	2.57	2.04	2.57	1.80	2.02
215/75R17.5	Dual	175	350	450	767	2.36	1.93	2.36	1.80	1.85
245/70R17.5	Dual	215	430	530	789	1.63	1.39	1.63	1.18	1.47
245/70R19.5	Dual	200	400	500	839	1.71	1.48	1.71	1.37	1.47
265/70R19.5	Dual	210	420	520	872	1.51	1.34	1.51	1.24	1.34
11R22.5	Dual	184	368	468	1054	1.52	1.45	1.52	1.63	1.23
315/80R22.5	Dual	247	494	594	1085	0.91	0.89	0.91	0.88	0.89
385/55R22.5	Single	329	329	329	998	1.91	2.78	1.87	3.98	2.04
385/65R22.5	Single	285	285	285	1071	2.23	3.64	2.19	5.76	2.25
445/45R19.5	Single	380	380	380	895	1.70	2.21	1.66	2.75	1.93
445/65R22.5	Single	340	340	340	1155	1.53	2.43	1.50	3.66	1.66

TIW: Tire Width; CAW: Contact Area Width, TW: Total Width, D: Diameter, PR: Primary Rutting, WA: Weighted Average, SR: Secondary Rutting, F: Fatigue Cracking.

COST 334 also estimated the relative damage between the steering axle and the reference axle. On average, assuming the same axle load, the steering axle was three to four times as aggressive as the reference axle on primary roads, and five to eight times as aggressive as the reference axle on secondary roads. However, since the steering axle usually carries a much smaller load than the reference axle, this comparison was not entirely correct. However, even under smaller load, it is still expected that a steering axle with 68.6kN on two single tires is much more detrimental than the reference axle.

In order to improve the efficiency of transportation operations, while concurrently balancing the overall damage of the vehicle on the road infrastructure, COST 334 has suggested the use of wide-base single tires on the steering axle. Table 3-7 illustrates the overall damage of the vehicle as compared to the reference axle if wide-base tires were used in the steering axle. Note that only the most common tires are used in each axle for illustration.

Table 3-7. Variation of Pavement Damage for Different Axles of a Typical European Truck (after COST 334 2001)

Axle	Tire Type	W mm	D mm	Primary Roads		Secondary Roads	
				TCF	Wide base vs. dual or single	TCF	Wide base vs. dual or single
Towed	Dual	410	973	1.57		1.43	
	Wide Base Single	328	1049	1.84	+17%	2.82	+97%
Driven	Dual	455	1038	1.04		1.00	
	Wide Base Single	427	1013	1.22	+17%	1.64	+64%
Steering	Single	245	1023	3.25		5.86	
	Wide Base Single	307	1035	2.07	-36%	3.21	-45%

In summary, one may conclude that the COST Action 334 resulted in significant advances in the understanding of the aggressiveness of different axle configurations. Although the results of this study are not directly applicable to the axle configurations in North America, the research approach followed in this study was adequate. One major obstacle to the applicability of the results of this study is that the new generation of wide-base tire in Europe refers to the 495/45R22.5, while the proposed new generation of wide-base tire in North America is the 445/50R22.5 (November 2000), and subsequently the 455/55R22.5 (October 2002). This discrepancy is due the difference in axle configurations between Europe and North America.

Based on the results of the COST Action 334, one may conclude that a great step forward has been achieved in reducing pavement damage due to the introduction of the new generation of wide-base tire. For primary roads, the damage ratio between the new generation of wide-base tire and the conventional dual-tire configuration was estimated at 1.53 for a towed axle. This comparison assumed a primary rutting failure mechanism only. The damage ratio between the conventional wide-base tire and a standard dual tire configuration was estimated at 2.23 for a towed axle. Although a robust analysis was conducted to quantify pavement damage due to primary rutting, other failure mechanisms such as fatigue cracking did not offer the same level of accuracy and demand further investigations. In addition, the top-down failure mechanism was not considered.

4. EXPERIMENTAL PROGRAM AT THE VIRGINIA SMART ROAD

An experimental program was conducted at the Virginia Smart Road to investigate the effect of two different tire configurations on flexible pavement damage: a dual tire assembly (MICHELIN 275/80R22.5 XDA2) and the new generation of wide-base tire (MICHELIN 445/50R22.5 XD2). The experimental program was conducted in three different stages between May 2000 and July 2001. The main difference between the three experimental stages was that while the wide-base and dual tire configurations were tested separately in the first experimental phase, the second and third experimental setups tested them concurrently by mounting the dual tire assembly in the first axle and the wide-base tire assembly in the second axle, and vice versa (see Figure 4-1). The following sections provide a detailed description of the experimental program as well as a summary of the results of the field evaluation. Field measurements were used in this study to validate and calibrate the developed theoretical models.



Figure 4-1. Concurrent testing of the dual and wide-base tire configurations

4.1. THE VIRGINIA SMART ROAD

The Virginia Smart Road, located in Southwest Virginia, is a unique state-of-the-art full-scale research facility for pavement research and evaluation of Intelligent Transportation Systems (ITS) concepts, technologies, and products. It is the first facility of its kind to be built from the ground up with its infrastructure incorporated into the roadway. When completed, the Virginia Smart Road will be a 9.6-km connector highway between Blacksburg and I-81 in Southwest Virginia, with the first 3.2km designated as a controlled test facility. The flexible pavement part of the Virginia Smart Road test facility includes 12 heavily instrumented flexible pavement sections; see Table 4-1.

Section length varies between 76 and 117m, with the exception of section A, which is 317m. Seven of the 12 sections are located on a fill, while the remaining five sections are located in a cut. Different layers are used in each section (all designations and mix designs are in accordance with Virginia Department of Transportation Specifications). The different layers are as follows:

- Wearing surface: Seven types of HMA wearing surface are used (SM-9.5A, SM-9.5A with high laboratory compaction, SM-9.5D, SM-9.5E, SM-12.5D, SMA-12.5, and open-graded friction course [OGFC]). Five of these seven mixes are SuperPave™ mixes. All of the mixes, with the exception of the OGFC, were constructed at 38-mm-thick. The OGFC was constructed at 19-mm-thick.
- Intermediate HMA layer: BM-25.0 at different thickness ranging from 100 to 244 mm.
- Three sections have the SuperPave™ SM9.5A fine mix placed under the BM-25.0 to examine the benefits of such a design on reducing fatigue cracking.
- Open-graded drainage layer [OGDL]: Out of the 12 sections, three sections were built without OGDL. Seven sections are treated with asphalt cement and two are treated with Portland cement. The thickness of this layer is kept constant at 75mm throughout the project.
- Cement Stabilized Subbase: 21-A cement-stabilized layer is used in 10 sections at a thickness of 150mm.
- Subbase layer: 21-B aggregate layer was placed over the subgrade at different thickness with and without a geosynthetic.

As the construction of the first phase of this project is completed (3.2km controlled test facility), the Virginia Smart Road is currently used as a pavement test facility by allowing only controlled traffic loading to pass over the different pavement sections.

Table 4-1. Pavement Design at the Virginia Smart Road

Section	Station Starts	Station Ends	Bunker Station	Lane Length (m)	Surface 38mm	BASE BM-25.0 (mm)	BASE SM-9.5A (mm)	OGDL (mm)	21A Aggr. Cem. Stab. (mm)	21-B Aggr. (mm)	Pave. Thick. (mm)	Fill/ Cut
A	100.54	103.71	103.71	104	SM-12.5D	150	0	75	150	175	588	Fill
B	103.71	104.61	103.71	90	SM-9.5D	150	0	75	150	175/GT	588	Fill
C	104.61	105.48	105.48	87	SM-9.5E	150	0	75	150	175/GT	588	Fill
D	105.48	106.65	105.48	117	SM-9.5A	150	0	75	150	175/GT	588	Fill
Bridge	106.65	107.70										
E	107.70	108.46	108.46	76	SM-9.5D	225	0	0	150	75/GT	488	Fill
F	108.46	109.40	108.46	94	SM-9.5D	150	0	0	150	150	488	Fill
G	109.40	110.30	110.30	90	SM-9.5D	100	50	0	150	150/GT	488	Fill
H	110.30	111.20	110.30	90	SM-9.5D	100	50	75	150	75	488	Cut
I	111.20	112.18	112.18	98	SM-9.5A*	100/RM	50	75	150	75	488	Cut
J	112.18	113.10	112.18	92	SM-9.5D	225	0	75	0/MB	150	488	Cut
K	113.10	113.96	113.96	86	OGFC+SM-9.5D	225/SR	0	75 (Cement)	0	150	488	Cut
L	113.96	115.00	113.96	104	SMA-12.5	150/RM	0	75 (Cement)	150	75	488	Cut

* High lab compaction

SR: Stress Relief Geosynthetic; GT: Woven Geotextile/ Separator; RM: Reinforcement Mesh; MB: Moisture Barrier

4.2. PAVEMENT INSTRUMENTATION

All instruments were embedded in the pavement sections during construction. Environmental instruments were installed in the centerline of the two-lane road, while load-associated instruments were installed in the wheel path at three different locations to account for traffic wander and for replications. Environmental instruments consist of thermocouples for temperature measurements, resistivity probes for predicting frost penetration, and two types of time domain reflectometry probes for moisture measurements. Loads-associated instruments include pressure cells and different types of strain gauges. Pressure and strain gage responses under the different layers were used in this study; therefore, descriptions of the pressure cells and the HMA strain gauges are presented below. Also presented is a description of the thermocouples since temperature readings were used to correct the results for temperature variation by shifting all results to a reference temperature of 25°C. Table 4-2 illustrates a description of the instruments installed at the Virginia Smart Road and used in this study.

Table 4-2. Instruments Installed at the Virginia Smart Road and Used in this Study

Instrument Type	Picture	Applications	Main Properties
Pressure Cell		<ul style="list-style-type: none"> Vertical Stress 	<ul style="list-style-type: none"> Diaphragm cell gauge Temperature resistance
HMA Strain Gage		<ul style="list-style-type: none"> Dynamic and static transverse and longitudinal strains in bounded layers 	<ul style="list-style-type: none"> Low stiffness Temperature resistant Good durability
Thermocouple		<ul style="list-style-type: none"> Temperature measurement 	<ul style="list-style-type: none"> In-House manufactured T-type thermocouple

The pressure cell used at the Virginia Smart Road consists of two circular steel plates welded together around their rims to create a cell approximately 150mm (used in HMA layers) or 200mm (used in aggregate layers and subgrade) in diameter and 12.7mm thick. The space between the plates is liquid-filled. The fluid of the 150mm-diameter cell has a boiling point of 200°C. This boiling point was chosen so as to be greater than the lay-down temperature of the HMA to prevent expansion of the cell diaphragm. A steel tube connects the liquid to an electrical pressure transducer. The pressure transducer responds to changes in total stress applied to the material in which the cell is embedded. The transducer, which is a strain gage type, is enclosed in a heavily protective 316 stainless

pipe to prevent damage from surrounding aggregate and to prevent problems with over-pressure.

Dynatest Past-II-AC H-type strain gages were used to measure the dynamic transverse and longitudinal strains in all HMA layers. The gage has an effective length of 102mm with two flanges, 75mm-long and 15mm-wide. The strain gage has a cross-section area of only 50mm², which requires an extremely low “strain force” of 0.11N/microstrain. The average modulus of the cell body is as low as 2.2GPa due to the special properties of the cell materials. This low stiffness avoids the reinforcement of the pavement layers by the presence of the gage. This type of strain gage is completely embedded in a strip of glass-fiber reinforced epoxy, a material with a relatively low stiffness and high flexibility and strength. Each end of the epoxy strip is securely fastened to a stainless steel anchor to ensure proper mechanical coupling to the HMA material after installation. The PAST transducer (1/4 bridge) has a resistance of 120 ohms, and a gage factor of 2.0. It can be incorporated into a full bridge setup with up to 12V excitation voltage. The gage can measure up to 1500 microstrains (tension or compression), with an expected fatigue life of 10⁶ cycles.

A twisted-stranded-shielded soldered pair of T-type thermocouple wire (constantan and copper) was used to measure temperature. 6.35mm inside-diameter copper tubing surrounds the exposed end of the thermocouple. The tubing is attached to the cable insulation by type TFM inner mount-melt heat shrinkable Teflon tubing. This is done to insulate the tubing from the exposed wire pair, and to provide a reservoir for epoxy. The shrink tubing is chosen especially for its thermal resistance, as it has a maximum operating range of 230°C. 3M DP-270 electrical grade epoxy is used to surround the thermocouple and to serve as a barrier to environmental effects.

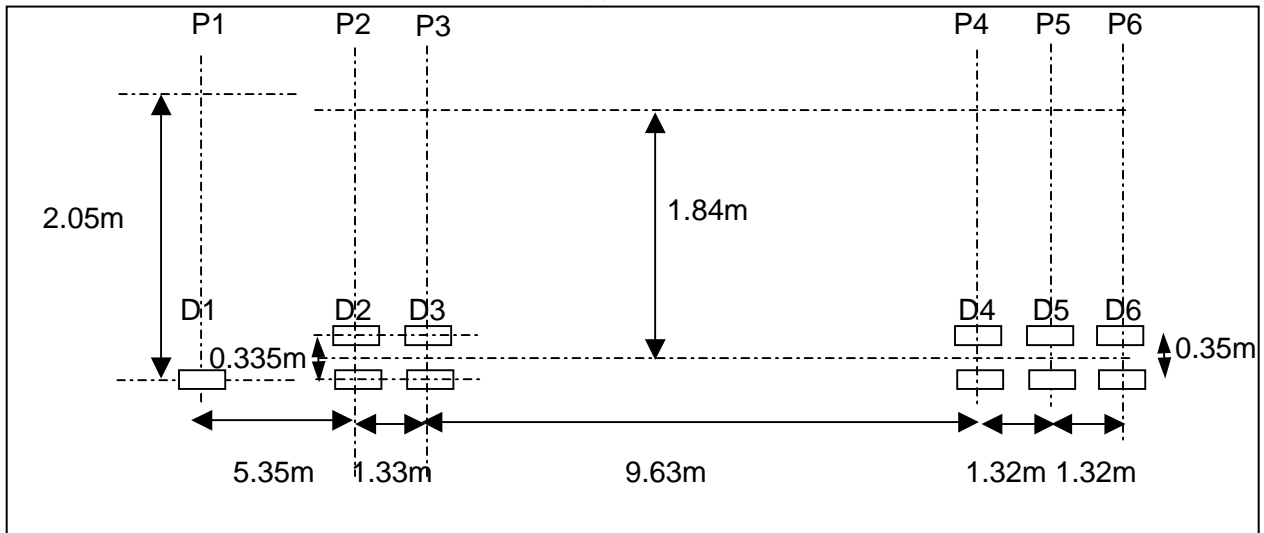
4.3. EXPERIMENTAL PROGRAM

As previously mentioned, the experimental program was conducted in three different stages. The first set of testing was conducted in May 2000, the second set of testing in November 2000, and the third set of testing in July 2001. The truck used for running the experimental program was a Freightliner Century Class 2000 with an engine power of 500hp at 2100rpm. Figure 4-2(a) shows the testing truck and Figure 4-2(b) shows a schematic of the truck layout.

Since other researchers found that the effect of lateral offset (between the center of the tire and the instrument) was very significant (Chatti et al. 1996), paint was used to mark the position of the instruments. All dynamic instruments were placed in three lateral positions: 0.5, 1, 1.5m from the shoulder, and a 10m line was painted at these three lateral positions. In addition, two more 10m lines were painted between the instruments at distances of 0.75 and 1.25m from the shoulder. Each condition was performed 10 times, twice on each lateral position. This ensured that the maximum strains and pressures would be measured in at least one of the runs. A global position system (GPS) unit was used to measure the exact truck speed. Data from the GPS unit was saved in a laptop placed inside the truck.



(a)



(b)

Figure 4-2. Truck Used for Testing: (a) Photograph While Preparing for Testing (b) a Schematic of Truck Layout

Two different load levels were considered for the tandem axle, as shown in Table 4-3. The first load configuration (L1) consisted of an axle load of 75.6kN for each of the tandem axles, while the second load (L2) configuration consisted of 37.8kN for each of the tandem axles. Concrete barrier walls (Jersey walls) were used to load the truck. Two portable low-profile weighing platforms were used to measure the wheel loads.

During the first testing program, the tandem axle consisted of either dual tires or wide-base single tires. Two speeds were used to compare between the newly developed wide-base tire and the conventional dual tires, 72 and 8km/h. However, to evaluate the speed effects using the wide-base single tires, two more speeds were considered: 24 and 40km/h. The tire inflation pressure was kept constant at 720kPa during testing. Since the tested conditions were performed during different periods of the day, it was necessary to correct for temperature variation to be able to compare between the tested conditions. To

avoid the temperature correction process, the second testing program was performed with the tandem axle consisting of either dual tires followed by wide-base tires or wide-base tires followed by dual tires. Two speeds were considered: 40 and 72km/h. However, since this testing program was performed in November, the temperature was too low to induce any measurable strains inside the pavement layers. Therefore, a third testing program was performed in July 2001 with the tandem axle consisting of dual tires followed by the wide-base tires. Four speeds were considered, 8, 24, 40, and 72km/h. Table 4-4 summarizes the 22 tested conditions during the three testing programs.

Table 4-3. Load Configuration

L1 (Dual Tires) (kN)				L1 (Wide base) (kN)			
D1	25.17	P1	25.89	D1	25.18	P1	25.89
D2	37.80	P2	37.19	D2	37.28	P2	36.21
D3	37.72	P3	38.34	D3	38.52	P3	36.65
L2 (Dual Tires) (kN)				L2 (Wide base) (kN)			
D1	24.55	P1	26.07	D1	24.82	P1	25.58
D2	18.95	P2	20.91	D2	19.22	P2	19.13
D3	18.86	P3	18.50	D3	19.13	P3	18.33

4.4. DATA COLLECTION

Dynamic data were collected during the truck testing and were saved in its raw format in a binary file as follows:

- *File header:* contains the sampling frequency of the wave and the number of samples saved before and after the trigger point, respectively.
- *Wave record:* contains the trigger time of the wave, the time (in seconds) elapsed between the trigger time of the previous and current wave, the label of the triggered instrument, the reference value with respect to which the instrument was triggered, and the different samples of the acquired wave.

The GPS unit, which was installed in the testing truck, was used to determine the truck's instantaneous speed, and the data was saved with a time stamp in a laptop synchronized with the computers located inside the bunkers. Using specially developed software, the obtained speed file was combined with the binary raw data from the bunkers and the information provided by the user to produce the final data files, which group the instrument responses by sections. The new binary files are formatted as follows:

- *File header:* contains the sampling frequency of the wave and the number of samples saved before and after the trigger point, respectively.
- *Wave record:* contains the trigger time of the wave, the time (in seconds) elapsed between the trigger time of the previous and current wave, the label of the triggered instrument, the reference value with respect to which the instrument was triggered, the different samples of the acquired wave, the run number, the

approximate distance from the edge of the lane, the instantaneous truck speed, and the direction of travel (downhill or uphill).

- *File footer*: this part contains three groups of information located at the end of the binary file:
 - *Test Info*: consisting of the tire pressure and truck target speed used during that test.
 - *Truck info*: consisting of the distances between the successive axles of the truck and trailer.
 - *Load info*: consisting of the load of each tire or axle of the truck and trailer.

Table 4-4. Summary of Testing Conditions

		Tires' Configuration	Load	Target Speed (km/h)
MAY 2000	Condition 1	Dual	L1	72.0
	Condition 2	Dual	L1	8.0
	Condition 3	Dual*	L1	72.0
	Condition 4	Dual*	L1	72.0
	Condition 5	Dual	L2	72.0
	Condition 6	Dual	L2	8.0
	Condition 7	Wide Base	L2	72.0
	Condition 8	Wide Base	L2	8.0
	Condition 9	Wide Base	L2	24.0
	Condition 10	Wide Base	L2	40.0
	Condition 11	Wide Base	L1	72.0
	Condition 12	Wide Base	L1	8.0
	Condition 13	Wide Base	L1	24.0
	Condition 14	Wide Base	L1	40.0
Nov. 2000	Condition 15	Dual + Wide Base	L1	40.0
	Condition 16	Dual + Wide Base	L1	72.0
	Condition 17	Wide Base + Dual	L1	40.0
	Condition 18	Wide Base + Dual	L1	72.0
July 2001	Condition 19	Dual + Wide Base	L1	8.0
	Condition 20	Dual + Wide Base	L1	24.0
	Condition 21	Dual + Wide Base	L1	40.0
	Condition 22	Dual + Wide Base	L1	72.0

*: Cases of differential dual tire pressures

The name of each output binary file was saved by concatenating the test date (month, day, and year), the section number, and the condition number (e.g. "05-10-2000_Section_A_Condition1"). Since there were 22 different conditions and 12 different sections, a total of 240 files were stored for analysis. Temperature data was collected continuously from the bunkers every 15 minutes. For each bunker, temperature data from the two corresponding sections was stored in a tab delimited text file in the form of a table (grouping the response of each instrument by column). The rows and columns of

that table were labeled respectively using the time at which data was collected and the instrument label. Using specially developed software, the temperature data was then grouped by section. The name of each temperature file is formed by concatenating the data when data was collected (month, day, and year) and the section number (e.g., "D05-10-2000ScA.tem). Since the testing was performed in four days at different periods of the day, the temperature data was used to shift all dynamic responses to a reference testing temperature of 25°C to be able to compare between all the results.

Figures 4-3 to 4-6 show some of the collected waveforms during testing. Figures 4-3 and 4-4 show the pressure response under the BM-25.0 of Section A for conditions 1 and 2, respectively. The first peak represents the effect of the driver side wheel of the steering axle, while the two following peaks represent the effect of the driver side wheels of the tandem axle. The main characteristics of pressure cell signals can be summarized as follows:

- The width of the response depends mainly on the speed of the vehicle. As shown in the strain responses, asymmetry of the signal is manifested. Since the speed was around 72km/h in condition 1 and only 8km/h in condition 2, the pressure pulse width for condition 1 is much narrower than that for condition 2. It is around 0.1 sec for condition 1 and around 1 sec for condition 2.
- Due to the dynamic nature of the load, pressure cell response coincides with the vertical principal stress only when the wheel is exactly on top of the instrument.
- The magnitude of the signal mainly depends on the load and its lateral position. A lateral offset of more than 250mm usually results in a reduction of more than 50% in the gauge response at shallow depths.

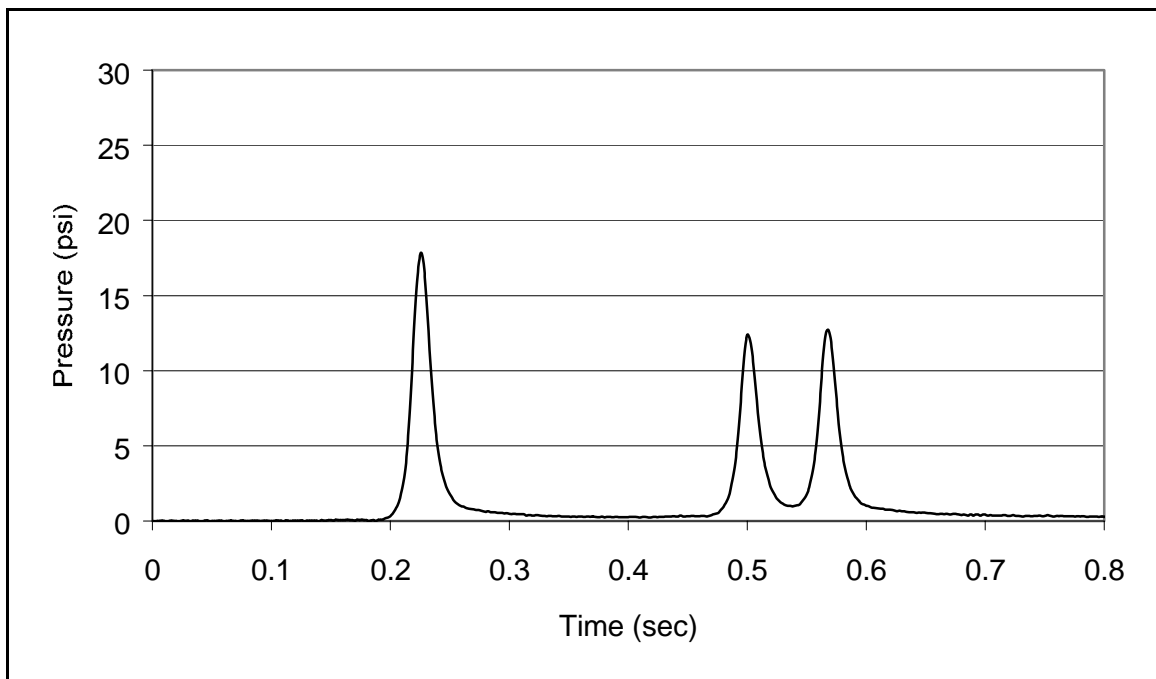


Figure 4-3. Pressure under BM-25.0 Condition 1 (Section A)

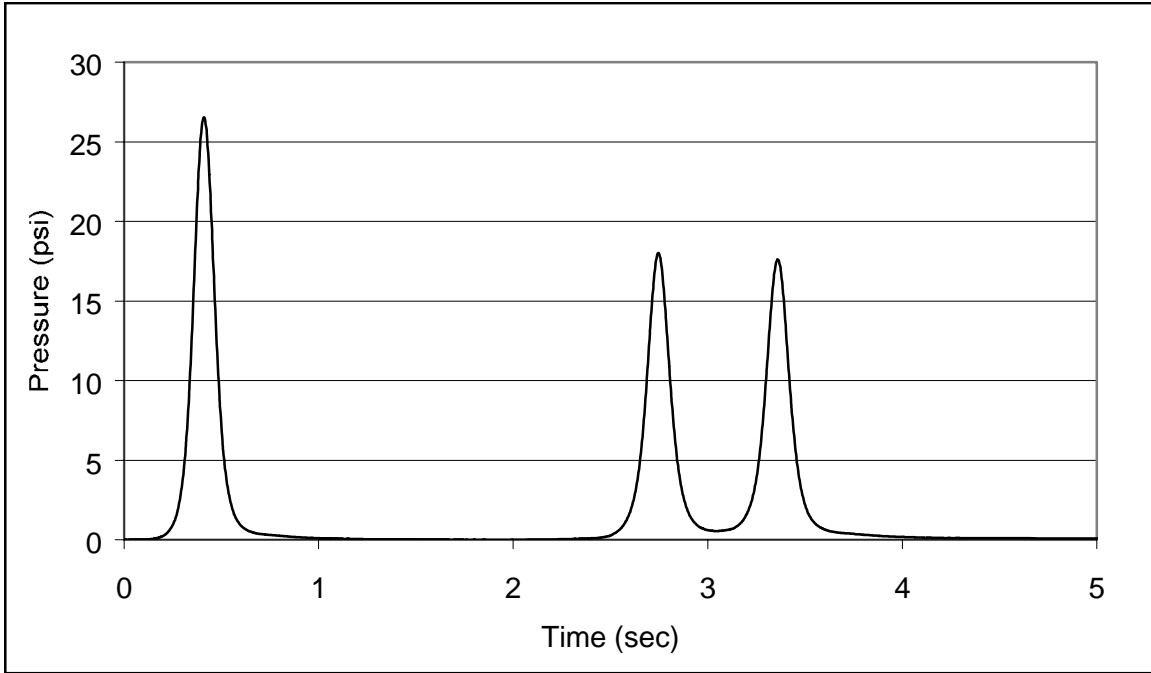


Figure 4-4. Pressure under BM-25.0 Condition 2 (Section A)



Figure 4-5. Strain under Wearing Surface Condition 2 (Section A)

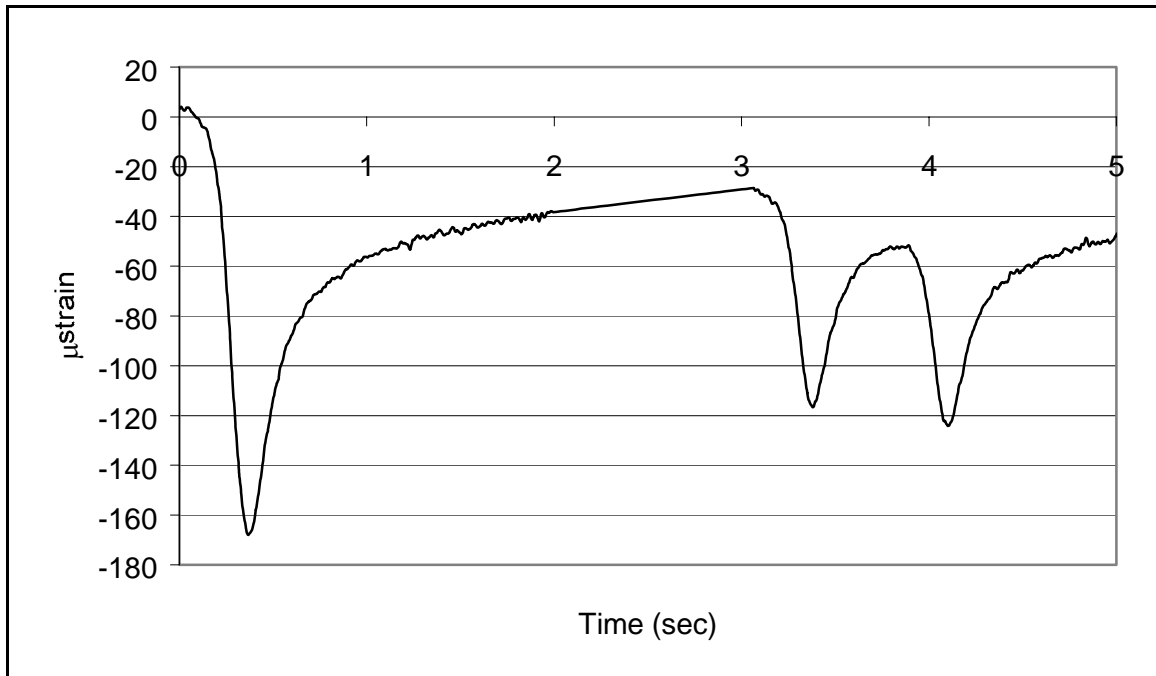


Figure 4-6. Strain under BM-25.0 Condition 2 (Section B)

Figure 4-5 shows the longitudinal strain under the wearing surface for condition 2, section A. Figure 4-6 shows the transverse strain under the BM-25.0 layer in section B for condition 2. The main characteristics of the transverse and longitudinal directions can be summarized as follows:

- These signals clearly prove the viscoelastic behavior of HMA: time retardation, relaxation with time, and asymmetry of the response.
- The longitudinal strain first shows compression, then tension, and finally compression again. The second compression peak is always lower than that of the first. In the longitudinal direction, relaxation of the material is very fast and usually returns to zero with no permanent deformation.
- The longitudinal strain shape is not affected by the lateral position of the tire; however, the magnitude of the strain is affected by the position of the wheel. If the tire load passes directly on top of the strain gauge, the transverse strain exhibits pure tension. If a small offset between the tire and the gauge exists, the transverse gauge would exhibit pure compression. It appears that the relaxation process in the transverse direction is much slower.
- If a second load passes on top of the same gauge before complete relaxation, accumulation of strain may occur in the transverse direction due to the slow relaxation rate (resulting in permanent deformation, as shown in Figure 4-6). Relaxation becomes even slower at high temperatures, since under such conditions HMA may exhibit close to pure viscous behavior.
- It was previously reported by Huhtala that the transverse strain is usually higher than the longitudinal strain, and, therefore, it is the most critical (Huhtala et al.

1992). The trend in this project suggests that the magnitude of the critical strain in both directions depends on the tire configuration. For the dual and wide-base assemblies considered in this project, the longitudinal strain was always greater than the transverse strain.

- The difference in the material response in both directions is not directly related to the viscoelastic nature of HMA or the anisotropy of the material; instead, the difference is due to the movement direction of the vehicle (Nilsson 1999). However, the difference in the rate of relaxation in the transverse and longitudinal direction clearly demonstrates the anisotropic nature of the material, which may be related to the compaction pattern used in construction practices.

Instrument responses to all the tested conditions were analyzed and the maximum recorded stresses and strains per layer were extracted. The temperature at the different layers during the testing was also recorded and tabulated with the corresponding stresses and strains. Conditions used to compare between dual configurations versus wide-base single tire configurations were tabulated together. Conditions 1, 3, and 4 were compared to condition 11; condition 2 was compared to condition 12; condition 5 was compared to condition 7; and condition 6 was compared to condition 8. Since the major focus in this study was given to section B, Tables 4-5 to 4-8 illustrate the results of this analysis for this pavement section. Results for the other sections have been presented elsewhere (Al-Qadi et al. 2000).

Table 4-5. Conditions 1, 3, and 4 vs. Condition 11 (Section B)

	Condition 1				Condition 3				Condition 4				Condition 11			
	Axle 1	Axle 2	Axle 3	Temp.	Axle 1	Axle 2	Axle 3	Temp.	Axle 1	Axle 2	Axle 3	Temp.	Axle 1	Axle 2	Axle 3	Temp.
Stress																
Under WS	64.7	68.7	72.5	31.5	27.8	47.8	48.2	38.7	63.5	55.3	64.5	23.3	71.1	75.7	79.7	22.8
Under OGDL	10.4	7.9	9.3	24.3	13.0	11.5	13.5	29.0	6.6	6.9	7.5	23.5	6.52	7.52	9.22	24.0
Under 21A	1.7	2.0	2.4	28.0	2.2	2.7	3.4	29.0	2.5	2.9	3.1	26.6	1.16	1.97	2.61	28.6
Under 21B	1.7	2.3	2.5	18.6	2.2	3.1	3.6	19.0	1.3	2.0	2.3	17.7	1.34	2.24	2.66	20.6
Transversal Strain																
Under WS	79.1	86.1	100.6	31.5	280.8	266.7	352.8	38.7	----	29.3	35.6	23.3	24.3	23.1	28	22.8
Under BM-25.0	----	----	----	----	64.6	50.5	59.6	33.5	----	----	----	----	----	----	----	----
Under OGDL	49.7	35.6	42.7	24.3	67.9	49.3	49.3	29.0	48.2	42.6	46.3	23.5	40.6	41	48.7	24.0
Longitudinal Strain																
Under WS	113	82.8	98.1	31.5	256.3	218.6	211.2	38.7	----	----	----	----	----	----	----	----
Under BM-25.0	----	----	----	----	----	50.4	57.5	33.5	----	----	----	----	----	----	----	----

Table 4-6. Conditions 2 vs. Condition 12 (Section B)

	Condition 2				Condition 12			
	Axle 1	Axle 2	Axle 3	Temp.	Axle 1	Axle 2	Axle 3	Temp.
Stress								
Under WS	75.7	59.6	61.4	41.2	73.2	62.4	65.6	30.8
Under OGDL	18.6	13.2	14.0	26.5	10.8	12.1	14.7	23.2
Under 21A	3.7	3.9	4.1	27.4	2.5	3.7	4.1	27.2
Under 21B	3.7	3.9	4.2	18.0	2.2	3.3	3.9	24.2
Transversal Strain								
Under WS	994.4	1071.3	1202.3	41.2	136.3	74.8	83.8	30.8
Under BM-25.0	168	116.7	124.1	31.5	43.7	44.1	57.6	23.1
Under OGDL	118.5	76.3	87.8	26.5	66.2	65.4	66.8	23.2
Longitudinal Strain								
Under WS	1002.3	1023.3	1063.5	41.2	146.7	201.2	238.2	30.8
Under BM-25.0	183.2	149.5	163.9	31.5	73.1	76.1	80.5	23.1

Table 4-7. Conditions 5 vs. Condition 7 (Section B)

	Condition 5				Condition 7			
	Axle 1	Axle 2	Axle 3	Temp.	Axle 1	Axle 2	Axle 3	Temp.
Stress								
Under WS	73.9	32.6	40.0	42.9	71.8	45.3	52.7	26.5
Under OGD	11.1	5.2	5.6	25.4	7.4	5.1	6.0	25.8
Under 21A	1.8	0.9	1.1	26.6	1.4	1.0	1.2	29.6
Under 21B	1.2	1.3	1.4	18.0	1.4	1.0	1.2	18.7
Transversal Strain								
Under WS	281.2	187.6	180.1	42.9	24.7	13.6	18.3	26.5
Under BM-25.0	----	----	----	----	----	----	----	----
Under OGD	56.7	30.6	36.4	25.4	54.5	34.3	37.5	25.8
Longitudinal Strain								
Under WS	----	----	----	----	68	60	75.4	26.5
Under BM-25.0	----	----	----	----	----	----	----	----

Table 4-8. Conditions 6 vs. Condition 8 (Section B)

	Condition 6				Condition 8			
	Axle 1	Axle 2	Axle 3	Temp.	Axle 1	Axle 2	Axle 3	Temp.
Stress								
Under WS	66.7	33.9	36.0	44.2	6.9	48.4	51.6	33.0
Under OGD	16.1	6.0	6.9	27.3	9.5	8.3	9.8	25.4
Under 21A	3.2	1.6	1.8	27.4	2.6	1.6	1.8	29.3
Under 21B	3.1	1.7	1.9	17.3	2.4	1.5	1.9	18.9
Transversal Strain								
Under WS	710.9	534.8	677.6	44.2	212.9	138.1	162.1	33.0
Under BM-25.0	129.4	72.7	81.7	33.2	46.5	42.1	49.3	26.4
Under OGD	106.4	53.7	60.0	27.3	60.4	52.7	57.5	25.4
Longitudinal Strain								
Under WS	641.8	512.9	664.1	44.2	255.7	247.7	260.9	33.0
Under BM-25.0	167.9	79.4	80	33.2	58.5	56.6	68.5	26.4

Table 4-9. Conditions 15 through 18 (Section B)

	Condition 15			Condition 16			Condition 17			Condition 18		
	Steering	Dual	Wide Base									
Stress												
Under OGDL	3.3	2.6	4.2	2.3	2.1	3.2	2.8	3.2	2.6	2.0	2.8	2.2
Under 21A	0.8	1.4	1.6	0.8	1.2	1.3	0.7	1.4	1.3	0.7	1.2	1.1

Table 4-10. Conditions 19 through 22 (Section B)

	Condition 19			Condition 20			Condition 21			Condition 22		
	Steering	Dual	Wide Base									
Stress												
Under OGDL	14.5	10.7	18.2	11.8	10.7	15.6	13.0	11.4	18.3	15.6	12.0	19.9
Under 21A	2.2	3.4	4.5	2.1	3.1	4.0	2.35	2.84	3.98	2.2	2.7	4.2
Transversal Strain												
Under OGDL	125.5	64.4	72.7	62.9	62.5	79.9	98.6	53.8	62.9	107.7	56.6	45.8
Longitudinal Strain												
Under BM-25.0	78.7	78.7	125.9	47.2	62.9	94.4	86.5	62.9	86.5	101.9	86.1	117.6

Based on the presented data and considering that the testing setup was different between the first (Conditions 1 through 14) and the second and third (Conditions 15 through 22) experimental program, the following observations may be made:

- Although the first set of data is the most complete of the three testing stages, the use of these data requires adequate correction for temperature to establish a sound comparison between dual and wide-base tires configurations because each tire assembly was tested separately.
- Since dual and wide-base tires were tested concurrently in the second and the third testing stage, no temperature correction is required in this case.
- The second testing program was conducted in November 2000. The pertinent testing temperature was too low to induce any measurable strains inside the pavement layers. Hence, a third testing stage was conducted in July 2001.

4.5. RESULTS AND DATA ANALYSIS

Stress and strain measurements under the BM-25.0 layer were used to study the aggressiveness of the different tires. This is because the strain under the BM-25.0 layer has always been correlated to the number of load repetitions to cause fatigue cracking in flexible pavements, while the stress under the HMA layer has been correlated with the rate of rutting (Finn et al. 1986).

4.5.1. Results from the First Testing Program

To be able to compare between the different tire assemblies, all results were shifted to a reference temperature of 25°C. To shift instrument responses to a temperature of 25°C, the results of the steering axle were used since the loading conditions were almost the same during all testing except for temperature variation. Therefore, conditions 1, 5, 7, and 11 were used to shift the 72km/h data, while conditions 2, 6, 8, and 12 were used to shift the 8km/h data. This was accomplished by plotting the measured values (stress or strain) versus the pertinent temperature during the test, omitting all outliers. An exponential regression line was then used to fit the data. The regression equation was then used to determine the response at the reference temperature of 25°C. The strain-temperature relationship at 72km/h was as follows:

$$\mu\text{strain} = 0.8567e^{0.1341T} \quad R^2 = 0.97 \quad (4-1)$$

where,
T = temperature in °C.

At a speed of 8km/h, the strain-temperature was as follows (see Figure 4-7 for illustration):

$$\mu\text{strain} = 10.824e^{0.0784T} \quad R^2 = 0.99 \quad (4-2)$$

The correction factor was then obtained using Equation (4-3):

$$CF = \frac{\text{Response@reference temp.}(25^{\circ}\text{C})}{\text{Response@testing temp.}} \quad (4-3)$$

The correction factor (CF) was found as follows:

$$CF = e^{-0.134(T-25)} \quad \text{For 72 km/h; } R^2=0.99 \quad (4-4)$$

$$CF = e^{-0.0784(T-25)} \quad \text{For 8 km/h; } R^2=0.99 \quad (4-5)$$

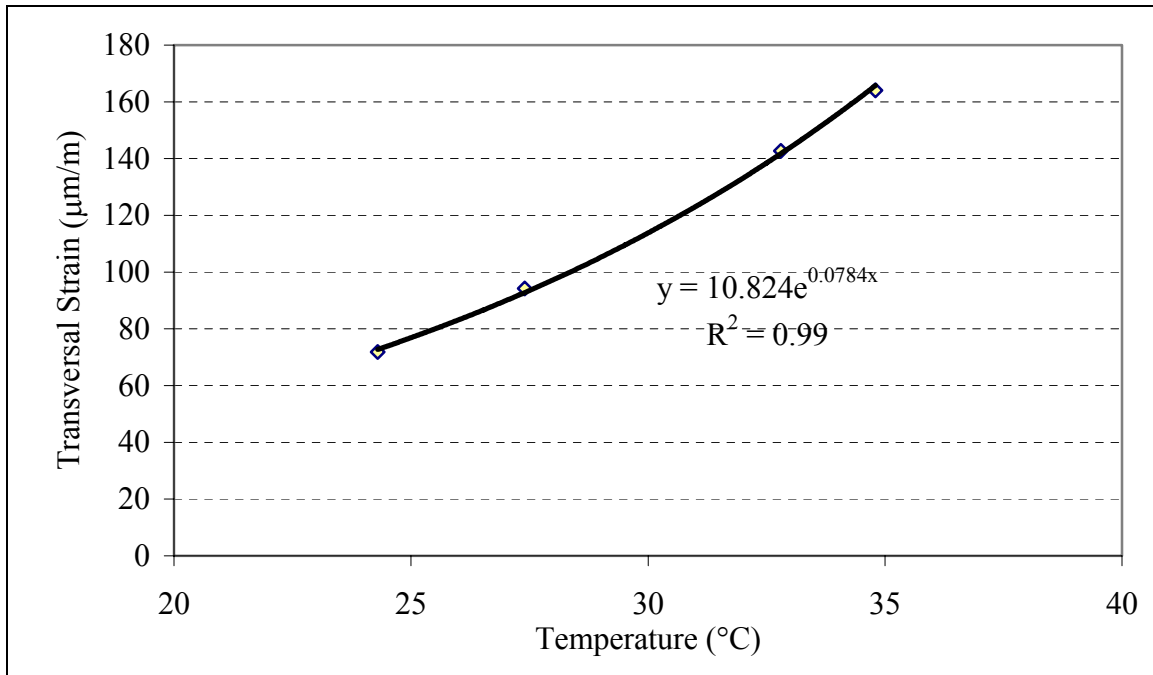


Figure 4-7. Transverse Strain versus Temperature at 8km/h (Steering Axle)

Once the correction factor was determined, strains and stress values obtained from the tandem axle were multiplied by their corresponding temperature correction factors to find shifted results as if all measurements were taken at the same temperature, 25°C. Figure 4-8 shows the maximum measured strain for the different comparable conditions. From this figure, it can be concluded that for the same test parameters (temperature, load, speed, and tire inflation pressure); the dual configuration resulted in smaller strains than did the new wide-base single tire configuration. The steering tire, on the other hand, resulted in greater strain values than the dual or wide-base tires. The difference is especially noticeable when the tandem axle is not fully loaded (load configuration L2).

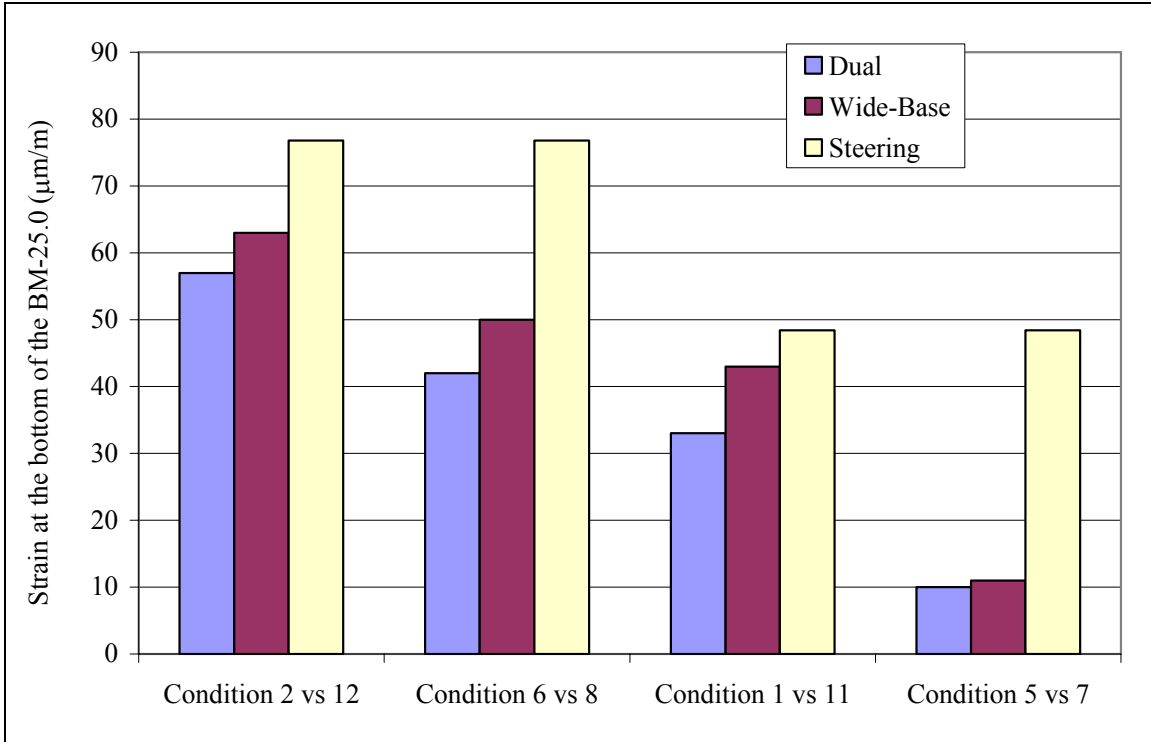


Figure 4-8. Measured Horizontal Strain for Different Testing Conditions

Figures 4-9(a and b) show the measured vertical compressive stress under the BM-25.0 layer and the 21-B layer. Under the BM-25.0, the newly developed wide-base tire resulted in greater stresses than the dual tires or the steering axle. This is mainly due to the fact that the load distribution from the wide-base tire is different than that of the dual tires. The stress due to the dual tires on the upper layers results from just one tire. As the depth increases, the stress from both tires will superimpose. This hypothesis was verified by the measured stress under the 21-B, where the wide-base tire and the dual tires produced approximately the same vertical compressive stress.

To study the effect of speed on the measured strain, results from conditions 9 through 12 were used for load configuration L1, and conditions 5 through 8 were used for load configuration L2. As expected with any viscoelastic materials, the measured strain was found to decrease with the increase in speed. This is due to the fact that when speed increases there will be a decrease in the time of contact between the tire and the pavement. The following relationships were found between tensile strain (in μ strain) and speed (in km/h) for L1 and L2, respectively:

$$\mu\text{strain} = 63.822e^{-0.006\text{speed}} \quad R^2=0.90 \quad (4-6)$$

$$\mu\text{strain} = 52.371e^{-0.0219\text{speed}} \quad R^2=0.94 \quad (4-7)$$

From the first testing program, it was concluded that the newly developed wide-base tire produced slightly greater horizontal strain under the BM-25.0 layer than the dual tires. The steering axle was found to induce more fatigue damage to the pavement than the dual

tires or the newly developed wide-base tire. Since damage to pavements is cumulative over time, the steering load damage should be considered in predicting pavement service life. On the other hand, the newly developed wide-base tire was found to induce greater vertical compressive stress under the BM-25.0 layer than the dual tires, but approximately the same vertical compressive stress under the 21-B layer.

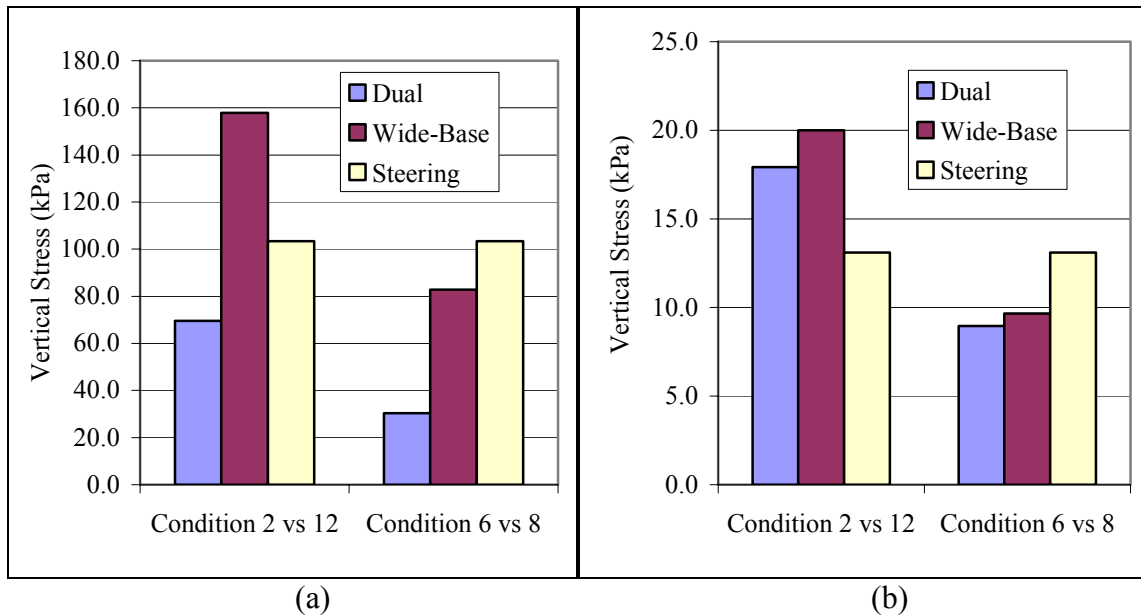


Figure 4-9. Measured Vertical Stresses under (a) BM-25.0 Layer and (b) 21-B Layer

4.5.2. Results from the Second Testing Program

The second testing program was conducted in November 2000. Two speeds were considered, 40 and 72km/h. The maximum recorded air-temperature was 12.9°C, the maximum recorded temperature under the wearing surface layer was 18.6°C, and the maximum recorded temperature under the BM-25.0 layer was 14.0°C. At these temperatures, no measurable strain was recorded (trigger value for strain-gages is 20μstrain). Figure 4-10 shows the measured vertical compressive stress under the BM-25.0. As shown in this figure, the newly developed wide-base tire induced greater stresses at the bottom of BM-25.0 layer as compared with dual tires.

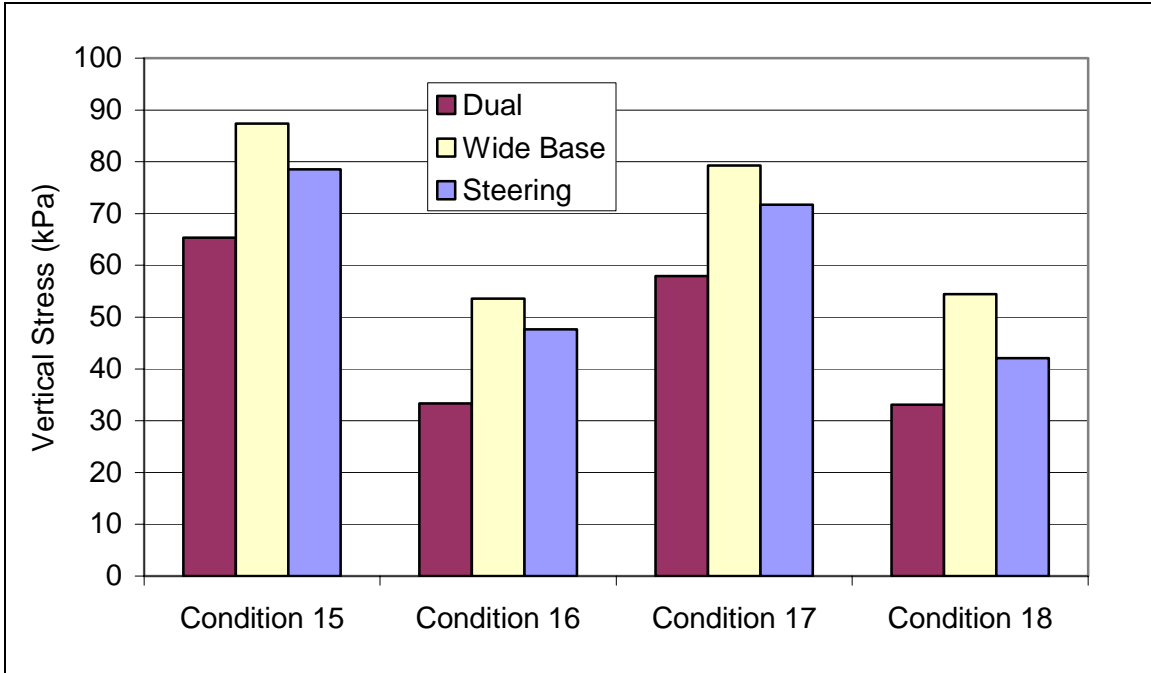


Figure 4-10. Measured Vertical Compressive Stress under BM-25.0 Layer

Based on the second testing program, it was concluded that for the testing conditions used (low temperature and high speed), the newly developed wide-base tire induced greater vertical stresses under the BM-25.0. This difference becomes less significant with increasing depth (Figure 4-11). However, the fatigue damage induced by both tire-assemblies is minimal under the tested conditions, and may be considered negligible.

4.5.3. Results from the Third Testing Program

During the third testing program, performed in July 2001, the temperature was high. The air, under SM-12.5D, and under BM-25.0 temperatures ranged between 20 and 40, 25 and 50, and 27 and 38°C, respectively, between 8:00AM and 4:00PM. Horizontal strains were measured under the BM-25.0 layer. Figure 4-12 shows the measured strains during all tested conditions. It was found that the steering tire load induces greater strains than the tandem axle tires. The measured strains induced from the newly developed wide-base tire were approximately equal to those induced from the dual tires. The measured stresses under the BM-25.0 layer from the newly developed wide-base tire were again higher than those induced from the dual tires. Under the 21-B, vertical compressive stresses induced from the dual tires were approximately equal to those induced from the newly developed wide-base tire (Figure 4-13).

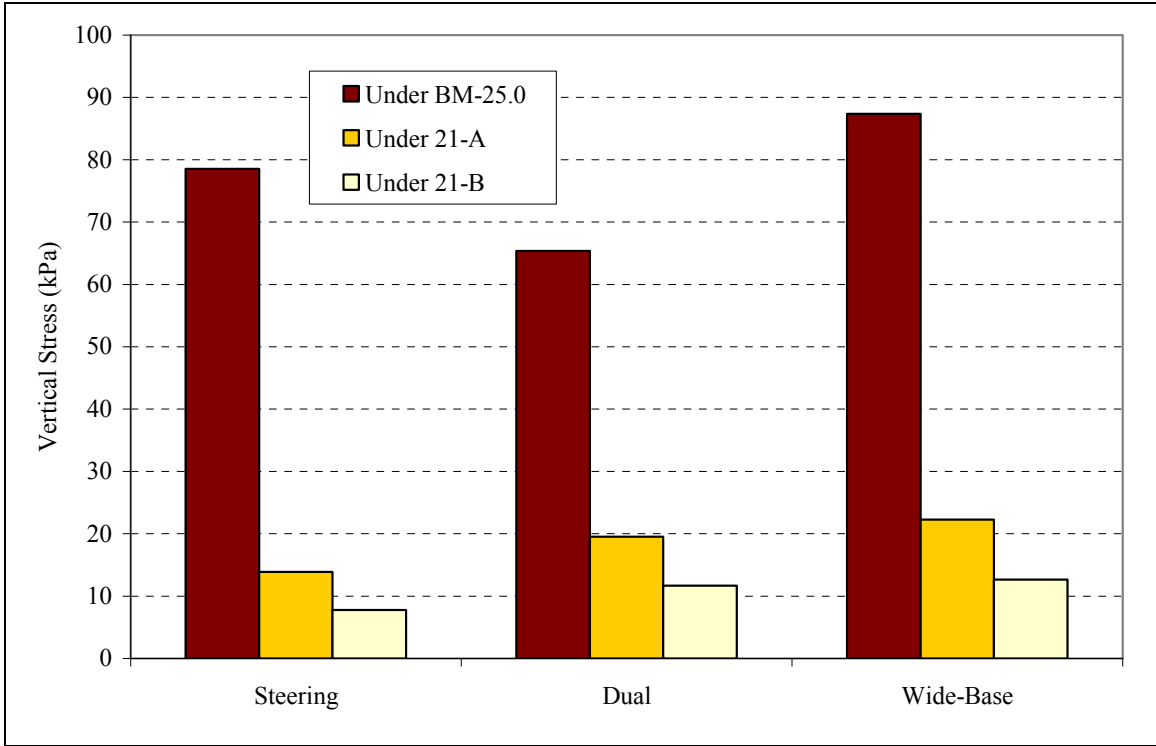


Figure 4-11. Variation of the Measured Compressive Vertical Stress with Depth

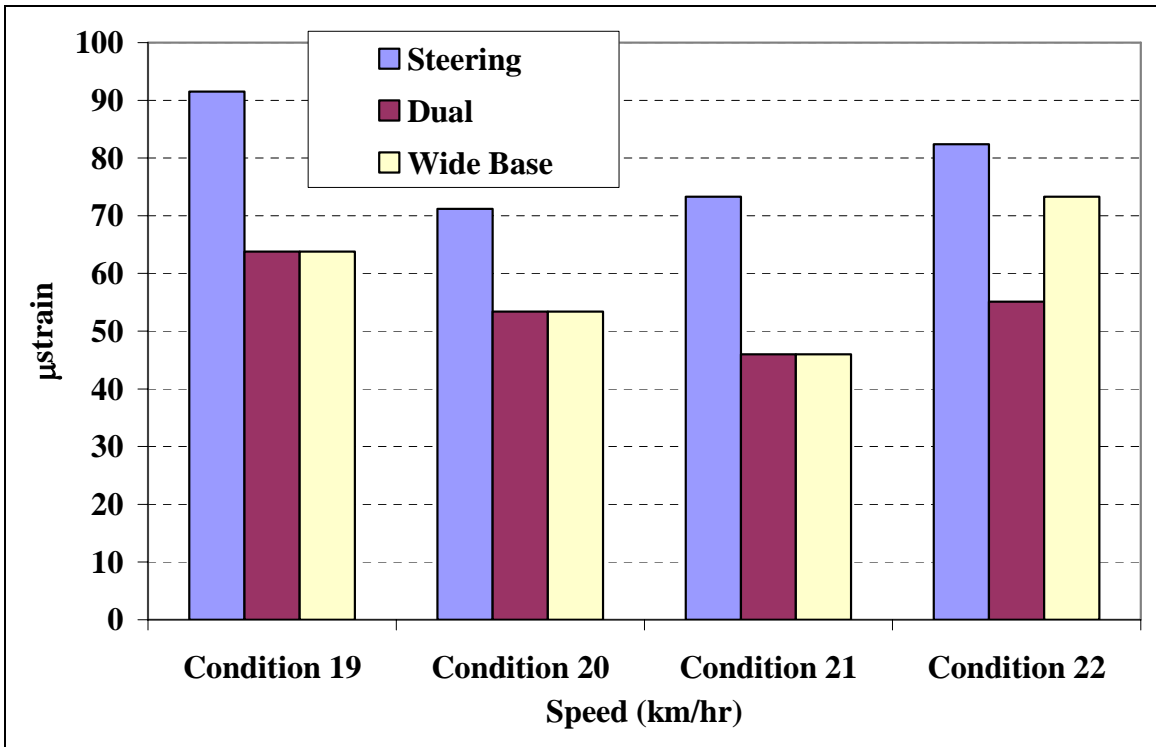


Figure 4-12. Measured Horizontal Strains under BM-25.0 Layer

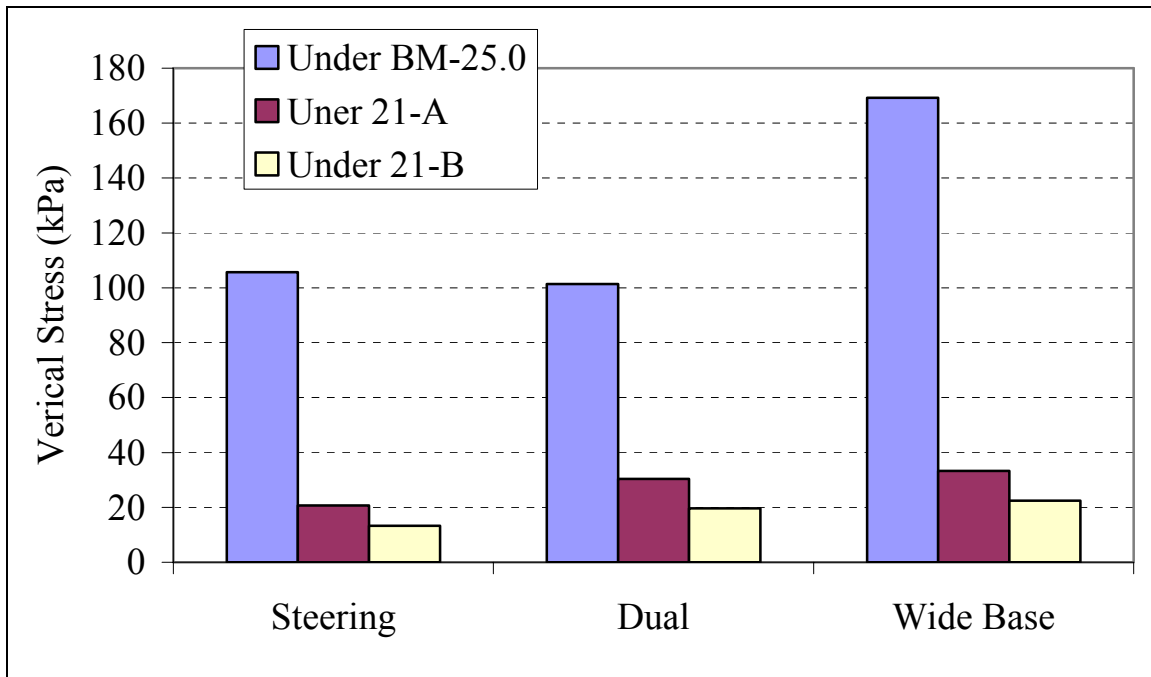


Figure 4-13. Measured Vertical Compressive Stress under Pavement Layers

4.5.4. Findings of the Experimental Program

The experimental program was performed under different loading and environmental conditions and at different speeds to fully understand the pavement behavior under different tires and axle configurations. Results of the first testing program indicated that the newly developed wide-base tire produced slightly greater horizontal strain under the BM-25.0 layer than the dual tires; strain at that location is believed to be responsible for fatigue cracking. In addition, the steering axle was found to induce more fatigue damage to the pavement than the dual tires or the newly developed wide-base tire. On the other hand, the newly developed wide-base tire was found to induce greater vertical compressive stress under the BM-25.0 layer than the dual tires, but approximately the same vertical compressive stress under the 21-B layer. Results of the second testing program showed that at low temperature and high speed, both the newly developed wide-base tire and dual tires induced minimal damage to the pavement. Results of the third experimental program indicated that induced strains from the newly developed wide-base tire were approximately equal to those induced from the dual tires.

Some variability is evident in the results of the experimental program, and a fully-calibrated FE approach may be utilized to validate some of the trends observed in the field. The large array of field measurements established the needed benchmark to calibrate and validate a realistic FE approach. In addition, some of the straining actions needed to assess pavement damage were not measured in the field but were needed to accurately quantify the aggressiveness of each tire configuration as related to different failure mechanisms.

5. FINITE ELEMENT FORMULATION AND VALIDATION

The commercial software ABAQUS version 6.3 was used for FE modeling of the pavement structure (ABAQUS 2001). The developed FE models were unique in different ways. First, geometry and dimensions of the developed theoretical models were selected to accurately simulate the axle configurations typically used in North America, and previously tested at the Virginia Smart Road. Second, these models incorporated laboratory-measured material properties. Finally, the developed FE models were successfully validated and calibrated based on actual stress and strain measurements obtained from the experimental program. This section provides detailed description of the developed models as well as the main assumptions made in the analysis.

All FE models developed in this study simulated the same pavement structure: Section B at the Virginia Smart Road. This section was selected for several reasons. In addition to its heavy instrumentation, Section B is a typical interstate highway pavement design, thus facilitating the validation of the developed FE models. Section B may be classified as a medium thickness pavement design with a total thickness of HMA layers of 188mm. However, given the large number of layers, the mechanical stiffness of this pavement design is considered high, which is typical of interstate highway pavement structures. Figure 5-1 presents the pavement design of this section. The following sections discuss some of the characteristics of the developed FE models.

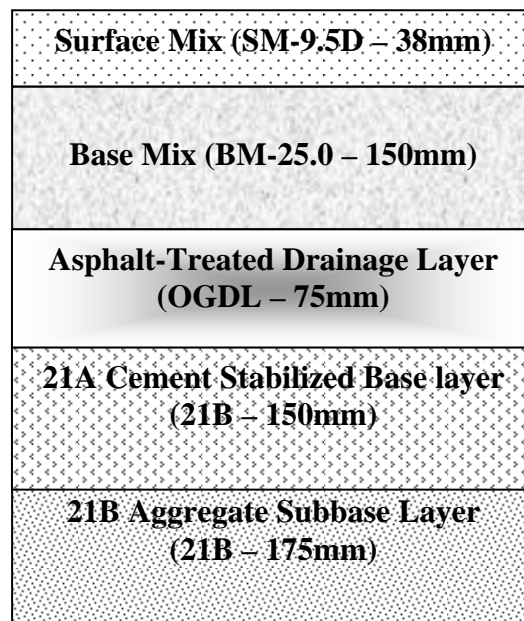


Figure 5-1. Pavement Design of Section B

5.1. MODEL DIMENSIONS AND GEOMETRY

Figure 5-2 illustrates the general layout of the developed FE models. The dimensions of the modeled portion were 1920mm x 1122mm. These dimensions were selected to reduce any edge effect errors, while keeping the elements' sizes within acceptable limits (computing constraints). To simulate the behavior of both dual tires and their combined effects on the pavement structure, no symmetry was considered in the developed model (see Figure 5-2). The generated mesh was designed to give an optimal accuracy (fine mesh around the load and coarse mesh far from it). To improve the rate of convergence, 8-node linear brick reduced integration elements (C3D8R) were used with variable thicknesses, depending on the layers. All layers were simulated with the same shape to preserve the continuity of nodes between consecutive layers.

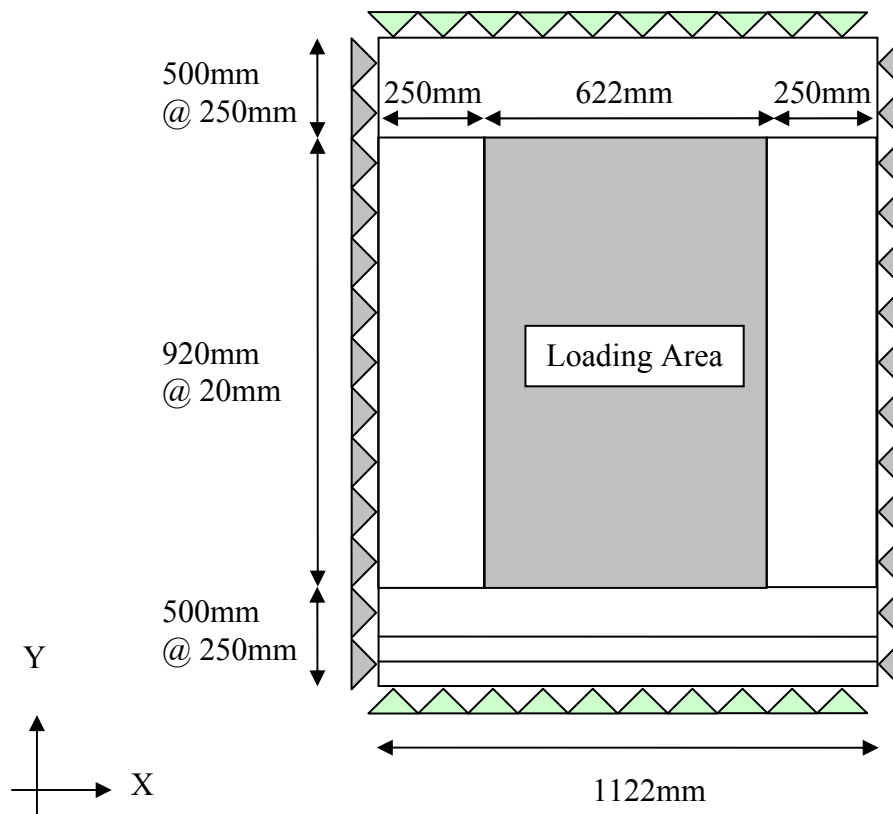


Figure 5-2. General Layout of the Developed FE Models

5.2. ELEMENT DIMENSIONS: SENSITIVITY ANALYSIS

The FE method is an approximation of the continuum solution (Holzer 1985). When dealing with 3D FE modeling, element dimensions need to be carefully selected since they directly affect the level of accuracy obtained from the model. Computational time and constraints also affect the possible level of accuracy. Therefore, to ensure the accuracy of the developed FE models, two convergence criteria were considered:

- The FE solution has to converge to the continuum model solution. To satisfy this criterion, a regular mesh refinement process was used with the finest mesh containing all previous meshes. The FE solution was then checked against a simplified solution. The layered theory solution was used in this study for validation. Therefore, for comparison purposes, the assumptions (e.g., static loading, fully-bonded conditions, uniform contact pressure, and linear elastic response of pavement materials) made in the developed FE models were intentionally simplified to exactly resemble the layered theory. These models were then modified to approach real field conditions.
- The accuracy of the FE model has to be acceptable within the context of the application. Bathe's criterion states that an FE mesh is sufficiently fine when jumps in stresses across inter-element boundaries become negligible (Bathe 1982). The jump in stresses may be considered within the same plane or at the interfaces between different layers.

To ensure the accuracy of the results and the convergence of the developed models, several aspects of the FE model were analyzed and refined until specific criteria were satisfied. Though the in-plane dimensions were selected to reduce the jumps across inter-element boundaries within the same XY plane while keeping the computation time within reasonable limits, only results of the sensitivity analysis for the element thickness (depth of the element) are presented in this report as an illustrative example.

For a continuum model, no jumps in vertical stresses should occur at the interface between the layers. Hence, the first criterion used in the evaluation of the accuracy of the model is the determination of the jump in vertical stresses that may occur at the interface. In this analysis, different element thicknesses ranging from 2.381mm to 38.1mm were considered. Table 5-1 presents the jump in vertical stress at the wearing surface – base mix interface, which is the most critical interface, being the closest to the load. As shown in this table, the continuity of stresses at the interface between the layers is highly affected by the selected element thickness. However, this problem can easily be controlled by appropriate refinement of the mesh. Considering that a minimum level of accuracy of 5% of the applied load is needed (i.e., 40kPa), it appears that only an element thickness of 9.53mm or smaller would provide an acceptable level of accuracy.

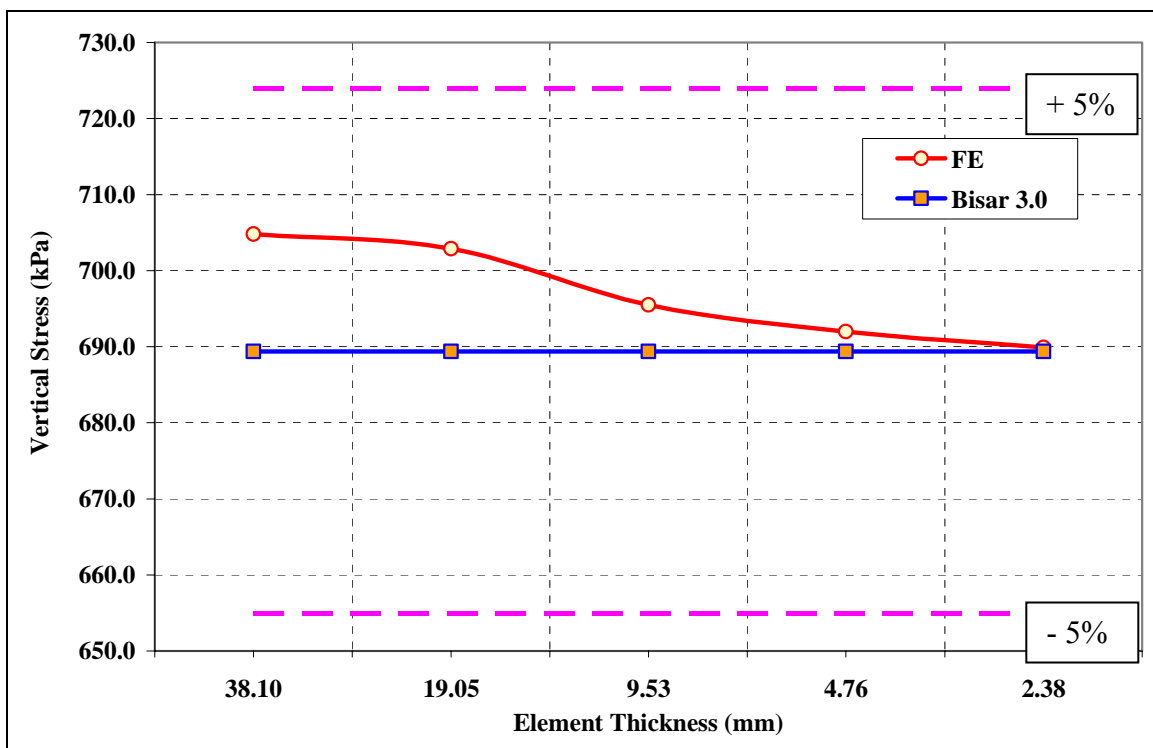
Table 5-1. Sensitivity Analysis

Case ID	Element Thickness (mm)	Model Size (dof)	Number of Elements	Data Storage (Gbytes)	Computational Time (sec)	Jump at WS – BM Interface (kPa)
A	38.10	172,476	42,916	2.35	3145	93.2
B	19.05	212,226	55,656	3.09	4871	52.2
C	9.53	291,726	81,136	4.19	6599	25.6
D	4.76	450,726	132,096	7.26	18565	9.90
E	2.38	760,776	231,468	12.91	30551	6.97

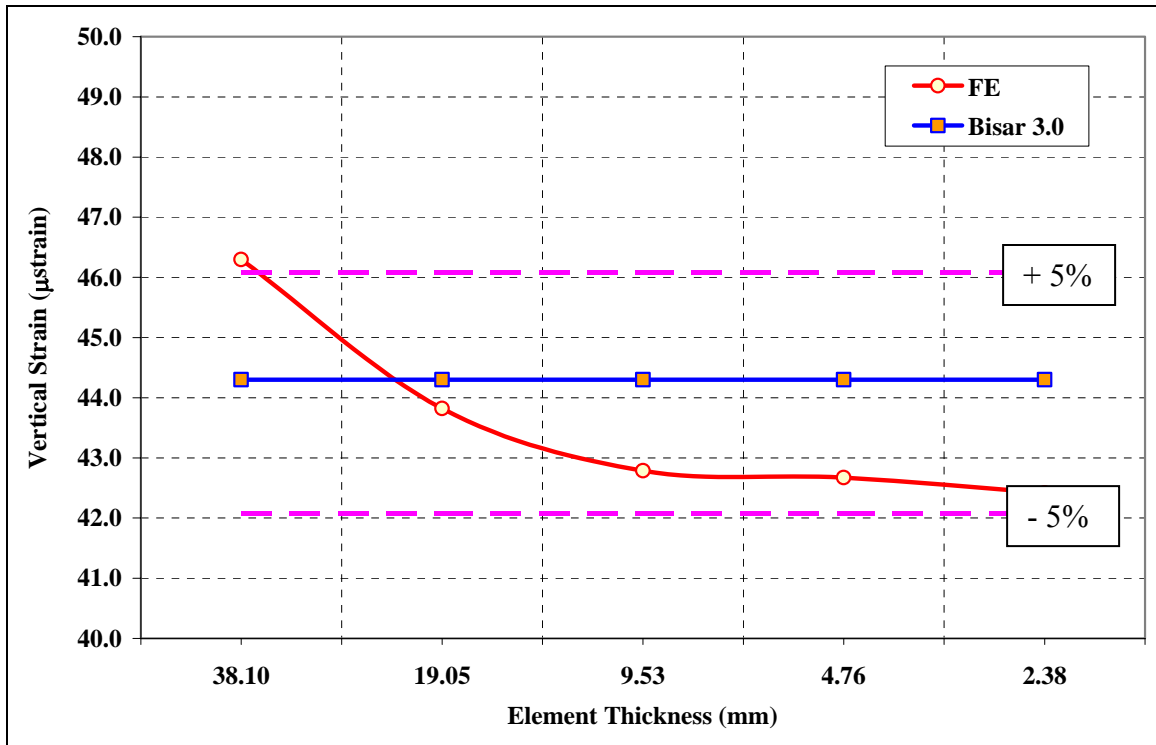
* dof : degree of freedoms

Another critical factor in the selection of the appropriate element thickness is to control the computational time and data storage space requirements for the selected element dimensions. Each layer of elements represents an additional 3,360 degrees of freedom to the model, which characterizes a significant increase in computational time and data storage space requirements. Table 5-1 illustrates the data storage and computational time requirements for the different investigated cases. It is worth noting that the computational time for the presented simplified model is only representative of the time required to run the modified model presented later in this chapter. This is due to the difficulty of obtaining an acceptable solution when nonlinearity is introduced to the analysis. Sources of nonlinearity include time-dependent material properties; geometric characteristic of the model; and contact and boundary conditions, such as the simulation of friction between the layers. All FE models were processed on a SGI Origin 2000 supercomputer.

To further evaluate the accuracy of each case, a similar model was developed for the same loading and material conditions using a multi-layer elastic software BISAR 3.0 (De Jong et al. 1973). Results presented in Figure 5-3(a) show the convergence of the vertical stress at the bottom of the wearing surface with mesh refinement. Similarly, Figure 5-3(b) illustrates the convergence of the vertical strain at the bottom of the base mixture with mesh refinement. However, results of these models do not appear to exactly converge to the BISAR's solution (though assumed close to the exact solution) as the mesh is refined. Using the same accuracy criterion applied to assess the jump in vertical stress across the layer interfaces, the limits of accuracy shown in Figures 5-3(a and b) indicate that an element thickness of 19.05mm or smaller should provide a level of accuracy of 5% or better, when compared to the BISAR's solution.



(a)



(b)

Figure 5-3. Convergence of (a) the Vertical Stress at the Bottom of the Wearing Surface (SM-9.5D) and (b) Vertical Strain at the Bottom of the Base-Mixture (BM-25.0)

Given that an FE model with an element thickness of 9.53mm or smaller would provide an acceptable level of accuracy, it was decided to use an element thickness of 9.53mm for all developed models in this study to save in computational time while providing an accurate description of the pavement system. This good agreement between the FE and the layered theory solution for this simplified case establishes the adequacy of the geometry, mesh, and boundary conditions of the FE model. Figures 5-4(a and b) illustrate the general layout of the developed FE model.

5.3. LOADING AREA AND MODEL

Two general approaches are used to model the contact of the tire with the pavement surface (Soon et al. 2003). In the first approach, the problem is dealt with as a two-solid contact mechanics. This implies that the actual contact stress between the tire and the pavement is not initially known, and depends on the interaction between the tire and the pavement surface. This is a very challenging problem with respect to the modeling process or the required computational time since a very fine mesh is needed to capture the high stress gradient at the surface, and the existence of singularities at the edges of the tire. In addition, in order to simplify this problem, linear elastic responses of the materials are usually assumed. In the second approach, one of the two solids is omitted

and is approximated by a known stress-field or a rigid surface. If pavement responses are of primary interest, the tire is removed, and its interaction is substituted by a known stress field. This allows the finest mesh to be used to model the different pavement layers, and more realistic time-dependent material properties may be implemented in the analysis. Given the limitations of the first approach, it was decided to adopt the second method in this study. Exact contact dimensions and stress fields were provided by the manufacturer, and were also interpreted based on stress measurements at the Virginia Smart Road.

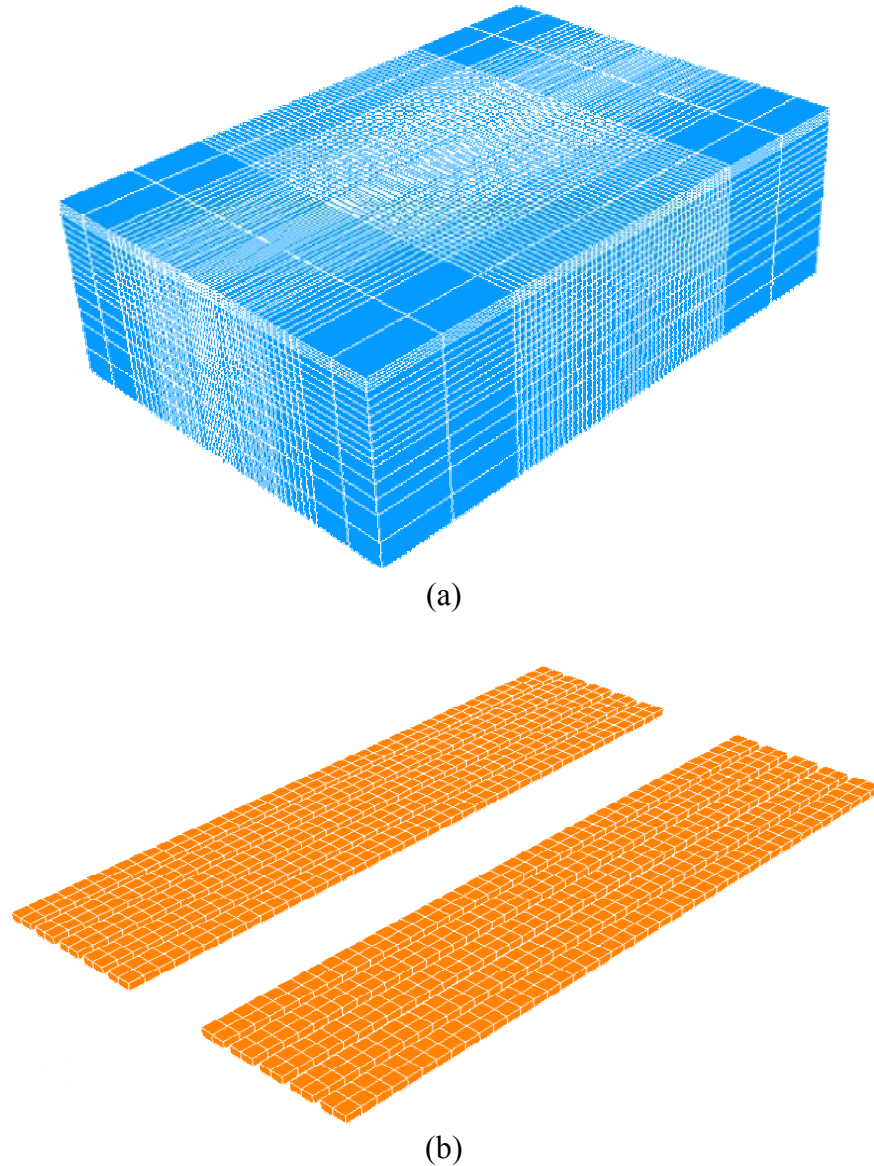


Figure 5-4. (a) General Layout of the Developed FE Model and (b) Refined Mesh in the Loading Path

5.3.1. Contact Dimensions

To accurately simulate pavement response to vehicular loading, one must determine the exact area of contact between the tire and pavement. In the layered theory, due to its use of an axisymmetric formulation, it is assumed that each tire has a circular contact area. The tire-pavement contact area is not circular; in fact, a rectangular shape is more realistic. In addition, tire's type and its inflation pressure, along with the magnitude of the load, all affect the shape of the footprint. Three-dimensional finite element method (FEM) allows for any shape for the contact area, and therefore, a more accurate modeling of the contact area is feasible.

The exact footprint shape and dimensions of the dual and wide-base tires were provided by the manufacturer at the exact load level (Load L1) tested at the Virginia Smart Road (see Figure 5-5). These dimensions were provided at one of the tire pressures tested in the field (720kPa). In addition to the two tire configurations tested at the Virginia Smart Road, the newly-developed wide-base tire (455/55R22.5) was also evaluated at a nominal tire pressure of 720kPa and at the same load level (Load L1) used in the experimental program. The modeled loading area accurately simulated the actual contact between the pavement and the tire under consideration. Figure 5-6 illustrates the modeled contact area for the wide-base and dual configurations.

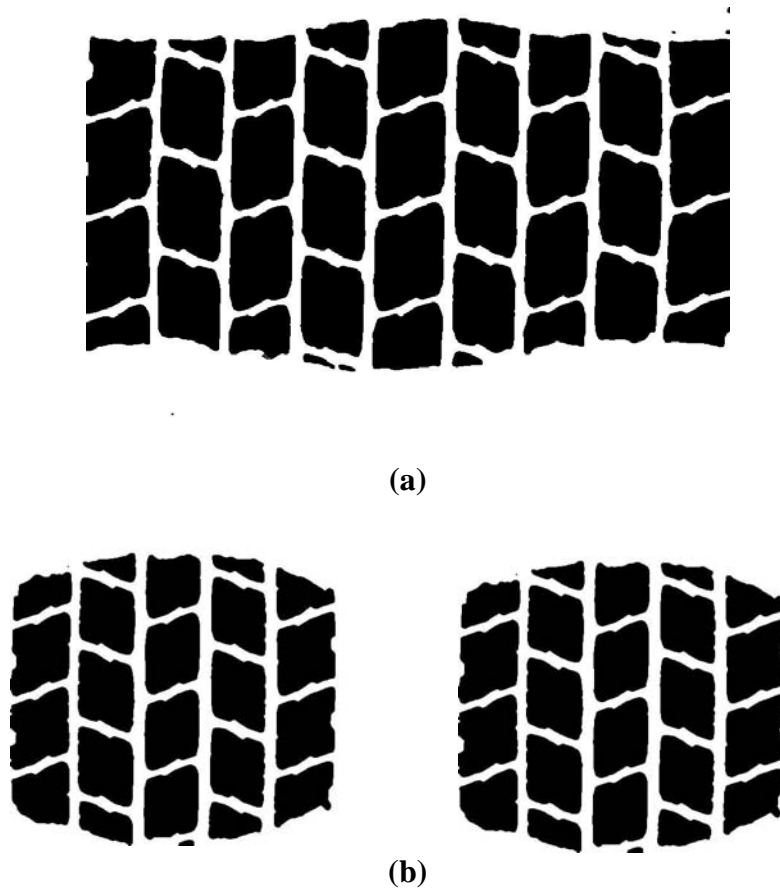
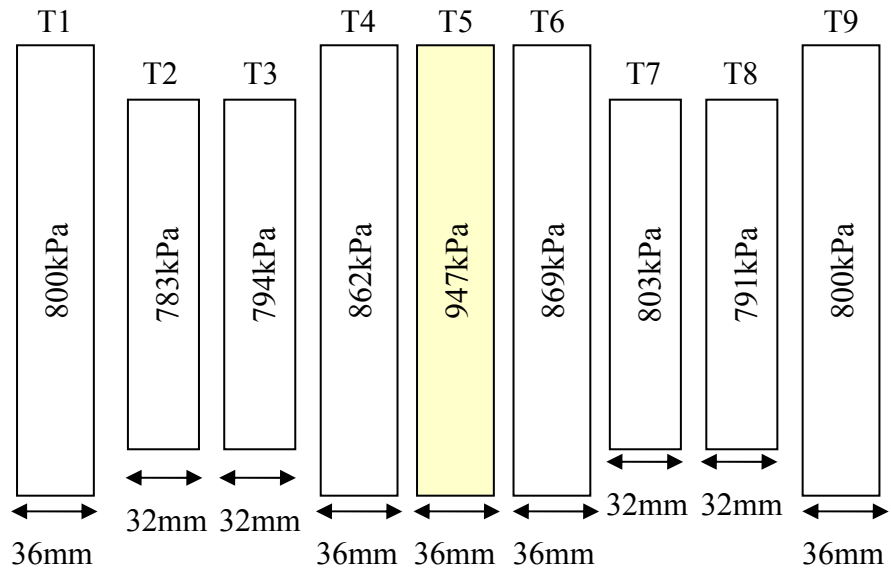
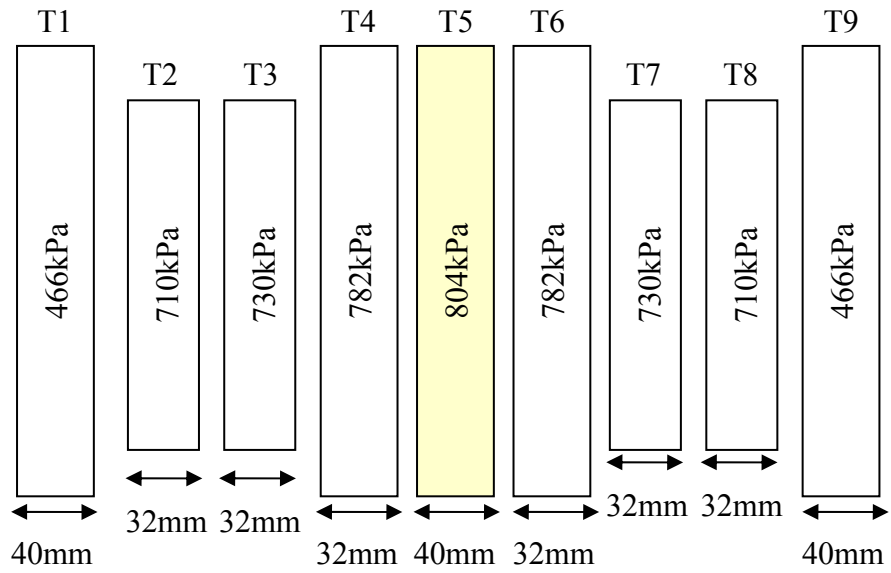


Figure 5-5. Tire Footprints for (a) the New Generation Wide-Base Tire (445/50R22.5) and (b) the Dual Tires Configurations



Wide-Base Contact Area

445/50R22.5



Wide-Base Contact Area

455/55R22.5

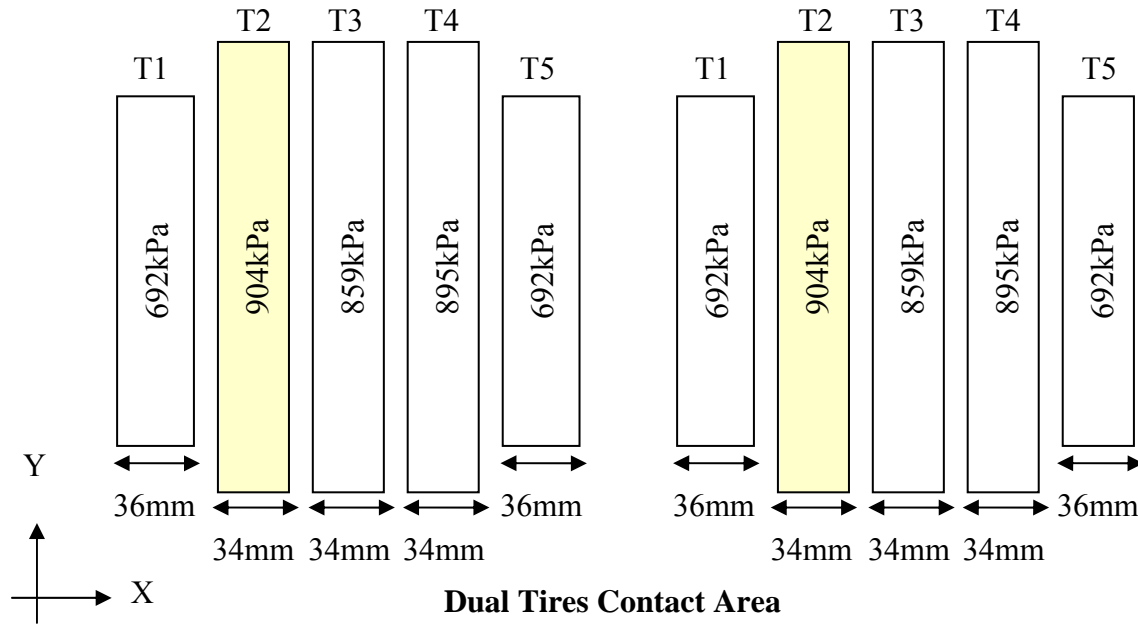


Figure 5-6. Modeled Contact Area

5.3.2. Tire Contact Pressure

Vertical contact pressures on each tire tread were measured by the manufacturer and made available to this study. Therefore, in contrast to the layered theory, which assumes that the load is applied uniformly over a circular contact area, the exact contact pressure conditions on each tire tread were incorporated in the developed FE models. The maximum vertical contact pressure assumed and measured by the manufacturer on each tire tread is shown in Figure 5-6.

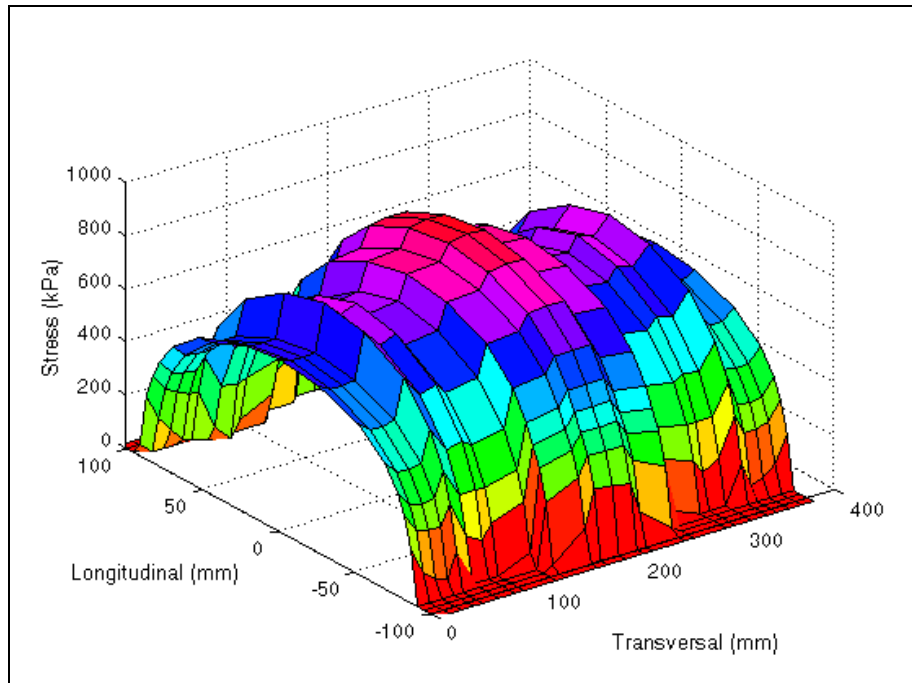
5.3.3. Movement of the Load

Four different speeds were considered in the FE analysis: 8, 24, 72, and 105km/h. With the exemption of the 105km/h, all these speeds were tested at the Virginia Smart Road. To simulate the movement of the load at the desired speed, a quasi-static approach was adopted in this study. As compared to regular dynamic methods, the major advantage of this approach is the faster converging rate and the significant reduction in computational time. It is worth noting that the main difference between quasi-static and regular dynamic methods is that the first neglects inertia effects of the load while the second considers it. Previous research by Monismith et al. (1988) has shown that for flexible pavements, this is an acceptable approximation. Based on a quasi-static approach, the amplitude and ramp loading concept was used. In this method, movement of the load was achieved by gradually shifting the loading area and amplitude over the refined loading path, shown in Figure 5-4(b) for the dual tire configuration. In total, up to 18 different increments (locations of the load) were required to achieve one full passage of

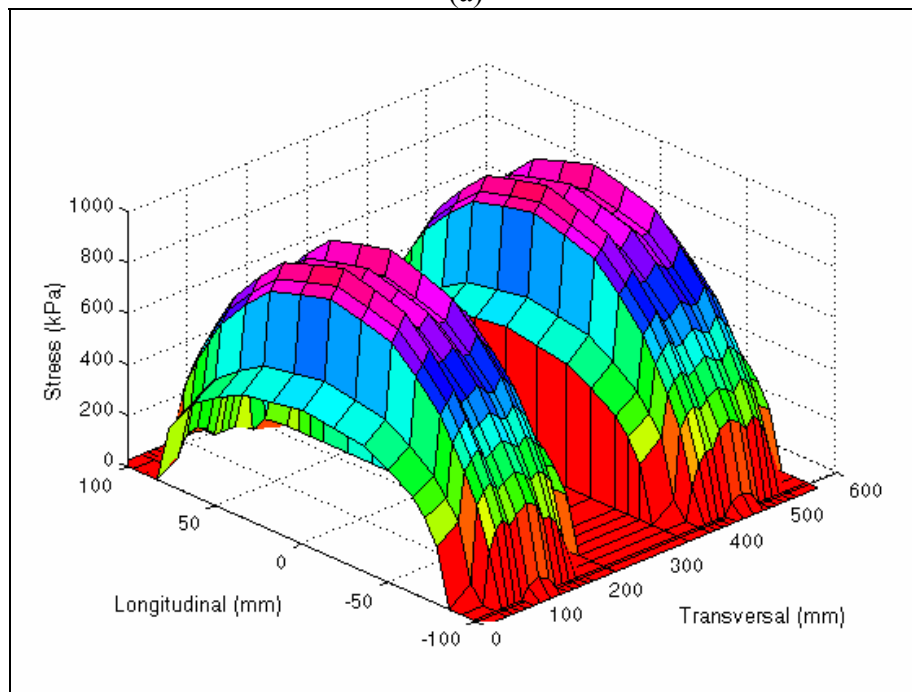
the tire over the entire model. The load was moved a 40-mm distance (2 elements) in each increment, and the loading time was adjusted to correspond to each simulated speed.

During the movement of the load, the stress transmitted to the pavement varies and is expected to be maximum at the center, and minimum at the edges. Two approaches were considered to simulate the longitudinal stress distribution underneath the tire. The first method was based on the modeled stress distributions if a two-contact body was simulated. These data were provided by the manufacturer for the different tire assemblies investigated in this study. Figures 5-7(a and b) illustrate the distribution of stress as determined by the manufacturer for the wide-base and dual tires, respectively. As shown in this figure, the stress is estimated to be relatively constant throughout the length of the tire footprint and drops sharply at the edges.

The second method considered the measured vertical stress in the field at the vicinity of the surface (depth =38.1mm) as representative of the longitudinal distribution of vertical stress. In this case, vertical stress measurements at the Virginia Smart Road at the bottom of the wearing surface for the wide-base and the dual tires were discretized into small rectangular shapes. The vertical stress was first normalized with respect to the maximum-recorded value. The normalized vertical stress was then multiplied by the average tire pressure measured on each tire tread. The maximum pressures were utilized in the maximum segments of the normalized histogram. Figures 5-8(a and b) illustrate this modeling process for the dual and wide base tires, respectively. It should be noted that the loading time was found to increase with depth and that considering the loading time at a depth of 38.1mm representative of the surface loading time may involve some approximations. The advantage of the second method over the first one was that the measured vertical stress was the resultant of the entire stress field at the surface, and represents the actual transmitted stress to the pavement. In contrast, the first method requires simulation of the lateral stresses (longitudinal and transverse) to be completely accurate, which was not considered in this study.

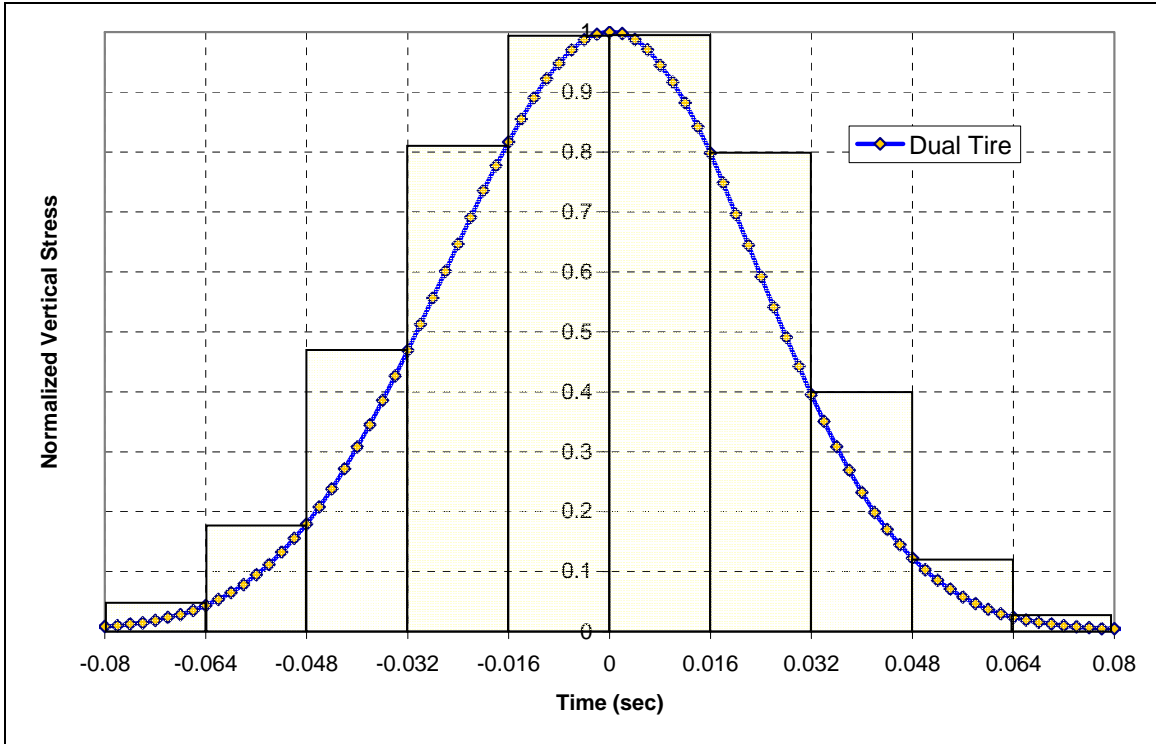


(a)

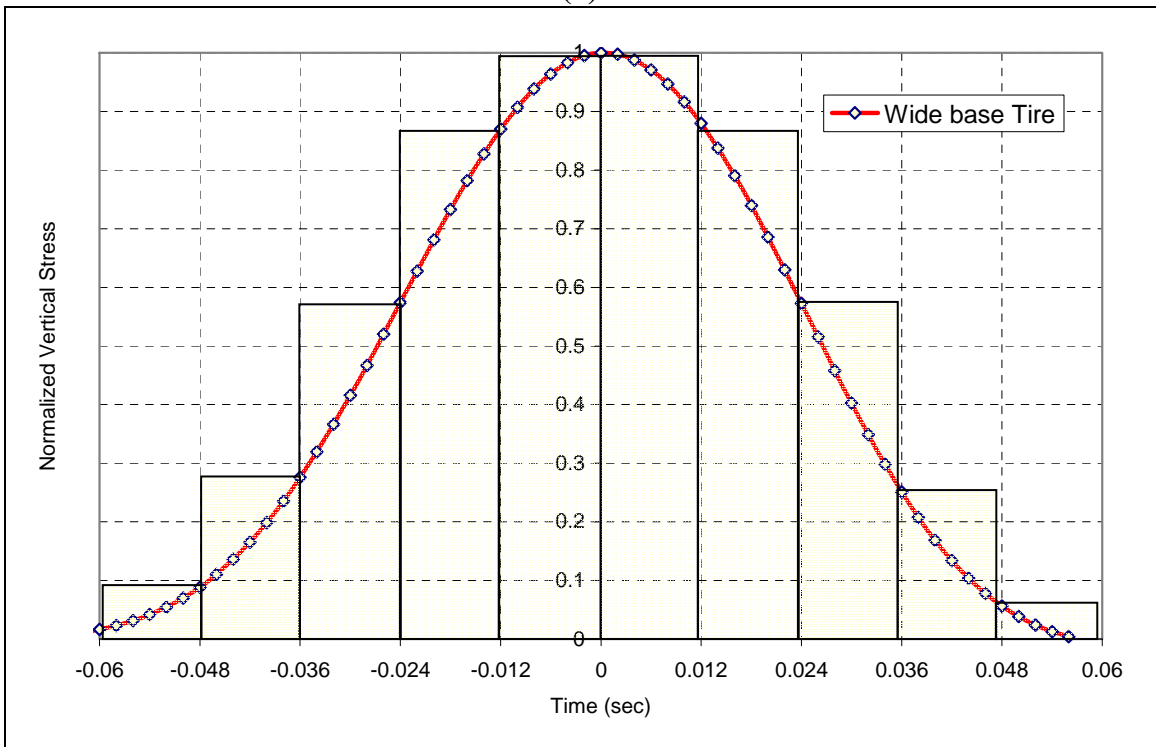


(b)

Figure 5-7. Vertical Contact Stress Distribution as Predicted from Numerical Simulation



(a)



(b)

Figure 5-8. Measured Load Amplitude Function for the Dual and Wide-Base Configurations

In general, both methods produced the same general trends in the FE analysis. However, as shown in Table 5-2, the first methodology of longitudinal stress distribution resulted in greater pavement responses to vehicular loading than the second approach, which was expected because the maximum pressure is assumed dominant in most regions of the tire footprint. The results of both methods were compared against instrument responses to vehicular loading to select the most realistic approach of modeling. Results showed that the second approach, which was based on the measured vertical stress, provides a more accurate modeling of pavement responses. Therefore, this method was adopted for the rest of the analysis.

Table 5-2. Comparison between the First and Second Method of Longitudinal Stress Distribution

Wide-Base Tire (Temperature = 5°C)				
Responses Location	ϵ_{xx}	ϵ_{yy}	ϵ_{zz}	σ_{zz}
Under W-Surface	26.18 (22.10)	41.66 (48.01)	86.40 (83.34)	707.90 (663.83)
Under Base-Mix	52.61 (36.89)	58.16 (43.03)	50.98 (36.75)	223.27 (161.20)

Dual Tires (Temperature = 5°C)				
Responses Location	ϵ_{xx}	ϵ_{yy}	ϵ_{zz}	σ_{zz}
Under W-Surface	24.53 (19.29)	36.58 (43.79)	78.50 (74.16)	640.87 (589.07)
Under Base-Mix	39.77 (27.33)	50.76 (36.18)	40.34 (28.14)	171.07 (117.67)

* Number in parentheses show calculated pavement responses based on the second approach.

5.4. BOUNDARY AND CONTACT MODELING

Elastic element foundations were used to simulate the subgrade's support of the pavement structure. These elements, which act as nonlinear springs to the ground, provide a simple way of including the stiffness effects of the subgrade without fixation of nodes at the bottom of the model. A medium level of resistance corresponding to a modulus of subgrade reaction of 175N/cm³ was assumed for the considered section. All contact between the layers was assumed to be of a friction type (Mohr-Coulomb theory), with a friction angle of 45°. This was shown to be representative of real field conditions (Al-Qadi et al. 2004).

5.5. MATERIAL CHARACTERIZATION

Different materials were used in the pavement structure of Section B. To adequately simulate pavement responses to different vehicular loadings, it was essential to characterize the properties of all relevant pavement materials. Material characterization was accomplished using field non destructive evaluation and laboratory testing. An elastic constitutive model was assumed for the granular layers and subgrade based on falling weight deflectometer (FWD) deflection measurements. Results of the backcalculation analysis are shown in Table 5-3.

Table 5-3. Backcalculated Pavement Moduli

Layer	Moduli (MPa)	Poisson's Ratio
Drainage Layer (OGDL)	1940	0.30
Cement-treated subbase (21-A)	11000	0.25
Granular subbase (21-B)	310	0.35
Subgrade	262	0.35

While an elastic constitutive behavior was assumed for granular and subgrade materials, three constitutive models were evaluated to simulate the behavior of HMA layers. The following sections describe each investigated constitutive model and the laboratory procedure adopted to define the governing parameters.

5.5.1. Elastic Constitutive Model

The resilient modulus test was used to determine the elastic properties of HMA (modulus of elasticity [E] and Poisson's ratio [ν]) at different loading times and temperatures. For HMA, the diametral indirect tensile test is considered one of the most popular and reliable means of evaluating these properties (Hugo and Schreuder 1993). This test consists of subjecting a cylindrical specimen to a compressive haversine loading in durations of 0.1sec, with rest periods of 0.9sec. With this loading pattern, a relatively uniform tensile stress may be assumed along the vertical diameter of the specimen. After a conditioning step (100 to 200 cycles), the permanent deformation is assumed to reach an asymptotic level, and all the strain is assumed recoverable. The elastic modulus is then defined as follows:

$$M_R = \frac{\sigma}{\epsilon_r} \quad (5.1)$$

where,

M_R = Modulus of resilience (elasticity);

σ = deviator stress; and

ε = recoverable strain.

Although the developed FE model assumed an elastic behavior for HMA materials (surface mix, base mix, and asphalt-treated drainage layer), temperature dependency was still considered. This was achieved by conducting the indirect modulus of resilience test at different temperatures (5, 25, and 40°C), and assuming an exponential fit for the measured values. Since the asphalt-treated drainage layer was characterized through nondestructive testing and a laboratory-measured modulus could not be determined for this layer, a similar temperature dependency as the base mix was assumed. Temperature dependency was not considered for granular materials, however. Table 5-4 illustrates the test results. It is worth noting that to define the instantaneous response of a viscoelastic material, ABAQUS still requires the definition of the elastic modulus at the temperature of interest.

Table 5-4. Laboratory-Measured and Backcalculated Moduli and Poisson’s Ratios

Mix Type	Temperature = 5°C		Temperature = 25°C		Temperature = 40°C	
	Resilient Modulus (MPa)	Poisson’s Ratio	Resilient Modulus (MPa)	Poisson’s Ratio	Resilient Modulus (MPa)	Poisson’s Ratio
SM-9.5D	9155	0.22	4230	0.33	1905	0.36
BM-25.0	8930	0.23	4750	0.30	1790	0.35
OGDL	4830	----	2415*	0.30*	965	----

* Backcalculated at a temperature of 23°C; temperature dependency is assumed similar to the BM-25.0.

5.5.2. Viscoelastic Constitutive Model Based on Creep Compliance

Characterization of the viscoelastic properties for HMA surface and base mixes was performed using the indirect creep compliance test. Experimental data were first obtained by conducting the creep compliance test at different temperatures, then shifting the data to a reference temperature—for this study, 5, 25, and 40°C—in order to establish one smooth master curve. To describe the viscoelastic behavior of a material, ABAQUS assumes that a Prony series expansion adequately describes the material response with respect to time (Generalized Kelvin model):

$$D(t) = D_0 + \sum_{i=1}^N D_i (1 - e^{-t/\tau_i}) \quad (5.2)$$

where,

$D(t)$ = creep compliance at time t ; and

D_i (Prony series coefficients) and τ_i (retardation times) = material constants

To obtain the material constants in Equation (5.2), a set of retardation times were assumed to cover the range of testing, and the fitting process was then reduced to find the coefficients of the Prony series through a linear least squares curve fit. In general, seven to 10 Prony series terms were used to obtain an accurate fit; see Figure 5-9 for illustration. The fitted creep compliance was then used to predict the relaxation modulus, $E(t)$. The interconversion process was based on the approximation developed by Park and Kim (2002). Assuming that both the creep compliance and the relaxation modulus may be described by a power law model, the relationship between the two material properties is defined as follows:

$$E(t) D(t) = \frac{\sin n\pi}{n\pi} \quad (5.3)$$

where,

n = positive constant, obtained by fitting a localized power law model ($D(t) = D_1 t^n$) to the different regions of behavior.

Similarly, a Prony series function was fitted to the relaxation modulus variation with time. Then, the bulk [$K(t)$] and shear [$G(t)$] moduli variation with time were estimated using the following relations assuming that Poisson's ratio (ν) does not change with time:

$$K(t) = \frac{E(t)}{3(1 - 2\nu)} \quad (5.4)$$

$$G(t) = \frac{E(t)}{2(1 + \nu)} \quad (5.5)$$

Table 5-5 illustrates the fitting parameters for the surface and base mixes at a temperature of 25°C. Based on this process, characterization of the viscoelastic properties of HMA was completed at three temperatures (5, 25, and 40°C), and all required parameters for this constitutive model were defined.

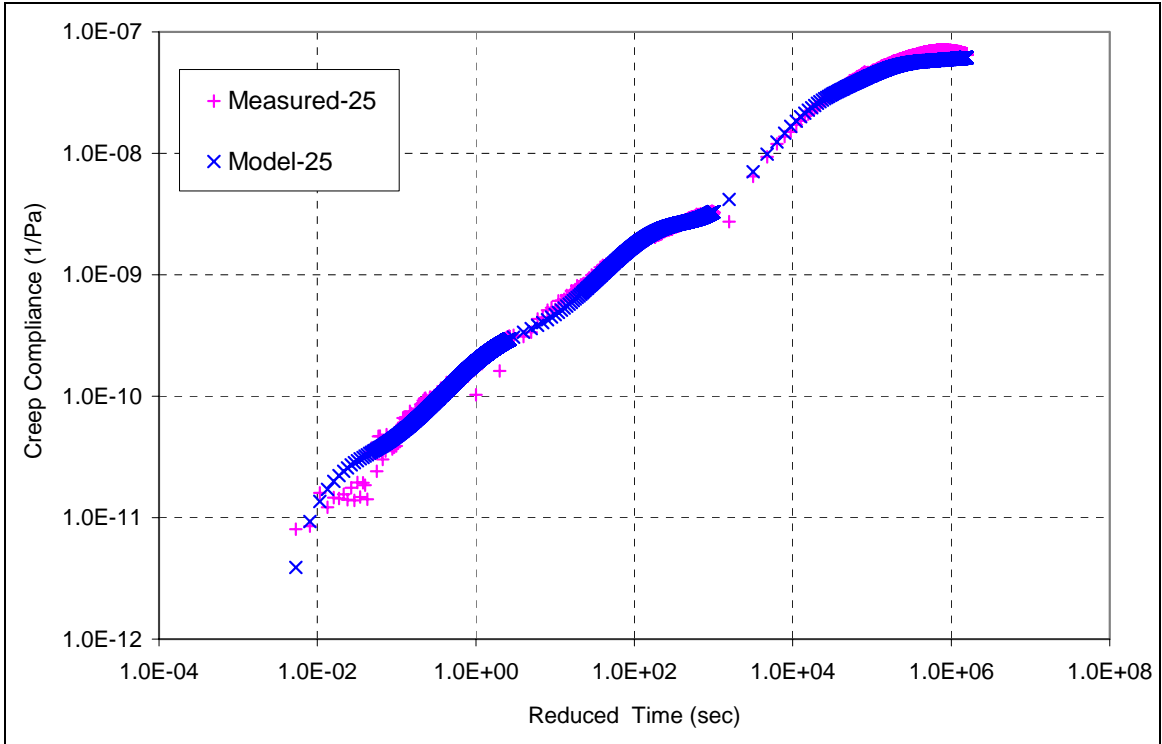


Figure 5-9. Prony Series Fitting of the Creep Compliance at a Temperature of 25°C

Table 5-5. Fitting Parameters for the Viscoelastic Model

(a) Surface Mixture

		T (°C)	N	D _i	Values	τ _i	Values
Surface Mixture (SM-9.5D)	25		10	D ₀	-1.18E-11	----	
				D ₁	3.46E-11	τ ₁	1.0E-02
				D ₂	5.74E-13	τ ₂	1.0E-01
				D ₃	2.28E-10	τ ₃	1.0E+00
				D ₄	-1.6E-11	τ ₄	1.0E+01
				D ₅	2.42E-09	τ ₅	1.0E+02
				D ₆	-2.9E-09	τ ₆	1.0E+03
				D ₇	2.26E-08	τ ₇	1.0E+04
				D ₈	3.37E-08	τ ₈	1.0E+05
				D ₉	7.24E-08	τ ₉	1.0E+06
				D ₁₀	-3.4E-07	τ ₁₀	1.0E+07

(b) Base Mixture

Base Mixture (BM-25.0)	T (°C)	N	D _i	Values	τ _i	Values
	25	25	8	D ₀	3.91E-11	----
			D ₁	-1.27E-11	τ ₁	1.0E-02
			D ₂	1.36E-10	τ ₂	1.0E-01
			D ₃	1.62E-10	τ ₃	1.0E+00
			D ₄	1.12E-09	τ ₄	1.0E+01
			D ₅	1.69E-09	τ ₅	1.0E+02
			D ₆	9.60E-09	τ ₆	1.0E+03
			D ₇	1.13E-08	τ ₇	1.0E+04
			D ₈	-1.27E-09	τ ₈	1.0E+05

5.5.3. Viscoelastic Model Based on the Variable Creep Loading Test: The Time Hardening Model

A time hardening model was considered in the analysis to simulate the viscoelastic behavior of HMA layers under variable loads (Kraus 1980):

$$\dot{\epsilon}^c = A\sigma^n t^m \quad (5.6)$$

where,

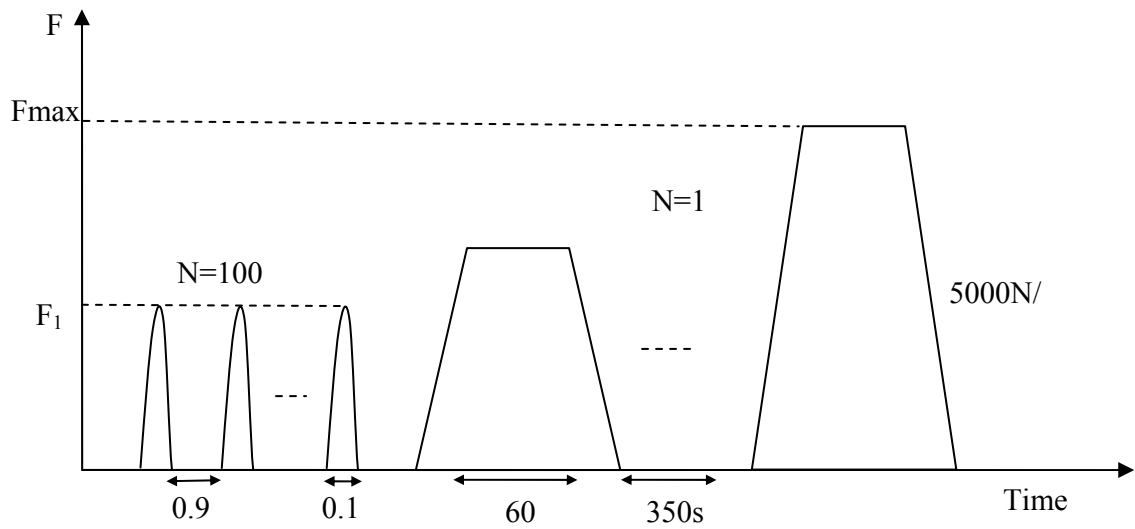
$\dot{\epsilon}^c$ = creep strain;

σ = constant stress;

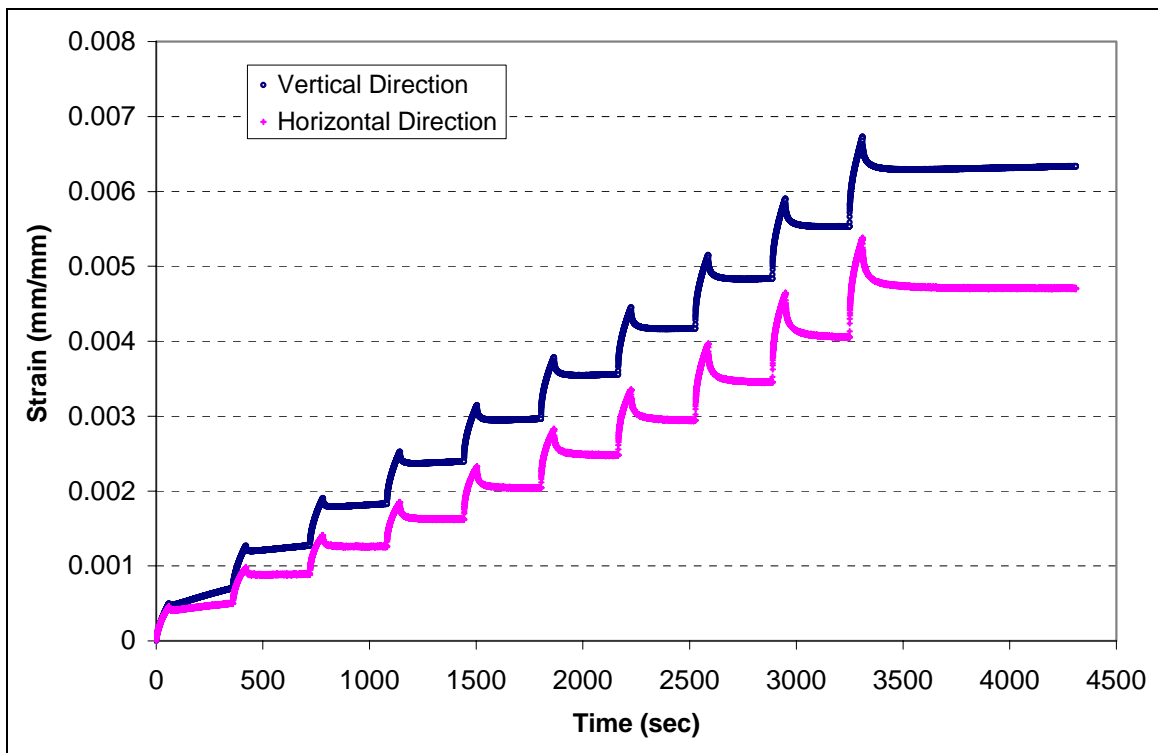
t = time; and

A, m, n = fitting parameters function of the temperature.

To determine the fitting parameters of Equation (5.6), a newly-developed laboratory variable creep load test was conducted at three temperatures (20, 30, and 40°C). This test consisted of applying 10 different load levels to the specimen while holding each load for a period of 60sec, see Figure 5-10(a). The main reason for inducing different stress levels on the material is to simulate variable strain rate levels in HMA to model its viscous behavior. A recovery rest period of 350sec was set between each load level to allow the material to recover some of the viscous deformation as shown in Figure 5-10(b). Table 5.6 illustrates the fitting parameters as well as the goodness of fit for the surface and base mixture at the three tested temperatures.



(a)



(b)

Figure 5-10. (a) Schematic of the Suggested Test Setup and (b) Strain Accumulations with Time for the Base Mix at 20°C in a True Time Scale

Table 5-6. Fitting Parameters for the Time Hardening Model

Mixture	Temperature (°C)	TIME HARDENING PARAMETERS			RMSE	R ²
		A	m	n		
Surface Mix	20	3.2700E-04	1.1293	-0.4187	2.36E-06	0.98
Surface Mix	30	2.2400E-03	0.5563	-0.5976	5.16E-05	0.96
Surface Mix	40	2.4800E-03	0.6962	-0.6134	4.38E-05	0.95
Base Mix	20	1.9500E-03	0.5000	-0.5829	7.59E-05	0.88
Base Mix	30	7.4500E-04	0.7650	-0.4289	4.80E-06	0.98
Base Mix	40	5.2200E-04	0.5000	-0.4000	2.72E-05	0.79

5.5.4. Comparison of the Three Constitutive Models

Comparison of the three constitutive models to simulate HMA behavior indicated the superior performance of the viscoelastic models in simulating pavement responses to vehicular loading. These models provided several advantages compared to the elastic model. First, the developed viscoelastic models successfully simulated the time retardation of the response as well as the asymmetry of the signal, as shown in Figure 5-11. In addition, the fast relaxation of the material in the longitudinal direction was manifested in the calculated pavement responses; see Figure 5-11.

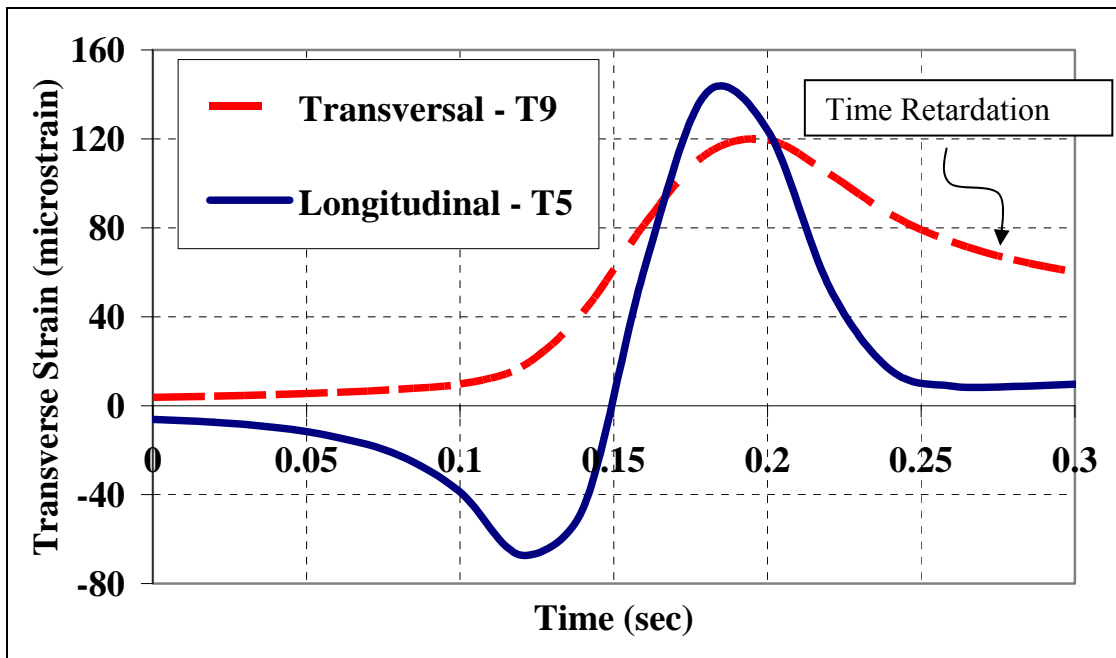


Figure 5-11. Calculated Pavement Strains in (a) the Transverse and (b) Longitudinal Direction at the Bottom of the Wearing Surface for the Dual Tires Assembly

Another advantage was that the viscoelastic models also predicted the permanent deformation (rutting) at the pavement surface before and after load application (Figure 5-12). The rapid recovery of most HMA strains is indicative of the viscoelastic behavior of the material. This could have detrimental effects when successive axles are applied due to the lack of recovery time. This capability allowed calculating primary rutting for a single load application without the need to use a transfer function. These transfer functions are commonly used to relate pavement responses to pavement performance. Two additional load increments were added to this analysis to allow the material to recover some of the exhibited viscous deformations.

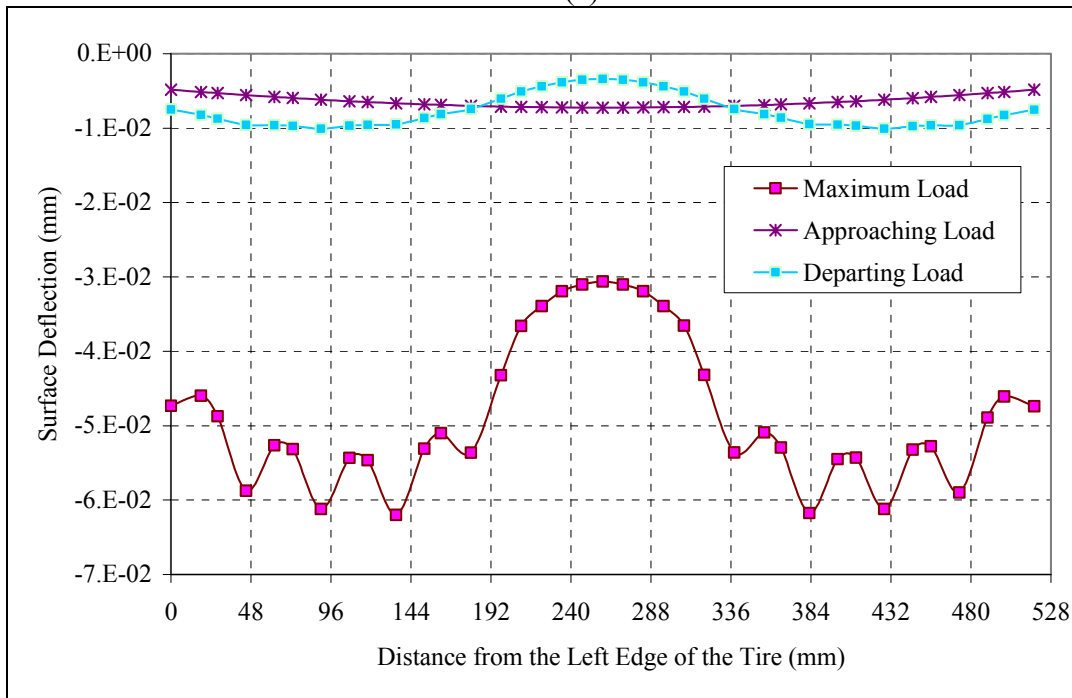
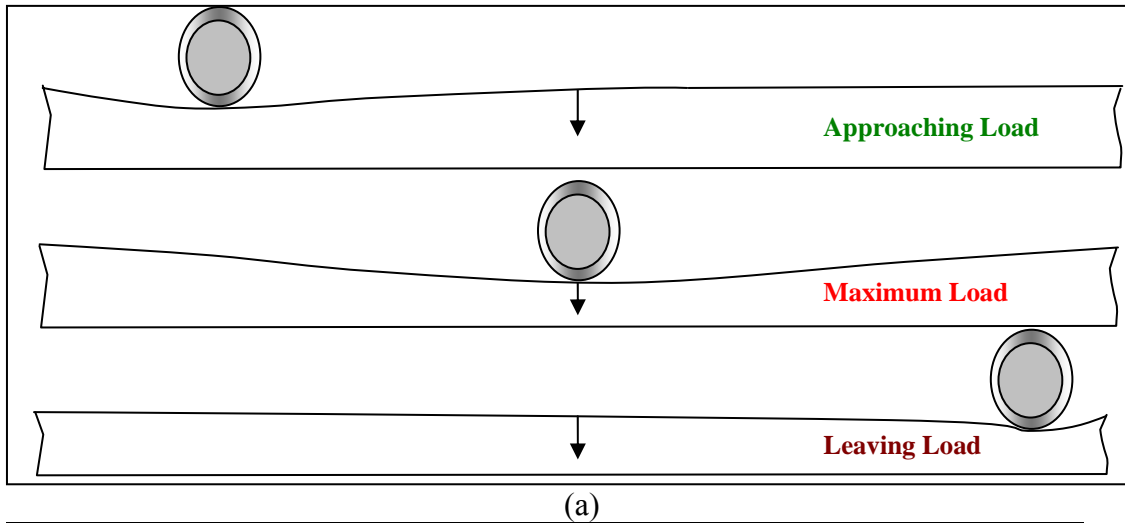
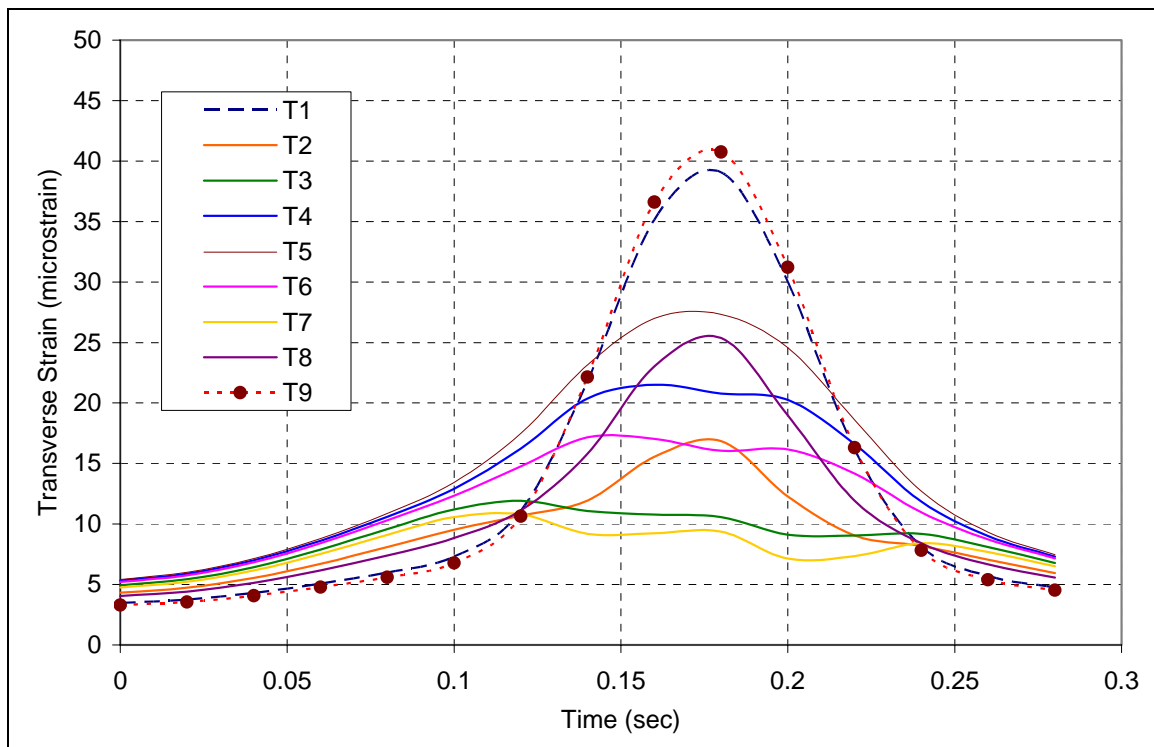


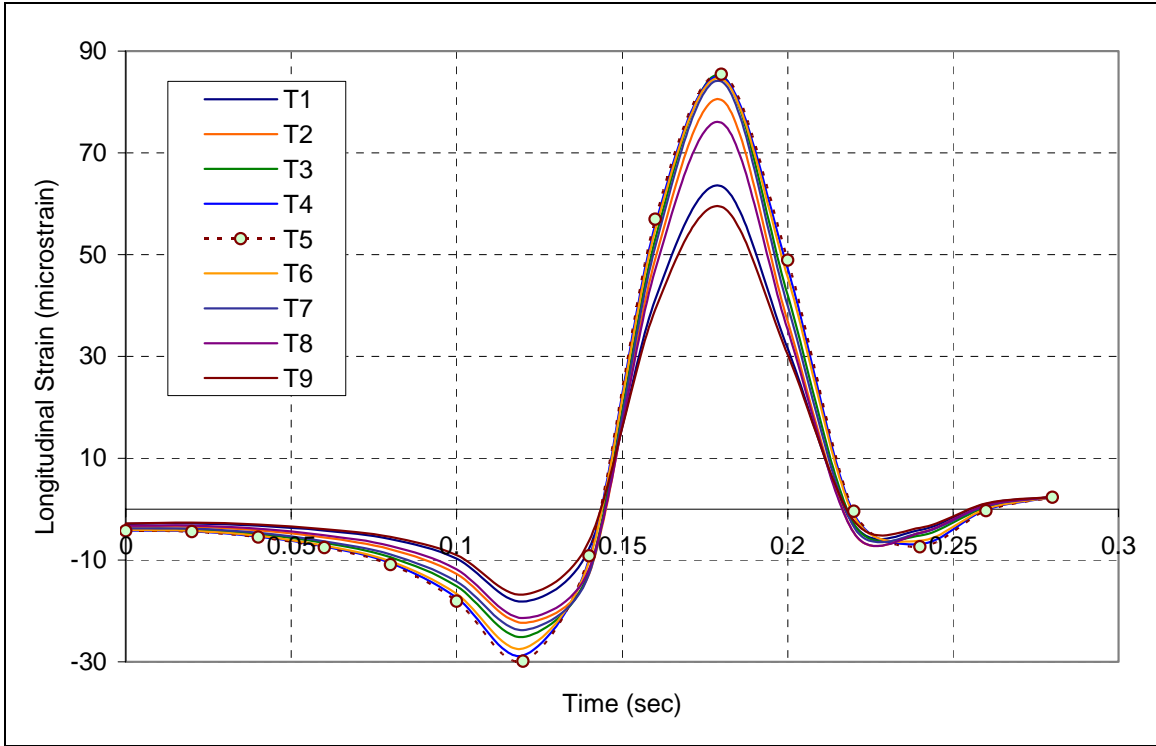
Figure 5-12. (a) Illustration of the Primary Rutting Calculation Concept and (b) Pavement Surface Profile before and after Load Application

5.6. MODEL RESPONSE

Figures 5-13(a and b) present the calculated transverse and longitudinal strains at the bottom of the wearing surface (depth = 38.1mm) based on the elastic FE model for the wide-base tire at a temperature of 25°C. Several observations may be drawn from these figures. First, the shape of the calculated strains and stresses are similar to the measured ones. Second, the longitudinal strain is greater than the transverse strain, which is in agreement with field observations for the considered axles. Since a non-uniform contact pressure distribution was simulated, pavement response to the different treads is different. For the wide-base tire, the maximum transverse strain occurs at the edges of the tire (Tread 9), while the maximum longitudinal strain occurs at the middle of the tire (Tread 5). This is in agreement with the literature. The elastic model could not simulate permanent deformation or delayed recovery, a known characteristic of HMA materials. This is in disagreement with field measurements, and supports the use of a viscoelastic model to simulate pavement responses at intermediate and high temperatures. Figure 5-14 illustrates the calculated vertical stress at the bottom of the BM-25.0 layer; this figure illustrates the advantages of adopting a three-dimensional modeling strategy. This allows the determination of 3D stress distribution in the longitudinal and transverse directions and under the different treads, which can not be estimated in plane strain and axisymmetric simulation techniques.



(a)



(b)

Figure 5-13. (a) Transverse and (b) Longitudinal strain at the Bottom of the Wearing Surface (Wide-Base – Elastic at 25°C)

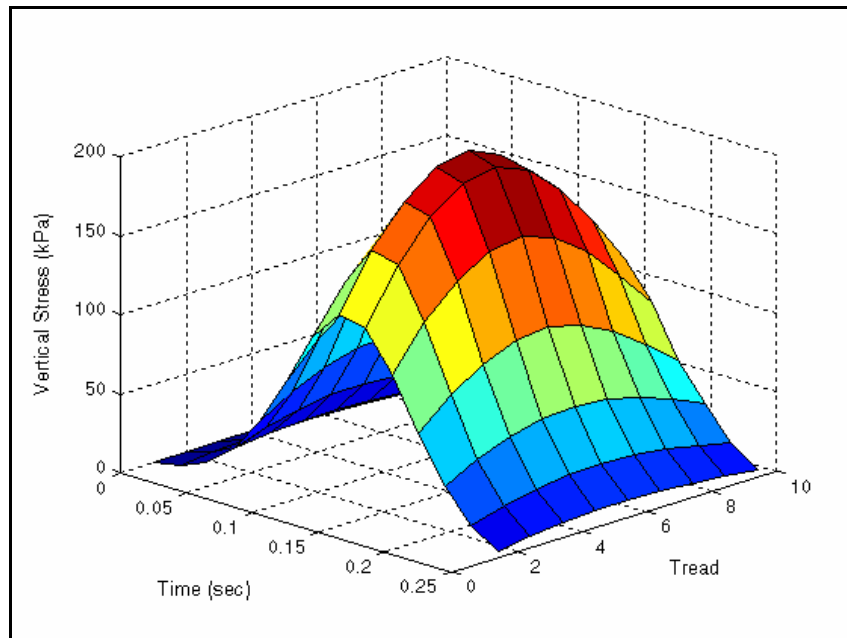
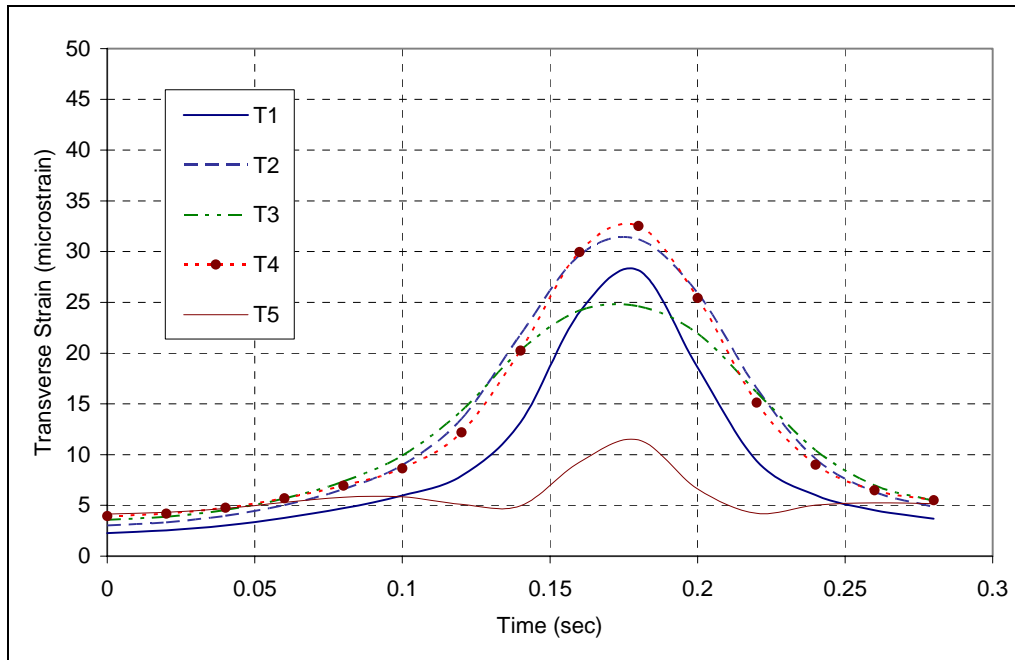
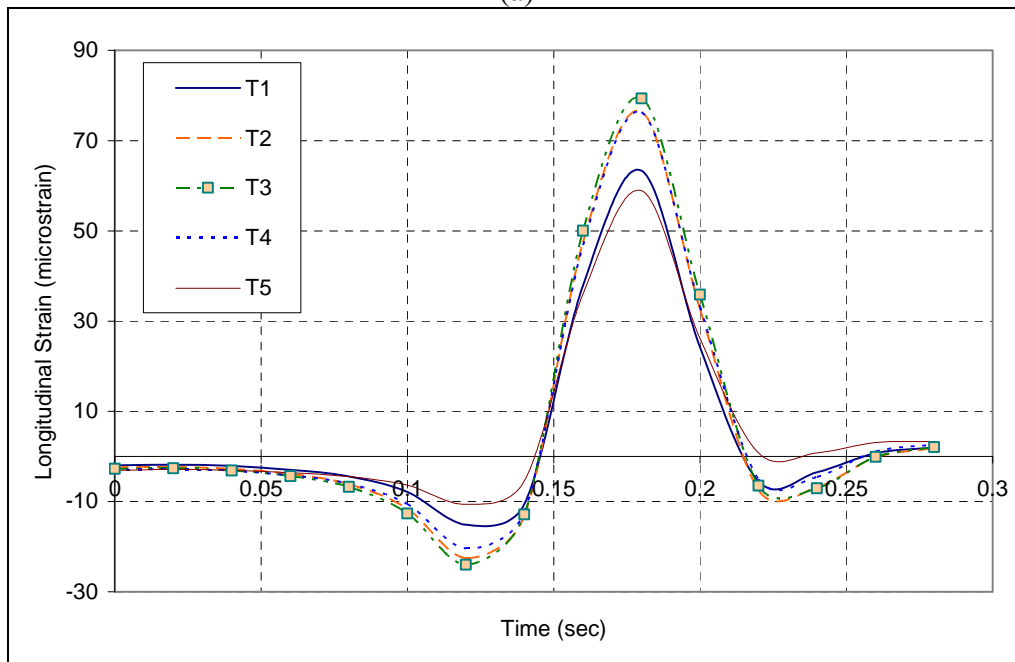


Figure 5-14. Vertical Stress Distribution under the BM-25.0 (Elastic 25°C – Wide-Base)

Similarly, Figures 5-15 (a and b) and 5-16 present the calculated transverse and longitudinal strains at the bottom of the wearing surface (depth = 38.1mm) and vertical stress at the bottom of the BM-25.0 (depth = 188.1mm) for the dual tires. For this tire configuration, the maximum transverse strain occurs close to the inside edge of the tire (Tread 4), while the maximum longitudinal strain occurs at the middle of the tire (Tread 3).



(a)



(b)

Figure 5-15. Transverse and Longitudinal Strains at the Bottom of the Wearing Surface (Dual Tires – Elastic at 25°C)

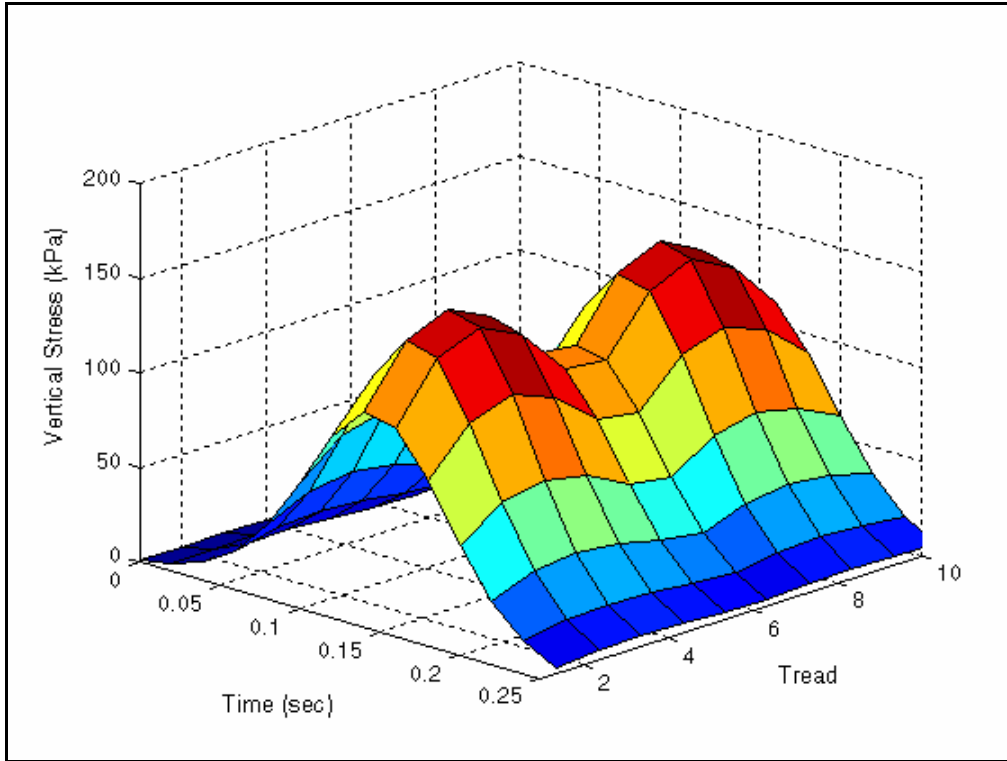


Figure 5-16. Vertical Stress Distribution under the BM-25.0 (Elastic 25°C – Dual Tires)

5.7. MODEL VALIDATION

Based on all measurements obtained during the truck testing program, various sets of instrument responses were selected to calibrate and validate the developed FE models. This step was essential for accurately calibrating the various parameters in the simulation process to arrive at the best realistic conditions. Although an effort was made to approach real pavement conditions in the developed models based on the available laboratory results and modeling limitations, some approximations were inevitable. These same assumptions were used to develop the models for the second generation of wide-base tire (455/55R22.5) although no experimental data from the Virginia Smart Road were available for this tire configuration.

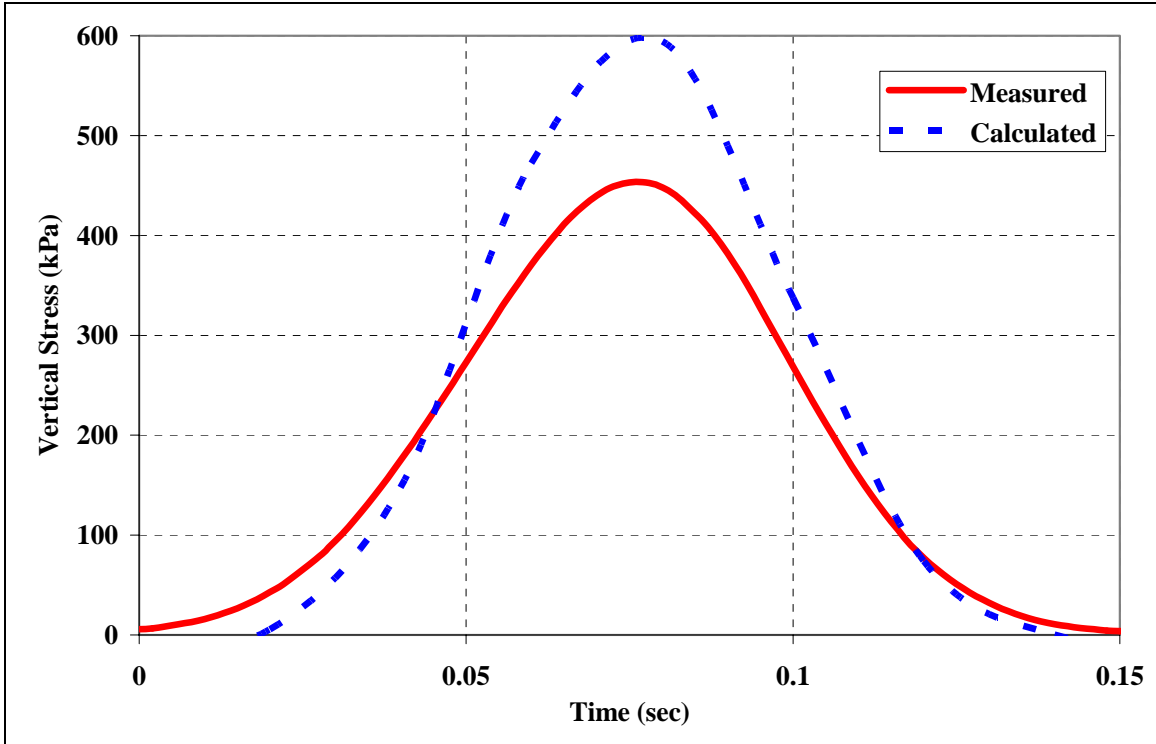
A critical factor in strain and stress analysis is the temperature at the time of testing. Previous research at Virginia Tech showed that the measured horizontal strain increased approximately 117 times from 0°C to 40°C when driving at a speed of 72km/h, and it increased approximately 35 times when driving at 8km/h (Loulizi et al. 2004). To establish a similar line of comparison, experimental results had to be shifted to a temperature of 25°C, one of the temperatures used in the theoretical models. The methodology used for shifting of the experimental results was previously explained in Chapter 4: Experimental program at the Virginia Smart Road. It is worth noting that based on previous research at Virginia Tech, a better agreement would be expected at low temperatures, and greater deviation would be anticipated at high temperatures (Al-Qadi et

al. 2004). To improve the model prediction at high temperatures, anisotropic characteristics of HMA need to be considered, which was outside the scope of this study.

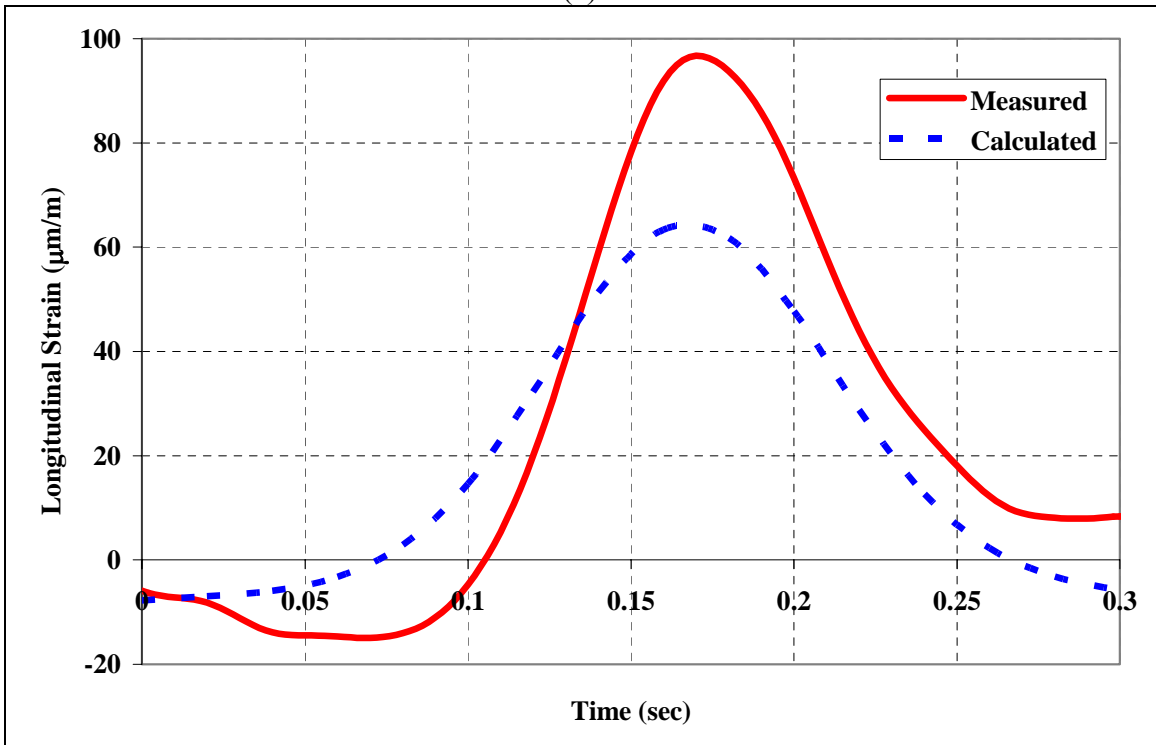
5.7.1. Elastic Model

The elastic model characterized HMA constitutive behavior using the resilient modulus results. Figures 5-17 (a and b) compare the measured vertical stress at the bottom of the wearing surface to the calculated one, and the measured longitudinal strain at the bottom of the BM-25.0 to the calculated one, respectively. As shown in these figures, the elastic FE model poorly predicts pavement responses at the reference temperature of 25°C. In this case, the error in the model prediction was 30% for the vertical stress and 36% for the longitudinal strain. This error was judged too high for predicting pavement damage due to different axle configurations. Another disadvantage of the elastic FE model is that the predicted pavement response was independent of the vehicle speed. Results from the experimental program at the Virginia Smart Road suggested that the measured maximum vertical compressive stress was independent of the vehicle speed but that the pulse width of the vertical stress increases with a decrease in speed. In contrast, it was found that the vehicle speed does affect the measured strain: as speed decreases, the measured strain significantly increases (Al-Qadi et al. 2004). Based on these observations, it was decided that the results of the elastic FE model would not be suitable to compare pavement damage caused by different tire assemblies.

An interesting observation, however, is that all developed models successfully predicted that the longitudinal strain is greater and therefore more critical than the transverse one, which is in agreement with field measurements for the considered axle configurations. In addition, the locations of the tensile and compressive fields are in agreement with field condition, which validates the contact conditions assumed in the FE models.



(a)

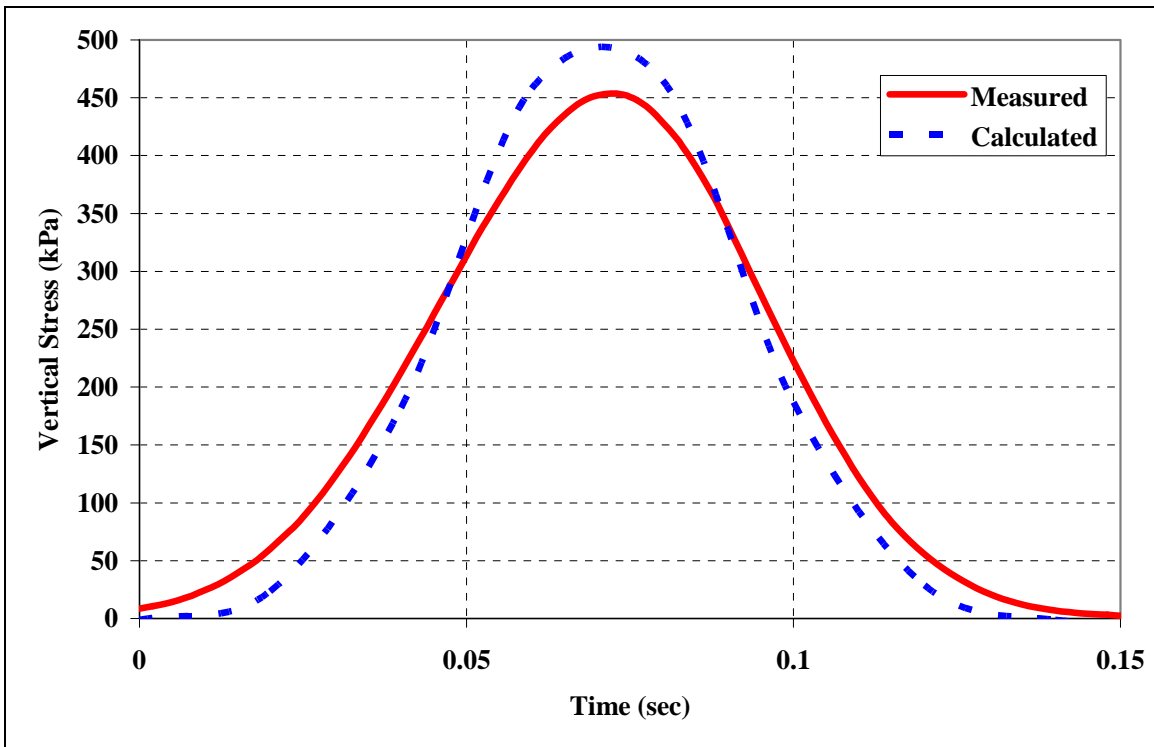


(b)

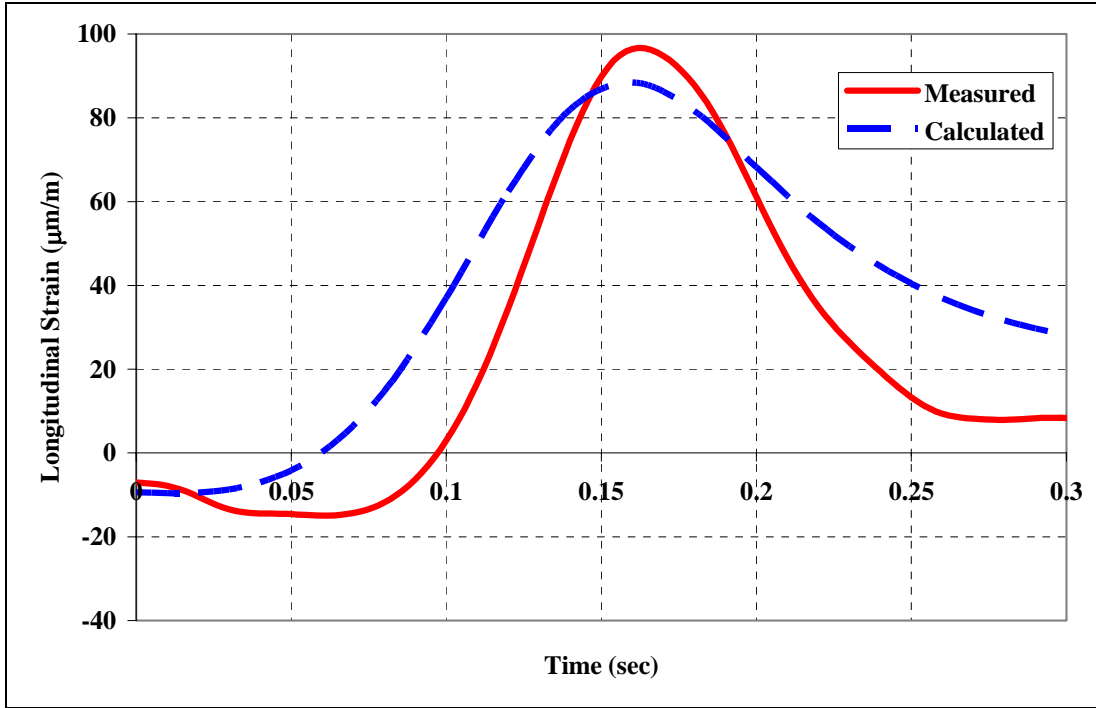
Figure 5-17. Comparison between Measured and Calculated (a) Vertical Stress at the bottom of the Wearing Surface (Condition 2) and (b) Longitudinal Strain at the bottom of the BM-25.0 (Condition 12)

5.7.2. Time Hardening Model

Figures 5-18 (a and b) compare the measured and calculated vertical stress at the bottom of the wearing surface, and the measured and calculated longitudinal strains at the bottom of the BM-25.0 at a speed of 8km/h. Assuming that the measured response is accurate, the model predicted the vertical stress and the longitudinal strain at an error of less than 5%. This is an acceptable level of accuracy. It appears that the time hardening FE model provides an acceptable prediction of pavement responses to vehicular loading. At greater speeds, however, the time hardening model was less accurate. This approach is only applicable when the stress state remains essentially constant or is slowly changing. Figure 5-19 compares the measured and calculated longitudinal strains at the bottom of the wearing surface at a speed of 24.1km/h. In this case, the error in the model prediction was 30%, which was significantly greater than the aforementioned error at 8km/h.



(a)



(b)

Figure 5-18. Comparison between Measured and Calculated (a) Vertical Stress at the bottom of the Wearing Surface (Condition 2) and (b) Longitudinal Strain at the bottom of the BM-25.0 (Condition 12)

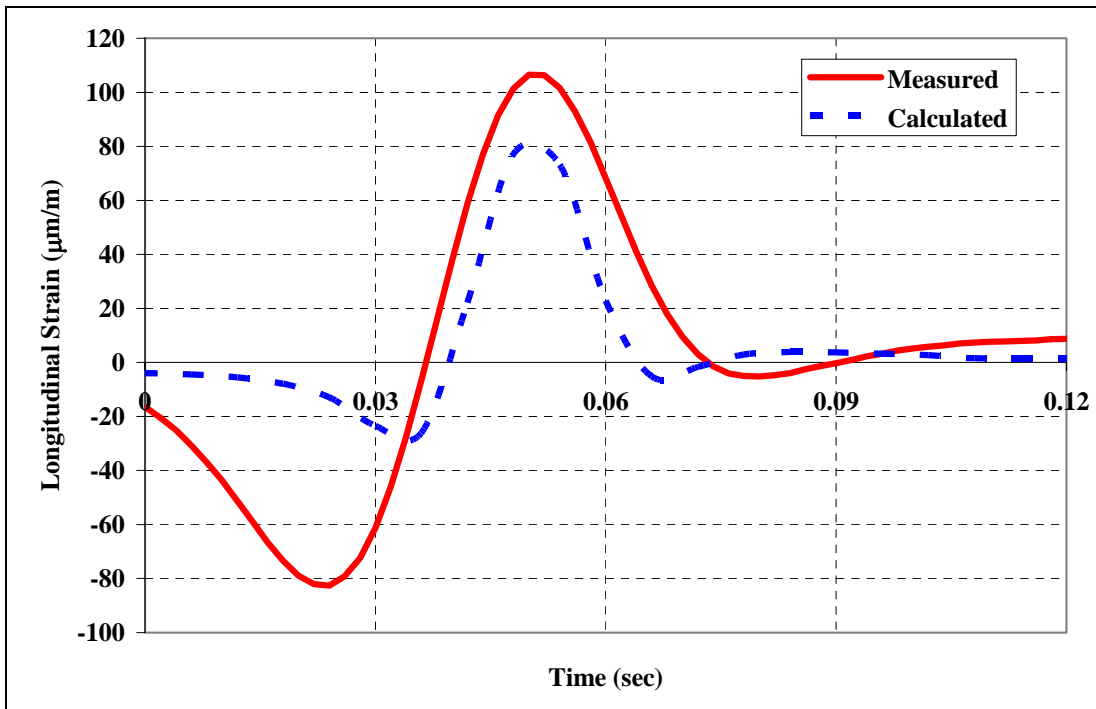
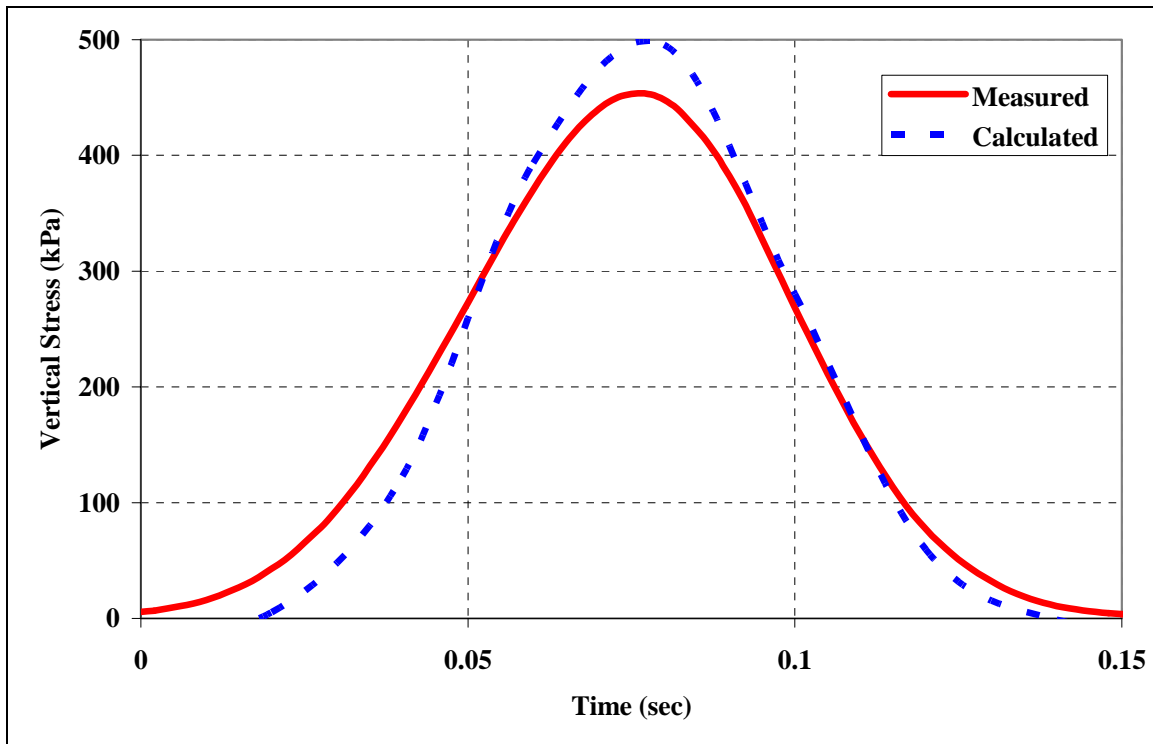


Figure 5-19. Comparison between Measured and Calculated Longitudinal Strain at the bottom of the Wearing Surface (Condition 13) at a Reference Temperature of 25°C

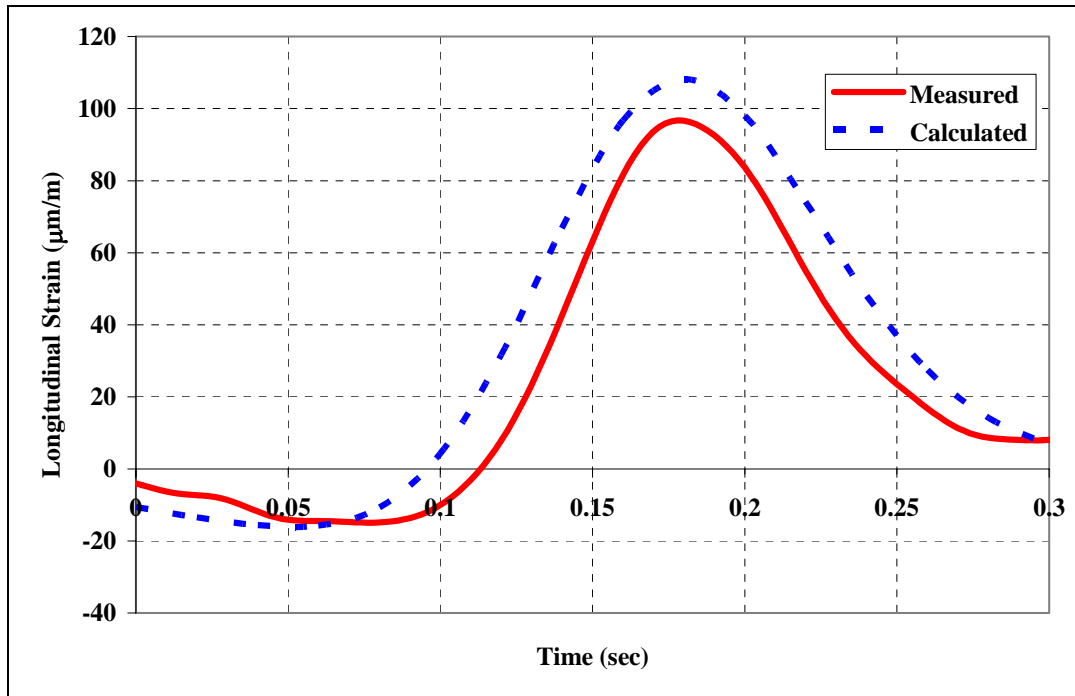
For all tested speeds, the average prediction error of the time hardening FE model was 28% for the vertical stress and 20% for the horizontal strain. Under a slow moving load (i.e., Conditions 2 and 12, which were conducted at a speed of 8km/h), however, the model accuracy was acceptable with an average error of less than 10%. It appears also from Figure 5-18(b) that rate of recovery of the BM-25.0 is more rapid than the predicted one. In summary, although the time hardening approach provides an acceptable prediction of pavement response to loading at low speeds, it may not be appropriate to compare the aggressiveness of the different tires.

5.7.3. The Generalized Kelvin Viscoelastic Model

The generalized Kelvin viscoelastic model was used to calculate HMA response to loading. Figures 5-20 (a and b) compare the measured and calculated vertical stresses at the bottom of the wearing surface, and the measured and calculated longitudinal strain at the bottoms of the BM-25.0 at a speed of 8km/h. Under slow moving loads, the predicted maximum pavement responses did not change significantly from the time hardening model. However, the generalized Kelvin FE model successfully predicted the rate of recovery exhibited in the field; see Figure 5-20(b).



(a)

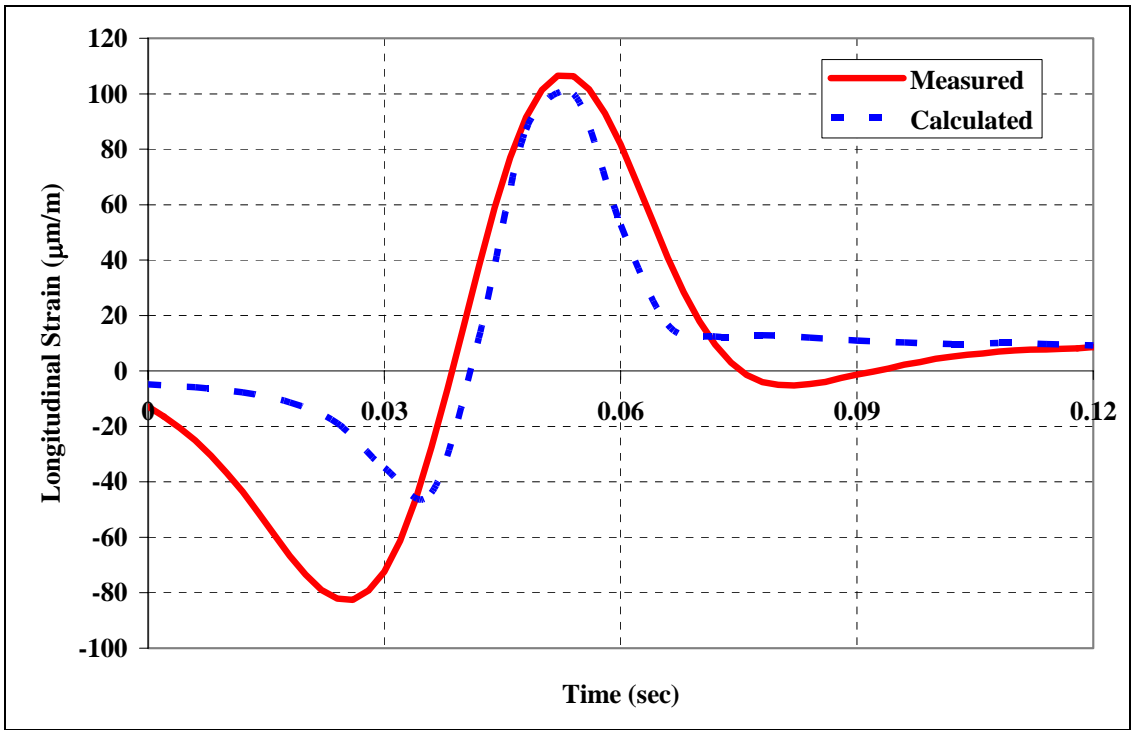


(b)

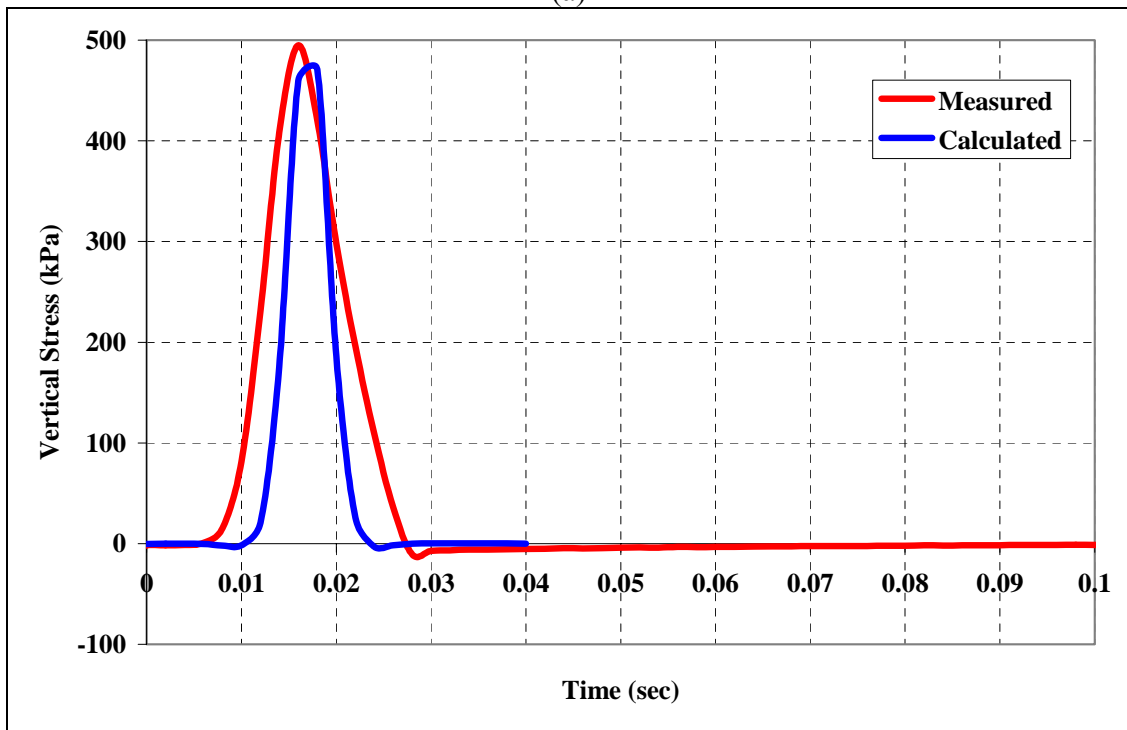
Figure 5-20. Comparison between Measured and Calculated (a) Vertical Stress at the bottom of the Wearing Surface (Condition 2) and (b) Longitudinal Strain at the bottom of the BM-25.0 (Condition 12)

At greater speeds, the results of the generalized Kelvin FE model were in better agreement with the measurements than the time hardening FE model. Figures 5-21 (a and b) compare the measured longitudinal strain at the bottom of the wearing surface to the calculated one at a speed of 24.1km/h, and the measured vertical stress at the bottom of the wearing surface to the calculated one at a speed of 72.4km/h, respectively. As shown in these figures, results of the generalized Kelvin FE model were in better agreement with field measurements than the elastic and the time hardening FE models. For these particular cases, the error in the model prediction was only 6 and 4% for the vertical stress and longitudinal strain, respectively. The rate of recovery was also well-predicted and a small permanent strain was manifested in the experimental and calculated responses; see Figure 5-21(a). For all the considered measurements, the model accuracy was acceptable, with an average error of 11% in predicting vertical stress, and 15% in predicting the horizontal strain. Hence, based upon this comparison, it appears that the generalized Kelvin FE model provides an acceptable prediction of pavement responses to vehicular loading.

In summary, results of the elastic and the time hardening FE models were not used in evaluating pavement damage due to the different tire assemblies. In general, the elastic FE model was found to underestimate the damage ratios between the new generation of wide-base tire and the conventional dual-tire assembly, while the time hardening model overestimated these ratios. Supported by the aforementioned findings, the main pavement damage analysis model in this study was derived based on the results of the generalized Kelvin viscoelastic model.



(a)



(b)

Figure 5-21. Comparison between Measured and Calculated (a) Longitudinal Strain at a Speed of 24km/h (Condition 13) and (b) Vertical Stress at a Speed of 72km/h (Condition 1) at the bottom of the Wearing Surface

6. RESULTS AND ANALYSIS

Pavement failure may occur as a result of the environment, repeated traffic loading, deficient construction, and/or poor maintenance strategies. Load-associated pavement distresses are the main focus of this study. Four failure mechanisms were considered in this research project, covering the most serious load-associated pavement distresses (other factors may also contribute to the acceleration of the deterioration): fatigue cracking, HMA rutting (primary rutting), subgrade rutting (secondary rutting), and surface initiated top-down cracking.

As previously mentioned, the main pavement damage analysis model in this study was derived based on the results of the generalized Kelvin viscoelastic model. This model allowed predicting permanent deformation (rutting) at the pavement surface before and after load applications. This provides an indication of the aggressiveness of tire loading with respect to primary rutting for a single load application. Moreover, this FE model successfully simulated the time retardation of the response as well as the asymmetry of the signal in the transverse direction and the quick relaxation of the material in the longitudinal direction. The following sections briefly describe the failure mechanism associated with each considered pavement distress and the adopted transfer functions to quantify and predict pavement damage.

6.1. FAILURE MECHANISMS

6.1.1. Fatigue Cracking

Fatigue cracking is caused by repeated axle load applications, usually lower than the strength of the material. It is a progressive localized damage due to fluctuating stresses and strains in the material and a build-up of irrecoverable strains (Hsu et al. 1996). Fatigue cracking usually starts at the bottom of the HMA layers, which represents the location of the greatest tensile strain in case of fully-bonded conditions between the different HMA layers. Fatigue cracking may also start at the bottom of the individual HMA layers if unbonded or friction conditions exist. To quantify load-associated fatigue pavement damage due to different axle configurations, a fatigue law suggested by Finn et al. (1986) was adopted in this study to predict the number of load repetitions to cause 45% fatigue cracking in the wheelpath:

$$\log N_f(45\%) = 16.086 - 3.291 \log \frac{\varepsilon_t}{10^{-6}} - 0.854 \log \frac{E_1}{10^3} \quad (6.1)$$

where,

N_f = Number of repetitions for fatigue cracking;

ε_t = tensile strain at the bottom of the HMA layers in microstrain; and

E_1 is the resilient modulus of HMA in psi.

Equation (6.1) is similar to the Asphalt Institute failure criterion presented in a logarithmic form. Since pavement fatigue damage is a bottom-up failure mechanism, the crack propagates through the entire HMA layers before appearing at the surface. Therefore, the criticality of this distress is more pronounced in flexible pavements surfaced with a thin to medium-thickness HMA layer (less than 100mm). In addition, this cracking pattern does not usually appear in high priority routes since a functional overlay is regularly applied to preserve the rideability of the pavement at high operating speeds.

6.1.2. Subgrade (Secondary) Rutting

Subgrade rutting is a longitudinal wheelpath depression that occurs when the subgrade exhibits permanent deformation or lateral migration due to loading. In this case, the pavement settles into the subgrade ruts, causing surface depressions in the wheelpath. The allowable number of repetitions to control secondary rutting can be determined from the following equation (Huang 1993):

$$N_s = 1.077 \times 10^{-8} (\epsilon_c)^{-4.483} \quad (6.2)$$

where,

N_s = number of repetitions for subgrade rutting failure (rut depth = 12.5mm); and

ϵ_c = compressive strain on top of the subgrade.

6.1.3. HMA (Primary) Rutting

Primary rutting is a longitudinal depression in the wheelpath caused by permanent deformation of the HMA in hot weather or under slow-moving loads. The viscoelastic models, presented earlier, were capable of predicting the residual permanent deformation after load application, which may provide an indication of the rutting damage after one load application. In addition, the following transfer function was used to determine the number of cycles to cause rutting failure (AASHTO 2002):

$$\log\left(\frac{\epsilon_p}{\epsilon_r}\right) = -3.74938 + 0.4262 \log(N_r) + 2.02755 \log(T) \quad (6.3)$$

where,

ϵ_p = permanent strain at the surface fixed at 15mm;

ϵ_r = recoverable strain;

N_r = number of repetitions corresponding to ϵ_p ; and

T = pavement temperature (°C).

Equation (6.3) may be re-written as follows (Prophète 2003):

$$N_r = \left(\frac{15}{h \varepsilon_{vr} 10^x} \right)^{1.74} \quad (6.4)$$

where,

$$x = -3.74938 + 2.02755 \log(T) \quad (6.5)$$

h = HMA thickness (mm).

6.1.4. Surface Initiated Top-Down Cracking

Surface-initiated top-down cracking has recently been recognized as a major failure mode that appears just outside the wheel path. This cracking gradually progresses to form parallel cracks within 0.3 to 1m from the original crack (Svasdisant et al. 2002; Kumara et al. 2002). Researchers debate the real cause of top-down cracking. However, it appears that the high tensile strains induced by tires at the top of the pavement layer are the most recognized factor that contributes to this failure mechanism. It has also been reported that the pavement structure has little effect on the reduction of the tensile stresses around the tire and that the major influencing factor is the distribution of the contact stresses around the tire (Meyers et al. 2000). Based on this fact, analysis of the surface tensile strain developing around the tire was considered and used to measure the aggressiveness of the tire in terms of top-down cracking.

To date, a transfer function does not exist to determine the number of cycles to failure through top-down cracking. In this study, considering that top-down cracking could be dealt with as a special type of fatigue cracking, the fourth power law was assumed valid to relate the damage between the wide-base and dual configurations to the surface tensile strain as follows:

$$DR_{TD} = \frac{2}{4} \left(\frac{\varepsilon_w}{\varepsilon_d} \right)^4 \quad (6.6)$$

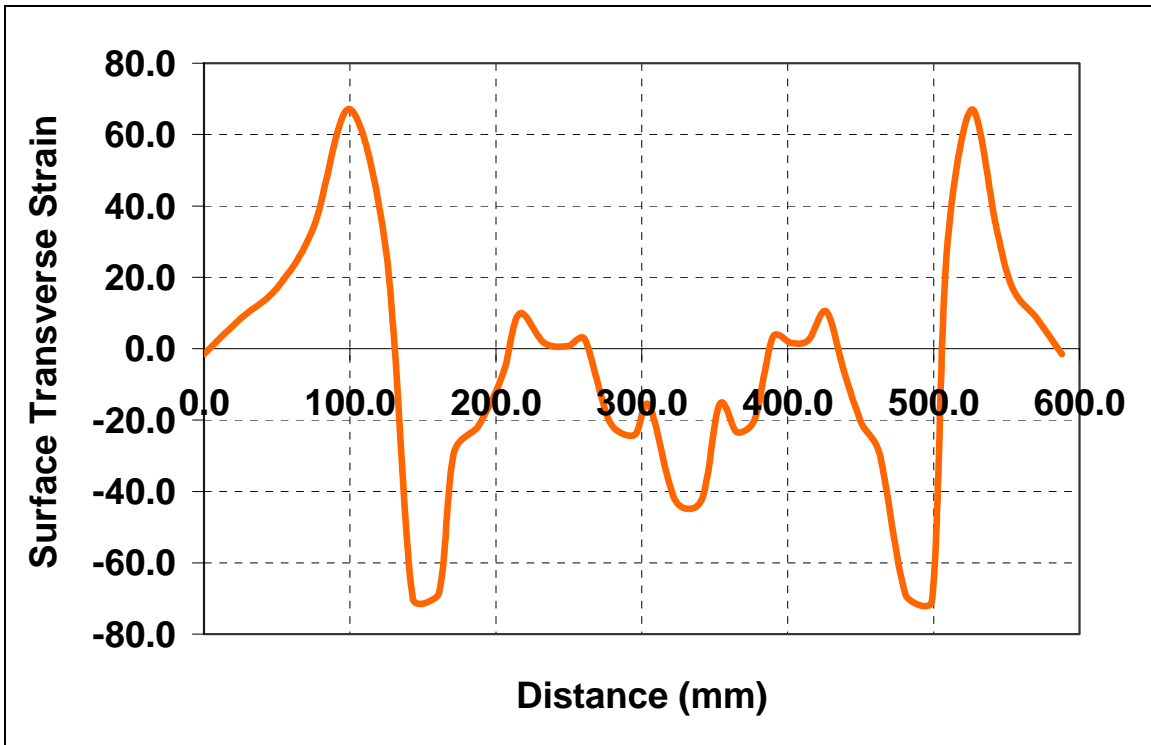
where,

DR_{TD} = damage ratio between the wide-base and dual tires configurations for the top-down failure mechanism;

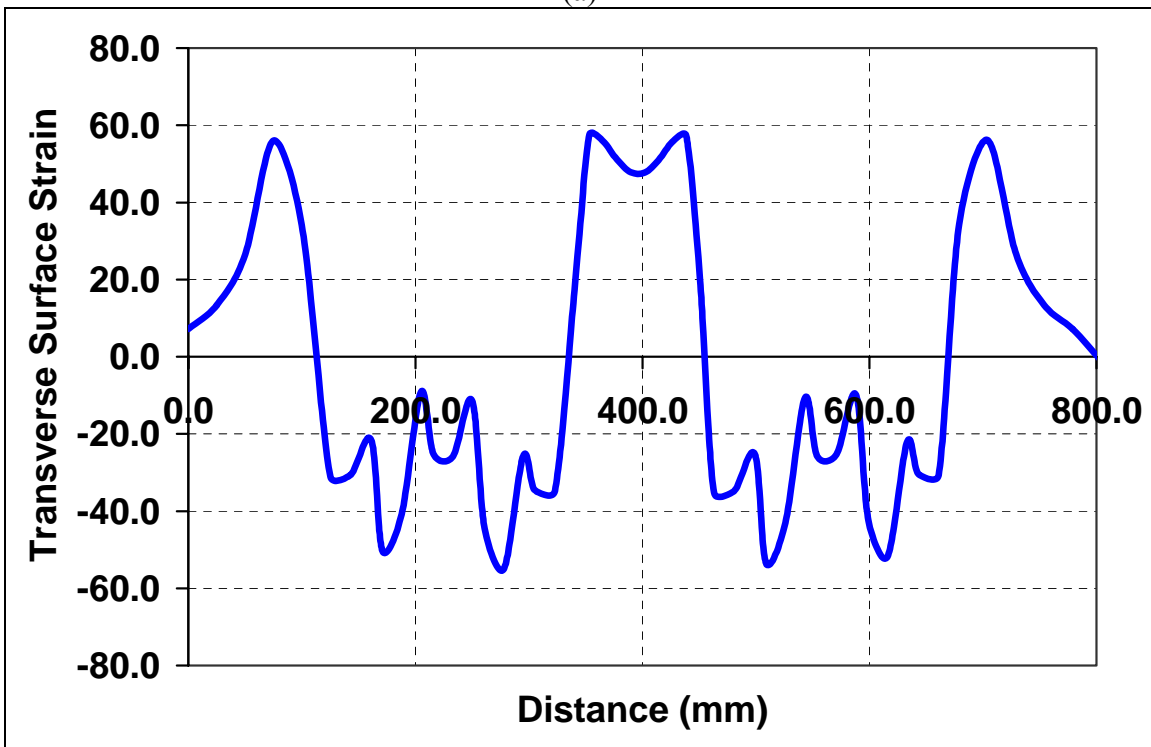
ε_w = surface tensile strain for the wide-base tire; and

ε_d = surface tensile strain for the dual tires.

Figures 6-1(a and b) show the calculated transverse strain at the pavement surface for both the new single wide-base and dual tire configurations at a temperature of 25°C.



(a)

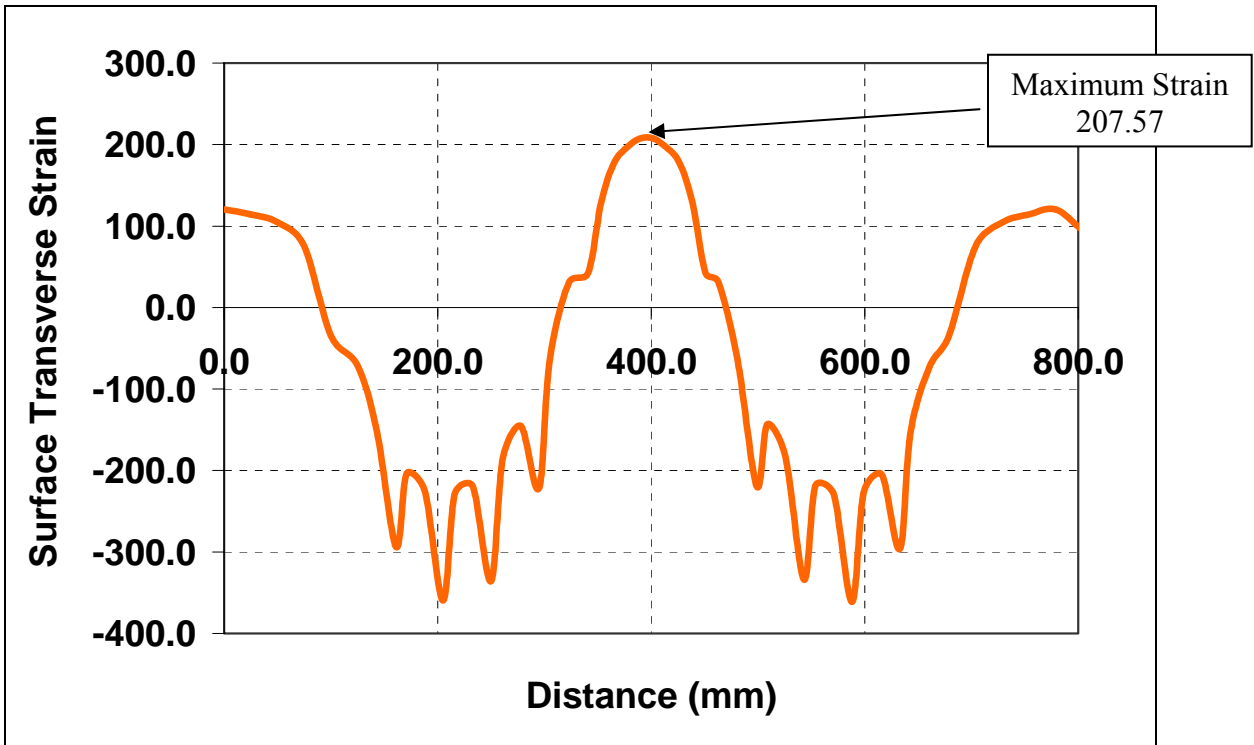


(b)

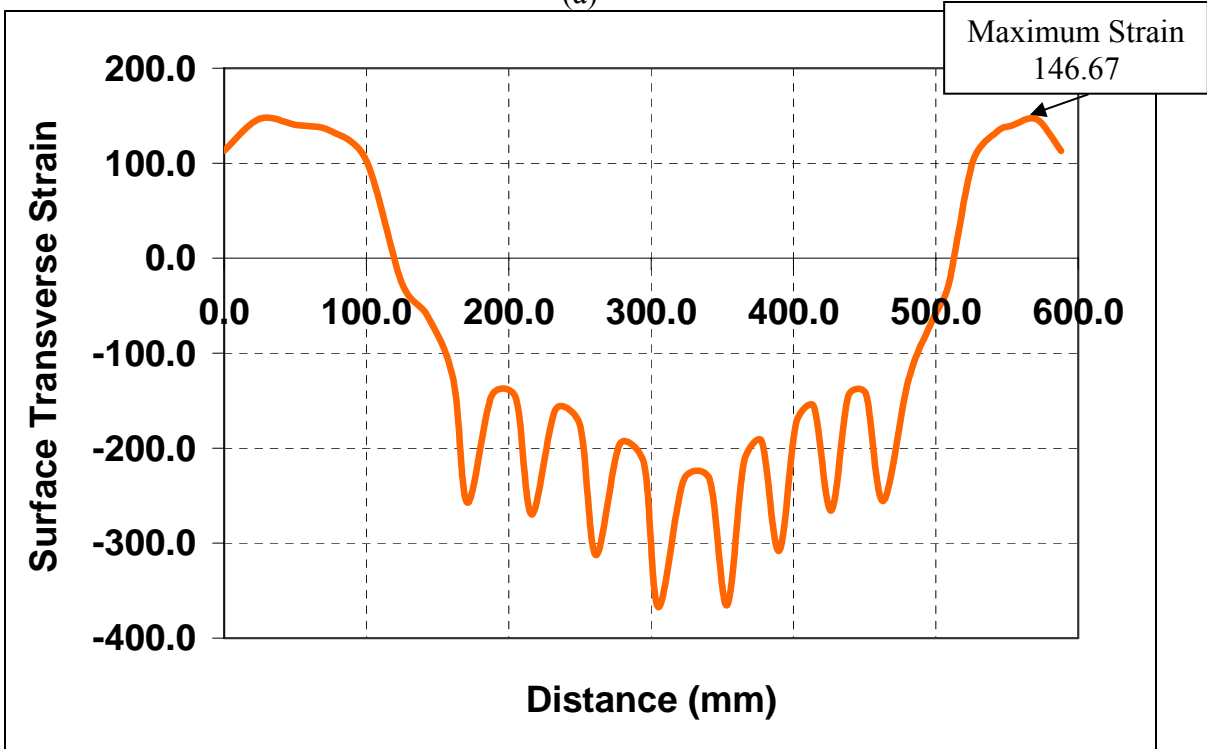
Figure 6-1. Comparison between Calculated Surface Strain at a Temperature of 25°C for (a) the New Generation of Wide-Base Tire and (b) the Dual Tires

As shown in these figures, the calculated tensile surface strain was slightly higher for the new single wide-base tire than for the dual-tire configurations. However, the dual-tire configuration results in three critical areas with high tensile strain: two at the edges of the tires and one between the tires. In contrast, the single wide-base tire eliminates the central zone of tensile strain, and therefore, top-down cracks may only appear at the edges of the tire. If over the pavement service life, the dual tires result in four cracks and the wide-base tires result in two cracks, the serviceability index of the pavement exposed to dual tires would be less than the serviceability index of the pavement exposed to wide-base tires. However, the timing of the appearance of the crack may be sooner or latter for the wide-base than the dual tires, depending on the applicable pavement design; this was considered through the ratio of strain raised to the fourth power.

An interesting observation is that the surface strain for the wide-base tire was not always higher than that for the dual tires. This was dependent on different factors such as the simulated speed, temperature, and the pavement design. During the course of this project, an experimental test site located at the University of Laval was also analyzed for surface-initiated top-down cracking. Results for the pavement structure are shown in Figures 6-2(a and b) at a temperature of 25°C. In this case, the dual-tire configuration resulted in greater strain than the wide-base tire. In addition, the dual-tire assembly would result in three critical locations instead of four, as it was observed at the Virginia Smart Road. Hence, pavement structures with different designs may not have the same trend of response to dual and wide-base tires. Therefore, different pavement designs ranging from thin to thick pavement structures should be considered in the analysis of pavement responses to dual and wide-base tires. More details are provided in Chapter 7 on the FE analysis of the Laval test site.



(a)



(b)

Figure 6-2. Comparison between Calculated Surface Strain at a Temperature of 25°C for (a) the Dual Tires and (b) the New Generation Wide-Base Tire (Laval Test Site)

6.2. DAMAGE RATIO

To compare the aggressiveness of the new generation wide-base tire to the conventional dual-tire assembly, the damage ratio for each failure mechanism (except for surface-initiated top-down cracking, see previous section) was calculated as follows:

$$DR_i = \frac{N_w}{N_d} \quad (6.7)$$

where,

DR_i = damage ratio between the wide-base and dual tires configurations for the considered failure mechanism (i.e., fatigue cracking, secondary rutting, primary rutting);

N_w = number of cycles to failure for the wide-base tire; and

N_d = number of cycles to failure for the dual tires.

This relation is based on a linear ratio of damage. To calculate the combined damage ratio (overall damage factor considering four pavement failure mechanisms) between the wide-base and dual-tire configurations, a distribution function was used:

$$CDR = a_1 DR_{TD} + a_2 DR_{FC} + a_3 DR_{SR} + a_4 DR_{PR} \quad (6.8)$$

where,

CDR = combined damage ratio between the wide-base and dual tires configurations;

DR_{TD} = damage ratio between the wide-base and dual tires configurations for surface-initiated top-down cracking;

DR_{FC} = damage ratio between the wide-base and dual tires configurations for fatigue cracking;

DR_{SR} = damage ratio between the wide-base and dual tires configurations for secondary rutting;

DR_{PR} = damage ratio between the wide-base and dual tires configurations for primary rutting; and

a_1 , a_2 , a_3 , and a_4 = distribution factors to account for the criticality of each failure mechanism.

The distribution factors (a_i) were determined based on a logarithmic distribution function as follows:

$$a_i = \frac{1/\log N_i}{\sum_{j=1}^{j=4} 1/\log N_j} \quad (6.9)$$

where,

a_i = damage distribution factor for the considered failure mechanism.

The reason a logarithmic distribution function was used is to balance the effect of each failure mechanism with respect to the overall damage induced by the tire. This is a common transformation used in statistics, and it is usually recommended when dealing with variables spreading over several orders of magnitude as it was the case here. In the field, even if one failure mechanism is manifested, this does not imply that the other distresses will not occur throughout the pavement service life. These are progressive failure mechanisms that contribute gradually to pavement failure. This makes the use of a logarithmic transfer function more appropriate and, hence, it was adopted in this analysis. Since the number of cycles for surface-initiated top-down cracking could not be determined, a fatigue damage distribution factor was assigned to this distress given its high criticality as it appears directly at the surface.

6.3. RESULTS AND ANALYSIS

The following sections present and compare the aggressiveness of the new generation of wide-base tire to the conventional dual tires. First, each failure mechanism was dealt with separately. Then the combined damage ratios and the equivalent axle load between the two tire configurations were determined at different temperatures and at the most critical speed. When applicable, the calculated damage ratios were compared to the ones determined based on field measurements at the reference temperature, 25°C. Although the damage ratios were determined at different speeds and temperatures, the exact damage ratios can be easily obtained if one assumes a representative temperature for the considered pavement location and select the most critical vehicle speed. Low vehicle speeds were found to be the most critical to the pavement structure, and result in far more damage than high vehicle speed. In this analysis, the lowest and highest vehicle speed (8 and 105km/h) were used to calculate the pavement damage ratio at the most unfavorable and the most encountered operating conditions on highway setup. Similar trends were encountered at the other simulated speeds.

6.3.1. Fatigue Cracking

Fatigue cracking is associated with the tensile strain at the bottom of the HMA layers. Utilizing the results of the FE model at the three considered temperatures (5, 25, and 40°C), Tables 6-1 and 6-2 present the calculated tensile strain at the bottom of the BM-25.0 as well as the predicted number of repetitions before fatigue failure occurs based on Equation (6.1) at the studied two speeds (8.0 and 105km/h) for the first generation of wide-base tire and the dual-tire assembly. Based on the results presented in these tables, one may conclude that the first generation of wide-base tire (445/50R22.5) would cause more fatigue damage than the conventional dual-tire assembly. Results shown in Table 6-1 also indicated that there was a good agreement between field and calculated damage ratios. On the other hand, as shown in Tables 6-3 and 6-4, the newly developed wide-base tire (455/55R22.5) was less damaging than the first generation of wide-base tire. However, the damage is still greater than that of the conventional dual tires assembly.

It is evident from these results that the increase in temperature results in more fatigue damage to the pavement, while the increase in speed causes significantly less fatigue damage to the pavement. On the other hand, the damage ratios between the new generation of wide-base tire and the dual tire assembly increased with the increase in temperature and speed. With respect to the effect of temperature, this was expected since the pavement structure is more compliant at high temperatures and is therefore more responsive to the tire stress distribution. With respect to the effect of speed, it appears that the strain induced by the dual tire assembly decreased more rapidly with the increase in speed than the strain induced by the new generation of wide-base tires.

Table 6-1. Fatigue Damage Ratios (Speed = 8km/h – 445/50R22.5)

Temperature (°C)	Wide-Base Tire		Dual Tires		DR _{FC}
	Tensile Strain	N _{fatigue}	Tensile Strain	N _{fatigue}	
5	43.03	1.87E+08	36.18	3.31E+08	1.77
25	108.19	1.32E+07	86.93	2.72E+07	2.05
40	361.02	4.04E+05	286.94	8.61E+05	2.13
Damage ratio based on field measurements at a reference temperature of 25°C					1.97

Table 6-2. Fatigue Damage Ratios (Speed = 105km/h – 445/50R22.5)

Temperature (°C)	Wide-Base Tire		Dual Tires		DR _{FC} Fatigue
	Tensile Strain	N _{fatigue}	Tensile Strain	N _{fatigue}	
5	36.57	3.19E+08	31.49	5.23E+08	1.64
25	61.83	8.34E+07	49.41	1.74E+08	2.09
40	184.48	3.68E+06	138.31	9.51E+06	2.58

Table 6-3. Fatigue Damage Ratios (Speed = 8km/h – 455/55R22.5)

Temperature (°C)	Wide-Base Tire		Dual Tires		DR _{FC}
	Tensile Strain	N _{fatigue}	Tensile Strain	N _{fatigue}	
5	37.54	2.93E+08	36.18	3.31E+08	1.13
25	95.28	2.01E+07	86.93	2.72E+07	1.35
40	321.19	5.94E+05	286.94	8.61E+05	1.45

Table 6-4. Fatigue Damage Ratios (Speed = 105km/h – 455/55R22.5)

Temperature (°C)	Wide-Base Tire		Dual Tires		DR _{FC} Fatigue
	Tensile Strain	N _{fatigue}	Tensile Strain	N _{fatigue}	
5	37.14	3.04E+08	31.49	5.23E+08	1.72
25	59.17	9.64E+07	49.41	1.74E+08	1.81
40	180.50	3.96E+06	138.31	9.51E+06	2.40

6.3.2. Subgrade Rutting

Secondary rutting is associated with the compressive strain at the top of the subgrade. Utilizing the results of the Generalized Kelvin FE model at the three considered pavement temperatures (5, 25, and 40°C), Tables 6-5 and 6-6 present the calculated compressive strain on top of the subgrade as well as the predicted number of repetitions before secondary rutting failure occurs based on Equation (5.2) at the two considered speeds (8 and 105km/h) for the first new generation of wide-base tire and the dual tires assembly. Based on these results, one may conclude that the first generation of wide-base is slightly more damaging than the conventional dual tire assembly with respect to secondary rutting damage. As previously observed with fatigue damage, there was a reasonably good agreement between field and calculated damage ratios. Similarly, Tables 6-7 and 6-8 present the damage ratios between the second size new generation of wide-base tire (455/55R22.5) and the conventional dual tires assembly at the two considered speeds. In this case, the new generation of wide-base tire was less damaging than the dual-tire assembly at slow speed, but more damaging at high speed. However, the relative damage was less than that caused by the 445/50R22.5 tire.

Table 6-5. Subgrade Rutting Damage Ratio (Speed = 8km/h – 445/50R22.5)

Temperature (°C)	Wide-Base Tire		Dual Tires		DR _{SR}
	Comp. Strain	N _{rutting}	Comp. Strain	N _{rutting}	
5	35.79	9.22E+11	35.40	9.68E+11	1.05
25	57.84	1.07E+11	55.64	1.28E+11	1.19
40	60.42	8.81E+10	58.88	9.90E+10	1.12
Damage ratio based on field measurements at a reference temperature of 25°C					1.27

Table 6-6. Subgrade Rutting Damage Ratio (Speed = 105km/h – 445/50R22.5)

Temperature (°C)	Wide-Base Tire		Dual Tires		DR _{SR}
	Comp. Strain	N _{rutting}	Comp. Strain	N _{rutting}	
5	31.48	1.64E+12	29.94	2.05E+12	1.25
25	44.58	3.44E+11	42.24	4.39E+11	1.27
40	54.93	1.35E+11	50.99	1.89E+11	1.40

Table 6-7. Subgrade Rutting Damage Ratio (Speed = 8km/h – 455/55R22.5)

Temperature (°C)	Wide-Base Tire		Dual Tires		DR _{SR}
	Comp. Strain	N _{rutting}	Comp. Strain	N _{rutting}	
5	31.78	1.57E+12	35.40	9.68E+11	0.62
25	51.81	1.76E+11	55.64	1.28E+11	0.73
40	54.07	1.45E+11	58.88	9.90E+10	0.68

Table 6-8. Subgrade Rutting Damage Ratio (Speed = 105km/h – 455/55R22.5)

Temperature (°C)	Wide-Base Tire		Dual Tires		DR _{SR}
	Comp. Strain	N _{rutting}	Comp. Strain	N _{rutting}	
5	30.70	1.83E+12	29.94	2.05E+12	1.12
25	44.17	3.59E+11	42.24	4.39E+11	1.22
40	53.56	1.51E+11	50.99	1.89E+11	1.25

6.3.3. Primary HMA Rutting

Primary HMA rutting is associated with the compressive strain at the pavement surface. This failure mechanism is a major concern under slow moving load or at high pavement temperatures. Utilizing the results of the Generalized Kelvin FE model at the three considered pavement temperatures (5, 25, and 40°C), Tables 6-9 and 6-10 present the calculated compressive strain at the pavement surface as well as the predicted number of repetitions before primary rutting failure occurs based on Equation (6.4) at the two considered speeds (8 and 105km/h) for the first new generation of wide-base tire and the dual tires assembly. Based on these results, one may conclude that the new generation of wide-base is more damaging than the conventional dual tire assembly. In addition, one may notice the criticality of this failure mechanism at high temperature and at low speed. Similarly, Tables 6-11 and 6-12 present the damage ratio between the second size new generation of wide-base tire (455/55R22.5) and the conventional dual-tire assembly. In this case, the wide-base tire configuration was less damaging than the dual-tire assembly at slow speed, and as damaging or slightly greater at high speed. Overall, the 455/55R22.5 tire was found to be less damaging than 445/50R22.5 tire.

Table 6-9. Primary Rutting Damage Ratio (Speed = 8km/h – 445/50R22.5)

Temperature (°C)	Wide-Base Tire		Dual Tires		DR _{PR}
	Comp. Strain	N _{rutting}	Comp. Strain	N _{rutting}	
5	70.03	2.38E+09	61.80	2.96E+09	1.24
25	515.90	2.52E+05	491.23	2.75E+05	1.09
40	2270.00	3.65E+03	2010.00	4.51E+03	1.24

Table 6-10. Primary Rutting Damage Ratio (Speed = 105km/h – 445/50R22.5)

Temperature (°C)	Wide-Base Tire		Dual Tires		DR _{PR}
	Comp. Strain	N _{rutting}	Comp. Strain	N _{rutting}	
5	61.85	2.95E+09	57.82	3.32E+09	1.12
25	183.00	1.53E+06	154.00	2.07E+06	1.35
40	837.82	2.07E+04	650.00	3.21E+04	1.56

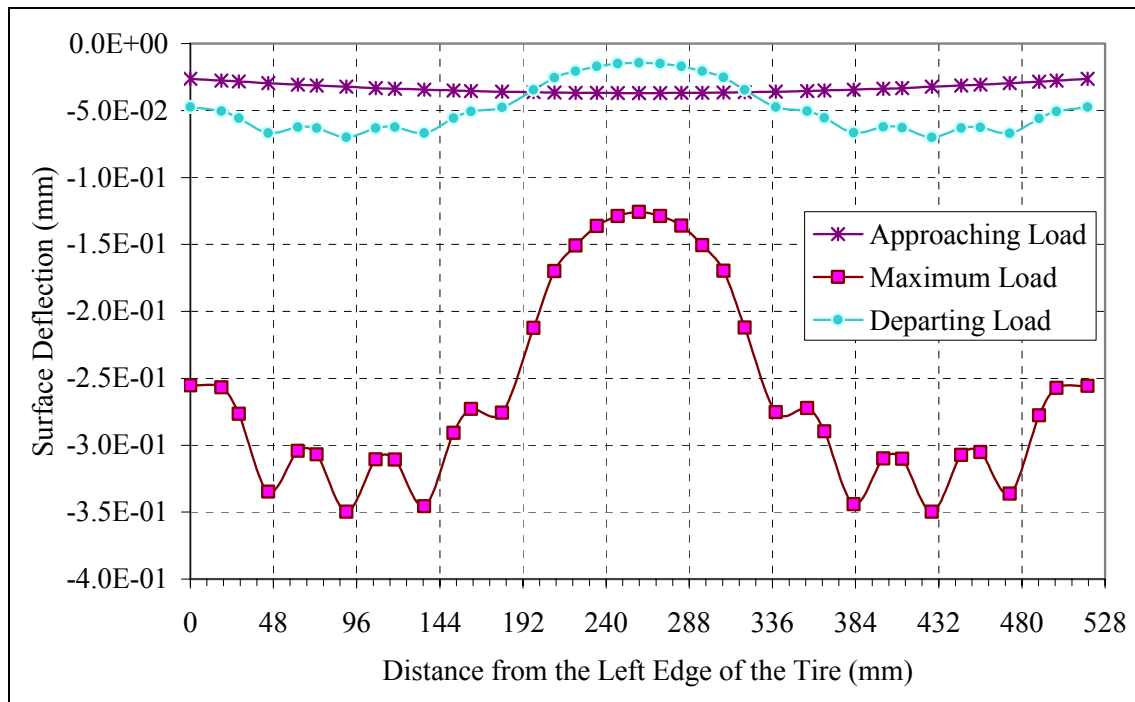
Table 6-11. Primary Rutting Damage Ratio (Speed = 8km/h – 455/55R22.5)

Temperature (°C)	Wide-Base Tire		Dual Tires		DR _{PR}
	Comp. Strain	N _{rutting}	Comp. Strain	N _{rutting}	
5	55.70	3.54E+09	61.80	2.96E+09	0.83
25	474.87	2.91E+05	491.23	2.75E+05	0.94
40	1941.29	4.79E+03	2010.00	4.51E+03	0.94

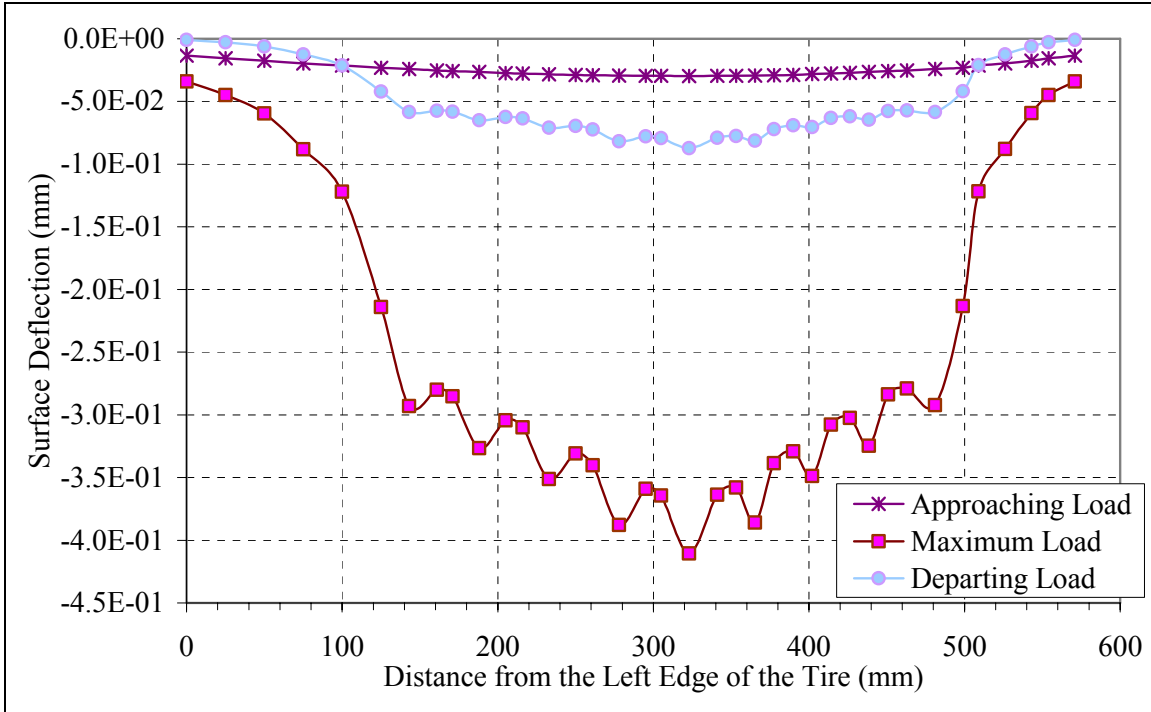
Table 6-12. Primary Rutting Damage Ratio (Speed = 105km/h – 455/55R22.5)

Temperature (°C)	Wide-Base Tire		Dual Tires		DR _{PR}
	Comp. Strain	N _{rutting}	Comp. Strain	N _{rutting}	
5	57.90	3.31E+09	57.82	3.32E+09	1.00
25	161.61	1.90E+06	154.00	2.07E+06	1.09
40	720.12	2.69E+04	650.00	3.21E+04	1.20

Since HMA layers were modeled using a viscoelastic constitutive model, the predicted permanent deformation was associated with the primary rutting failure mechanism. This capability allowed calculating primary rutting for a single load application without the need to use a transfer function. In this case, two additional load increments were added to this analysis to allow the material to recover some of the exhibited viscous deformations. Figures 6-3(a and b) present the results of this analysis for the dual and the first generation of wide-base tire assemblies at a temperature of 40°C and a speed of 8km/h, respectively. These could be considered the critical operating conditions for the primary rutting failure mechanism.



(a)



(b)

Figure 6-3. Pavement Surface Profile before and after Load Application at a Temperature of 40°C and a Speed of 8km/h

Based on these results, the primary rutting pavement damage ratios between the 445/50R22.5 tire and the conventional dual tire assembly were determined. Tables 6-13 and 6-14 present the results of this analysis at the three considered temperatures and at two speeds (8 and 105km/h). Based on these results, one may conclude that the 445/50R22.5 tire is slightly more damaging than the conventional dual-tire assembly. Similarly, Tables 6-15 and 6-16 present the damage ratio between the 455/55R22.5 tire and the conventional dual-tire assembly. The 455/55R22.5 tire was found to be slightly more damaging than the dual-tire assembly at the two considered speeds. In general, there was a good agreement between the damage ratios predicted based on the adopted transfer function and those predicted based on the calculated rut depth after load application.

Table 6-13. Primary Rutting Damage Ratio (Speed = 8km/h – 445/50R22.5)

	Wide-Base Tire	Dual Tires	DR _{PR}
Temperature (°C)	Rut Depth (µm)	Rut Depth (µm)	P. Rutting
5	3.00	3.27	1.09
25	19.00	21.35	1.12
40	70.00	87.30	1.25

Table 6-14. Primary Rutting Damage Ratio (Speed = 105km/h – 445/50R22.5)

	Wide-Base Tire	Dual Tires	DR _{PR}
Temperature (°C)	Rut Depth (μm)	Rut Depth (μm)	P. Rutting
5	0.20	0.22	1.10
25	9.50	12.00	1.26
40	21.90	31.70	1.45

Table 6-15. Primary Rutting Damage Ratio (Speed = 8km/h – 455/55R22.5)

	Wide-Base Tire	Dual Tires	DR _{PR}
Temperature (°C)	Rut Depth (μm)	Rut Depth (μm)	P. Rutting
5	3.13	3.00	1.04
25	19.00	20.70	1.09
40	70.00	75.70	1.08

Table 6-16. Primary Rutting Damage Ratio (Speed = 105km/h – 455/55R22.5)

	Wide-Base Tire	Dual Tires	DR _{PR}
Temperature (°C)	Rut Depth (μm)	Rut Depth (μm)	P. Rutting
5	0.20	0.23	1.15
25	9.50	10.60	1.12
40	21.90	27.50	1.26

6.3.4. Surface Initiated Top-Down Cracking

Surface-initiated top-down cracking is associated with the tensile strain at the pavement surface and the distribution of the contact stresses around the tire. To date, a transfer function does not exist to determine the allowable number of repetitions through the top-down cracking failure mechanism. Therefore, only the relative damage ratio between the two tire configurations was quantified. However, as its name implies, since top-down cracking appears directly at the pavement surface, they will directly affect the serviceability of the pavement structure and are therefore, considered a critical failure mechanism. Utilizing the results of the generalized Kelvin FE model at the three considered pavement temperatures (5, 25, and 40°C), Tables 6-17 through 6-20 present the calculated maximum surface strain around the tire edge as well as the predicted damage ratio between the first and second size new generation of wide-base tires and the dual-tire assembly based on Equation (5.6) at the two considered speeds (8 and 105km/h). Based on these results, one may conclude that the new generations of wide-base tires are significantly less damaging than the conventional dual-tire assembly with respect to surface-initiated top-down cracking.

Table 6-17. Surface Initiated Top-Down Cracking Damage Ratio (Speed = 8km/h – 445/50R22.5)

	Wide-Base Tire	Dual Tires	DR _{TD}
Temperature (°C)	Surface Strain	Surface Strain	Top-Down
5	8.76	8.70	0.51
25	67.14	58.88	0.85
40	367.00	429.00	0.27

Table 6-18. Surface Initiated Top-Down Cracking Damage Ratio (Speed = 105km/h – 445/50R22.5)

	Wide-Base Tire	Dual Tires	DR _{TD}
Temperature (°C)	Surface Strain	Surface Strain	Top-Down
5	8.50	7.67	0.75
25	24.30	20.10	1.07
40	137.39	126.00	0.71

Table 6-19. Surface Initiated Top-Down Cracking Damage Ratio (Speed = 8km/h – 455/55R22.5)

	Wide-Base Tire	Dual Tires	DR _{TD}
Temperature (°C)	Surface Strain	Surface Strain	Top-Down
5	6.32	8.70	0.14
25	40.64	58.88	0.11
40	249.72	429.00	0.06

Table 6-20. Surface Initiated Top-Down Cracking Damage Ratio (Speed = 105km/h – 455/55R22.5)

	Wide-Base Tire	Dual Tires	DR _{TD}
Temperature (°C)	Surface Strain	Surface Strain	Top-Down
5	7.15	7.67	0.38
25	13.92	20.10	0.12
40	88.99	126.00	0.12

6.3.5. Combined Damage Ratio

A logarithmic damage distribution function was suggested to define the criticality of the different failure mechanisms. Tables 6-21 and 6-22 present the calculated combined damage ratios (CDRs) at the different temperatures (5, 25, and 40°C) for the first new generation of wide-base (445/50R22.5) tire. Both the lowest and highest vehicle speeds were considered in this analysis as the lowest represent the most critical, while the highest represent the most encountered operating conditions on highway setup.

Results of this analysis suggested that the first new generation of wide-base tire induces more damage on the pavement structure than the dual-tire assembly. The increase in pavement damage is a function of various factors such as pavement temperature, vehicle speed, and pavement stiffness and design. The increase in pavement damage at 8km/h ranged between 14 to 28%. At a vehicle speed of 105km/h, the increase in pavement damage was more significant, ranging between 18 to 57%. The new generation of wide-base tire has a lower radius stiffness, which reduces the dynamic impact of the tire. Therefore, the pavement damage at high speed could be reduced when the dynamic loading is considered in the analysis.

Table 6-21. Combined Damage Ratios at Different Temperatures at a Speed of 8km/h (445/50R22.5)

Distress Temperature (°C)	A	B	C	D	CDR
	5	1.77 (0.28)	1.05 (0.20)	1.24 (0.25)	0.51 (0.28)
25	2.05 (0.25)	1.19 (0.17)	1.09 (0.34)	0.85 (0.25)	1.28
40	2.13 (0.24)	1.12 (0.13)	1.24 (0.39)	0.27 (0.24)	1.20

A: Fatigue Cracking, B: Subgrade Rutting, C: Primary Rutting, D: Top-Down Cracking.

Table 6-22. Combined Damage Ratios at Different Temperatures at a Speed of 105km/h (445/50R22.5)

Distress Temperature (°C)	A	B	C	D	CDR
	5	1.64 (0.28)	1.25 (0.20)	1.12 (0.25)	0.75 (0.28)
25	2.09 (0.25)	1.27 (0.18)	1.35 (0.33)	1.07 (0.25)	1.45
40	2.58 (0.24)	1.40 (0.15)	1.56 (0.37)	0.71 (0.24)	1.57

A: Fatigue Cracking, B: Subgrade Rutting, C: Primary Rutting, D: Top-Down Cracking.

Tables 6-23 and 6-24 present the combined damage ratios between the second size new generation of wide-base (455/55R22.5) tire and the conventional dual-tire assembly. Less damage was noted when 455/55R22.5 tire was used at low speed. The reduction in pavement damage ranged between 18 to 32%. However, at 105km/h, an increase between 5 to 23% in pavement damage was found. As noted earlier, wide-base tire usually has lower radius of stiffness, which reduces the dynamic impact of the tire.

Therefore, the pavement damage at high speed could be reduced when the dynamic loading is considered in the analysis.

Table 6-23. Combined Damage Ratios at Different Temperatures at a Speed of 8km/h (455/55R22.5)

Distress Temperature (°C)	A	B	C	D	CDR
	5	1.13 (0.28)	0.62 (0.20)	0.83 (0.25)	0.14 (0.28)
25	1.35 (0.25)	0.73 (0.18)	0.94 (0.33)	0.11 (0.25)	0.80
40	1.45 (0.24)	0.68 (0.15)	0.94 (0.37)	0.06 (0.24)	0.81

A: Fatigue Cracking, B: Subgrade Rutting, C: Primary Rutting, D: Top-Down Cracking.

Table 6-24. Combined Damage Ratios at Different Temperatures at a Speed of 105km/h (455/55R22.5)

Distress Temperature (°C)	A	B	C	D	CDR
	5	1.72 (0.28)	1.12 (0.20)	1.00 (0.25)	0.38 (0.28)
25	1.81 (0.25)	1.22 (0.18)	1.09 (0.33)	0.12 (0.25)	1.05
40	2.40 (0.24)	1.25 (0.15)	1.20 (0.37)	0.12 (0.24)	1.23

A: Fatigue Cracking, B: Subgrade Rutting, C: Primary Rutting, D: Top-Down Cracking.

Based on the calculated combined damage ratios, equivalent loads were determined to balance the damage induced by the new generation of wide-base tire with the dual-tire assembly. This assumes that the fourth power law, which is usually used for such application, is valid:

$$P_{\text{limit}} = \frac{P}{(\text{CDR})^{0.25}} \quad (6.10)$$

where,

P_{limit} = maximum load on a single tire to cause the same pavement damage induced by a dual tire configuration; and

CDR = combined damage ratio for the considered pavement temperature.

Results of this analysis, Tables 6-25 and 6-26, indicate that the recommended load reduction on an axle equipped with the 445/50R22.5 tire should range between 4.0 to 6.0% at a speed of 8km/h and between 5.0 to 11% at a speed of 105km/h to maintain the same effects on pavements as that of dual tires. However, given that the new generation of wide-base tire reduces the overall truck weight by approximately 450kg, if the carried weight is kept constant, the gross vehicle weight would be reduced by the difference in tire weight, when wide-base tires are used. Therefore, the actual load reductions may differ from the limits shown in Tables 6-25 and 6-26.

When using the 455/55R22.5 tire, at slow speed, the load carried by the axle may be increased by 5 to 10%, while at high speed, a small load reduction ranging between 2 to 5% is needed. One needs to consider the following as decision is made on load limits:

- More damage occurs in flexible pavements at low speeds due to the viscoelastic nature of HMA.
- 2% change in loading is within the margin of error of the FE model. Results from field validation or accelerated load testing can be used to fine-tune these results.
- Wide-base tire has a relatively low radius stiffness. This reduces the dynamic impact of the tire. Therefore, the pavement damage of the wide-base tire at high speed could be reduced when the dynamic loading is considered in the analysis.

Table 6-25. Recommended Load Limits at a Speed of 8km/h

Temperature (°C)	Tire Dual (kg)	Wide-Base Tire	
		445/50R22.5 (kg)	455/55R22.5 (kg)
5	9000	8700	9900
25	9000	8400	9500
40	9000	8600	9500

Table 6-26. Recommended Load Limits at a Speed of 105km/h

Temperature (°C)	Tire Dual (kg)	Wide-Base Tire	
		445/50R22.5 (kg)	455/55R22.5 (kg)
5	9000	8600	8900
25	9000	8200	8900
40	9000	8000	8500

7. THE LAVAL STUDY

In 2002, Michelin America has requested from the various Canadian Federal and Provincial Ministries of Transportation to review current load regulation limits to be applicable to the new generation of wide-base tire that was investigated in this study. This would avoid the current penalties set for the previous generation of wide-base tires being applied to the new generation of wide-base tire. Currently, load regulations in Quebec limit the maximum allowable load on an axle with single tires to 8000kg, compared to 9000kg for a standard dual tires axle. This represents a reduction of 11% during ten months of the year. For the two months of the spring thaw season, a 1000kg per axle load reduction is applied on all tire configurations.

To address this valid issue, the Québec Ministry of Transport commissioned the University of Laval to initiate a research study to compare the aggressiveness of four different tire assemblies (11R22.5 and 12R22.5 dual tires, and 385/65R22.5 single tire, and 455/55R22.5) on flexible pavements. The pavement response to loading was obtained from embedded instruments. Instruments responses to vehicular loading were then utilized in conjunction with the multi-layer elastic theory to estimate tire-induced damages. The developed models were validated using measured deflections utilizing Multi-Depth Deflectometer. Results of the study were used to propose load regulations for the aforementioned axle configurations. The following sections briefly describe the research efforts at the University of Laval. More details have been presented elsewhere (Prophète 2003). Finite Element models, similar to the ones used for analyzing the pavement section presented in Chapters 5 and 6, were developed for the Laval pavement test site.

7.1. THE LAVAL TEST SITE

Figure 7-1 illustrates a schematic of the pavement design of the instrumented test section. This section may be classified as a medium thickness pavement type with a total HMA layer of 100mm. However, the high number of pavement layers and the very high overall pavement thickness significantly increased the stiffness of the pavement structure making it representative of high priority routes.

7.1.1. Instrumentation

A limited number of sensors were installed in the Laval test site. The array of instrument used in the study was as follows:

- Thermocouples at different depths through the pavement structure.
- Multi-depth deflectometer (MDD), which allowed measuring the vertical deflection at different depths of the pavement structure.
- Strain gages installed by gluing the sensors to laboratory-made core samples, which were then installed as part of the HMA layer with a small tolerance:

- Two strain gages for longitudinal strain measurements at the bottom of the HMA layer.
- One strain gage for transverse strain measurement at the bottom of the HMA layer.
- Instrumented plate at a 25-mm depth in the HMA layer. The plate was instrumented with longitudinal and transverse strain gages, as well as thermistors. Measurements on the instrument plate were made at very low speed (quasi-static conditions).
- Tire imprint and height measurements were conducted at different loading and pressure conditions.

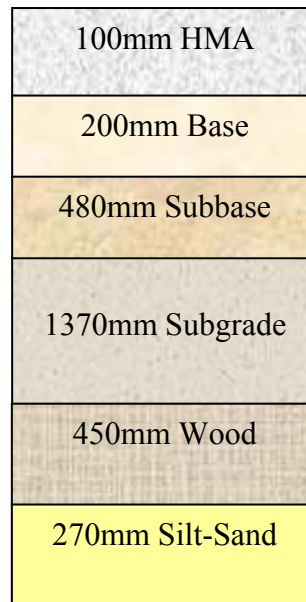


Figure 7-1. Pavement Cross-Section of the Laval Test Site

7.1.2. Experimental Program

To evaluate the aggressiveness of the different tire assemblies under different operating conditions, the experimental program was defined as follows:

- Four tire assemblies: 11R22.5 and 12R22.5 dual tires, and 385/65R22.5 single tire, and 455/55R22.5 (XONE).
- Four loading cases: 3000, 4000, 5000, 6000 kg per half-axle.
- Three tire pressures: 560, 730, and 900 kPa.
- One speed at 50 km/h.
- Two testing periods: one in the spring (temperature between 5 and 20°C), and one in the summer (temperature between 15 and 30°C with an average of 20°C).

7.1.3. Model Validation

As previously mentioned, a multi-layer elastic software (WinJulea) was used to simulate the pavement structure. Results from this software were then used to expand the scope of the experimental program. This model was calibrated based on field measurements. In addition, elastic layer moduli were backcalculated based on falling weight deflectometer (FWD) deflection measurements. This analysis considered two analysis periods representing the spring and summer seasons.

Comparison of the model results with the measurements of the MDD indicated a reasonable agreement in the spring (errors varied between -28.8 and 14.4%), but not an acceptable match in the summer (errors varied between -40.0 and 1%). This could be due to one or more of the following reasons: measurements of the MDD in the summer did not increase with depths, the effect of temperature variation during field testing, and the effect of speed on the theoretical analysis.

7.1.4. Results of the Laval Study

Three failure mechanisms were considered in the Laval study: fatigue cracking, subgrade rutting, and HMA rutting. Transfer functions, similar to the ones used in the analysis presented in Chapter 6, were adopted to quantify the number of cycles to failure. Aggressiveness of the different tire assemblies was compared based on a linear damage ratio, which was corrected for seasonal variations. To evaluate the combined damage of the different tire assemblies, the following relationship was used:

$$CD = \alpha D_{FC} + \beta D_R \quad (7.1)$$

where,

CD = combined damage of a given tire assembly;

D_{FC} and D_R = coefficient of damage based on fatigue cracking and rutting damage, respectively; and

α and β = linear damage distribution factors determined as follows:

$$\alpha = \frac{N_R}{N_{FC} + N_R} \quad \beta = \frac{N_{FC}}{N_{FC} + N_R} \quad (7.2)$$

where,

N_R = number of allowable repetitions to cause rutting failure (each rutting type was considered separately); and

N_{FC} = number of allowable repetitions to cause fatigue failure.

It is worth noting that damage was distributed linearly between the fatigue and the rutting failure mechanisms, and this resulted in an unbalanced distribution of zero for the rutting and one for the fatigue in the summer season. As discussed in Chapter 6, it is recommended to use a logarithmic distribution function to balance the overall damage of

the different failure mechanisms. The damage ratio between the reference tire (dual 11R22.5) and the different tire assemblies was evaluated for three different scenarios:

- Fatigue cracking and primary rutting in the summer.
- Fatigue cracking and secondary rutting in the summer.
- Fatigue cracking and secondary rutting in the spring.

Tables 7-1 through 7-3 present the results of this analysis for the three different scenarios. The tables also include the average damage distribution factors as reported by the Laval study. From the first glance at the results of the analysis, one may conclude that both the old and the new generation of wide-base tires produced the same pavement damage. The increased pavement damage due to the use of wide-base tires was approximately 80%. In addition, the damage distribution factors indicated that fatigue failure is the controlling mechanism for the considered pavement design. A surprising observation from the results presented in these tables is that the conventional wide-base tire caused less damage than the new generation of wide-base tire at some loads. This is unexpected since the new generation of wide-base tire is 18% wider and is especially designed to reduce the contact pressure at highway speeds.

Table 7-1. Damage Ratios between the Reference Tire and the Investigated Tire Assemblies in the Summer (after Prophète 2003)

Tire	Load (kg)					CDR	α/β
	3000	4000	5000	6000	7000		
11R22.5	1	1	1	1	1	1	0.95/0.05
12R22.5	1.12	0.98	1.06	1.03	---	1	0.96/0.04
385/65R22.5	2.53	1.84	1.65	1.34	1.43	1.80	0.98/0.02
455/55R22.5	2.56	1.83	1.60	1.45	1.40	1.80	0.99/0.01

Table 7-2. Damage Ratios between the Reference Tire and the Investigated Tire Assemblies in the Summer (after Prophète 2003)

Tire	Load (kg)					CDR	α/β
	3000	4000	5000	6000	7000		
11R22.5	1	1	1	1	1	1	1.00/0.00
12R22.5	1.07	0.98	1.06	1.03	----	1	1.00/0.00
385/65R22.5	2.53	1.85	1.65	1.34	1.43	1.80	1.00/0.00
455/55R22.5	2.56	1.84	1.60	1.45	1.40	1.80	1.00/0.00

The equivalent loads for different tire assemblies were determined based on the concept of load equivalency assuming the critical failure mechanism as fatigue cracking:

$$P_{\text{limit}} = \frac{P}{(\text{CDR})^{0.30}} \quad (7.3)$$

where,

P_{limit} = maximum load on a single tire to cause the same pavement damage induced by a dual-tire configuration; and

CDR = combined damage ratio for the considered tire assembly.

Table 7-3. Damage Ratios between the Reference Tire and the Investigated Tire Assemblies in the Spring (after Prophète 2003)

Tire	Load (kg)					CDR	α/β
	3000	4000	5000	6000	7000		
11R22.5	1	1	1	1	1	1	0.68/0.32
12R22.5	0.80	1.03	1.03	0.87	1.12	1	0.70/0.30
385/65R22.5	1.93	1.98	1.58	1.77	1.74	1.80	0.70/0.30
455/55R22.5	2.07	2.04	1.78	1.96	1.84	1.90	0.66/0.34

Based on this analysis, it was recommended that the maximum load carried by a single tire be reduced by 16% in the summer and spring. In addition, it was recommended that the load limit on all axle configurations be reduced by 20% in the spring thaw season to avoid excessive damage to the pavement in this time of year.

7.2. FINITE ELEMENT ANALYSIS OF THE LAVAL TEST SITE

Although theoretical calculations using the layered theory are relatively inexpensive and easy, uncertainty of the assumptions may affect the reliability of the results. For instance, assumptions such as uniform pressure, linear elastic response of HMA, and circular contact area significantly affect the analysis results. This effect becomes more pronounced when quantifying the damage due to different tire configurations. Because of using the multi-layer elastic theory in the Laval study, the longitudinal strain, which was found greater than the transverse strain at the Virginia Smart Road, was not considered. In addition, omitting HMA creep behavior would result in under predicting the pavement responses at high temperatures (Al-Qadi et al. 2004). The inaccurate MDD measurements, which were reported to increase with depth, along with the aforementioned drawbacks made it impossible to distinguish between the first and the new generations of wide-base tires in spite of the increase of the tire width and the reduction of the tire pressure in the new generation of wide-base tire over the first one. Hence, an advanced theoretical tool, such as finite element method, would be needed to overcome these shortcomings.

A FE analysis was conducted for the pavement design shown in Figure 6-1. Two FE models were developed. The first model (3D Circular FE) is a simplified model with its assumptions derived from the layered theory. The second model (3D Modified FE) follows the same assumptions made in Chapters 5 and 6. However, this analysis was conducted at a single temperature (25°C) using the recommended Generalized Kelvin model at a speed of 8km/h. The tire assemblies considered in this analysis were the new generations of wide-base tire (445/50R22.5 and 455/55R22.5) and a standard dual-tire assembly (275/80 R22.5). Figure 7-2 illustrates the general layout of the developed FE

model. To demonstrate the difference between the results of the modified FE model and the layered theory, the same pavement design was simulated using Bisar3.0 (De Jong et al. 1973).

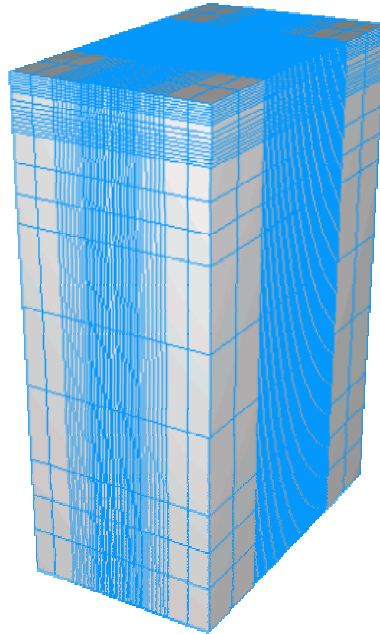


Figure 7-2. General Layout of the FE model

7.2.1. Results and Analysis

Table 7-4 compares the predicted linear damage ratios between the dual-tire assembly and the new generation of wide-base tire (445/55R22.5 and 455/55R22.5) at a single load of 4080kg using different analysis approaches. The predicted damage ratios using the multi-layer elastic model are also included in this table. Based on these results, the following observations may be made:

- The Laval results over-predicted the fatigue damage ratio between the dual-tire assembly and the second size new generation of wide-base (455/55R22.5) tires when compared to the results of the modified FE model.
- Significant discrepancies are evident between the modified FE model and the Laval test results in predicting the secondary rutting damage ratio. In fact, it is quite surprising that the Laval study predicted that the damage of the wide-base tire would be more than double the damage induced by the dual-tire assembly. This is in contradiction with the research conducted in this field (Huhtala 1986; Sebaaly 1992; COST 2001). It is well-documented that the difference in tire configuration is insignificant at greater depths. Under the considered loading and operating conditions, all other evaluation tools predicted that the subgrade rutting damage of the wide-base tire is equivalent or less than the subgrade rutting damage of the dual-tire assembly.

- A reasonable agreement was found between the Laval results and the modified FE model in predicting the primary rutting damage ratio between the dual-tire assembly and the second size new generation of wide-base tires (455/55R22.5).
- In all cases, the layered theory and the simplified FE model over-predicted the damage ratios between the dual-tire assembly and the new generation of wide-base tires. This was expected due to the aforementioned shortcomings of the elastic theory.
- As presented in Chapter 6, there was a good agreement between the results of the modified FE model and the results of the Virginia Smart Road experimental program.

Table 7-4. Comparison of Pavement Damage Ratios Based on Different Evaluation Methods

Section	Section B			Laval Section		
	A ⁻	B	C	A	B	C
Layered Theory	3.11	1.56	1.10	2.40	1.03	1.38
3D Circular FE⁺	3.03	1.07	0.97	2.14	0.85	0.64
3D Modified FE[#]	2.05	1.19	1.09	2.30	0.64	0.98
3D Modified FE⁼	1.35	0.73	0.94	1.54	0.17	0.87
Smart Road^{\$}	1.97	1.27	----	----	----	----
Laval Study[^]	----	----	----	2.31	2.22	0.82

⁻: A: Fatigue Cracking, B: Subgrade Rutting, C: Primary Rutting.

^{\$}: Based on the Virginia Smart Road experimental program.

[^]: Based on the Laval research study.

⁺: Simplified FE model.

[#]: First generation of wide-base tire (445/50R22.5).

⁼: Second generation of wide-base tire (455/55R22.5).

In addition to three failure mechanisms covered in Table 7-4, the modified FE model allowed investigating the aggressiveness of the different tire assemblies with respect to surface-initiated top-down cracking. Figures 7-3 (a, b, and c) show the calculated surface transverse strain for the dual-tire and the two wide-base assemblies (445/50R22.5 and 455/55R22.5). The wide-base tire resulted in significantly smaller strain at the surface than the dual-tire assembly. In addition, the dual-tire assembly resulted in four critical areas with high tensile strain: two at the edges of the tires and two between the tires. In contrast, the single wide-base tire eliminates the central zone of tensile strain, and therefore, top-down cracks may only appear at the edges of the tire. This may be accounted for by using the following relationship to estimate the damage ratio between the wide-base and dual-tire assemblies:

$$DR_{TD} = \frac{2}{4} \left(\frac{\varepsilon_w}{\varepsilon_d} \right)^4 \quad (7.4)$$

where,

DR_{TD} = damage ratio between the wide-base and dual tires configurations for the top-down failure mechanism;

ϵ_w = surface tensile strain for the wide-base tire; and

ϵ_d = surface tensile strain for the dual tires.

Given the surface strain distribution shown in Figures 7-3 for the Laval test section, Table 7-5 shows the final damage ratios between the dual and the new generation of wide-base tires (445/50R22.5 and 455/55R22.5) at a temperature of 25°C and a speed of 8km/h.

Table 7-5. Damage Ratio between the Wide-Base and Dual Tires

Distress Method	Smart Road (Section B)				Laval Test Section			
	A	B	C	D	A	B	C	D
3D FEM [#]	2.05	1.19	1.09	0.85	2.30	0.64	0.98	0.12*
3D FEM [▯]	1.35	0.73	0.94	0.11	1.54	0.17	0.87	0.07*
Smart Road	1.97	1.27	N/A [^]	N/A	xxx	xxx	xxx	xxx
Laval Study	xxx	xxx	xxx	xxx	2.31	2.22	0.82	N/A

A: Fatigue Cracking, B: Subgrade Rutting, C: HMA Rutting, D: Top-Down Cracking

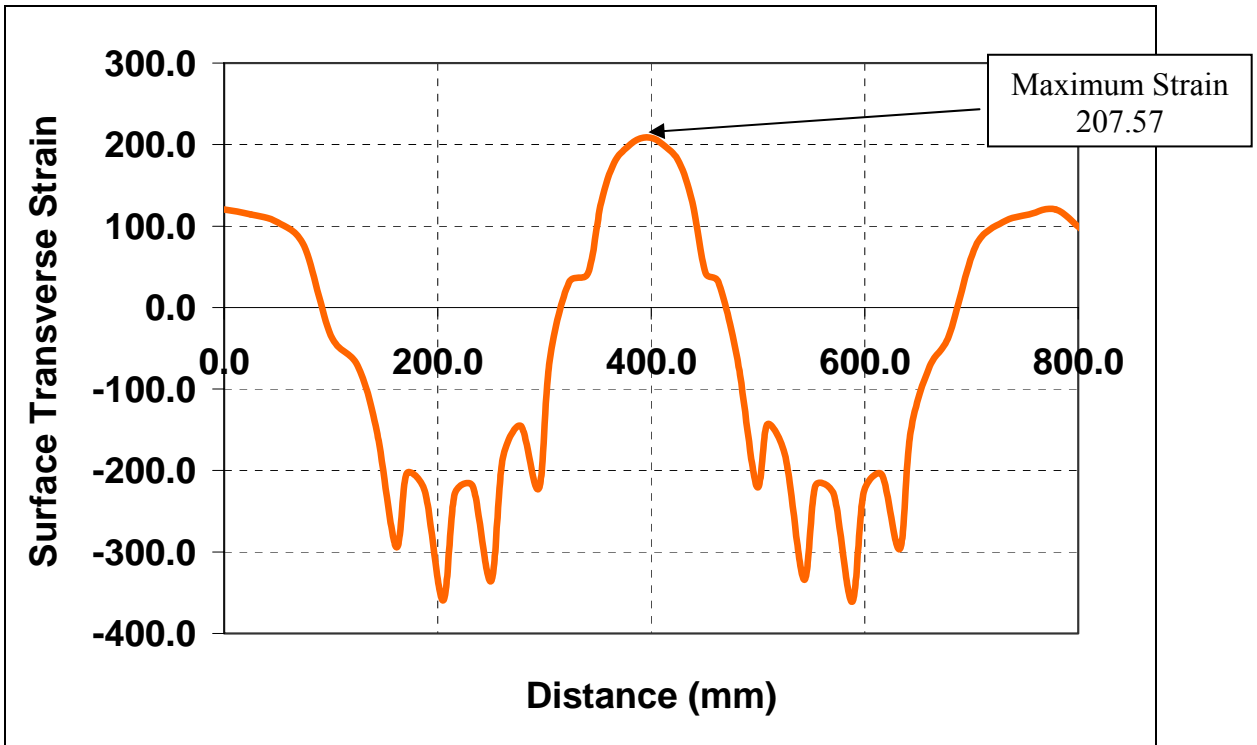
*: Based on Figure 7-3 and Equation 7-4.

[^]: No data available.

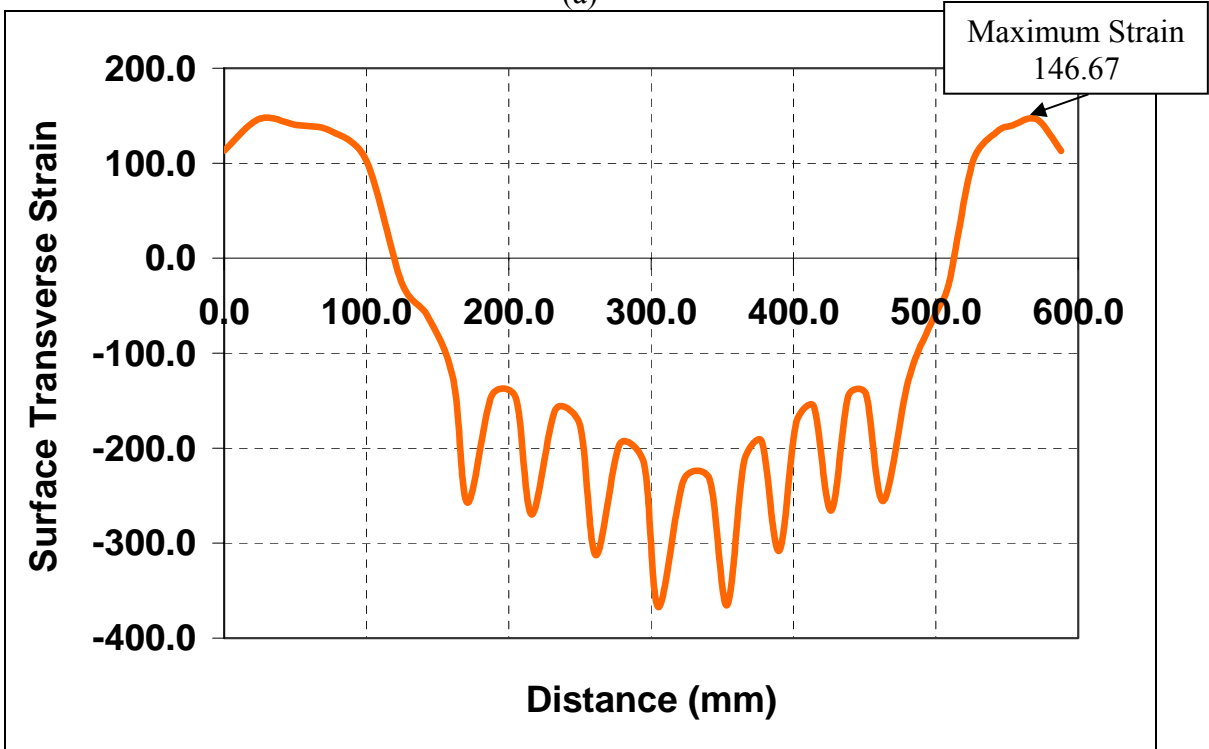
[#]: First generation of wide-base tire (445/50R22.5).

[▯]: Second generation of wide-base tire (455/55R22.5).

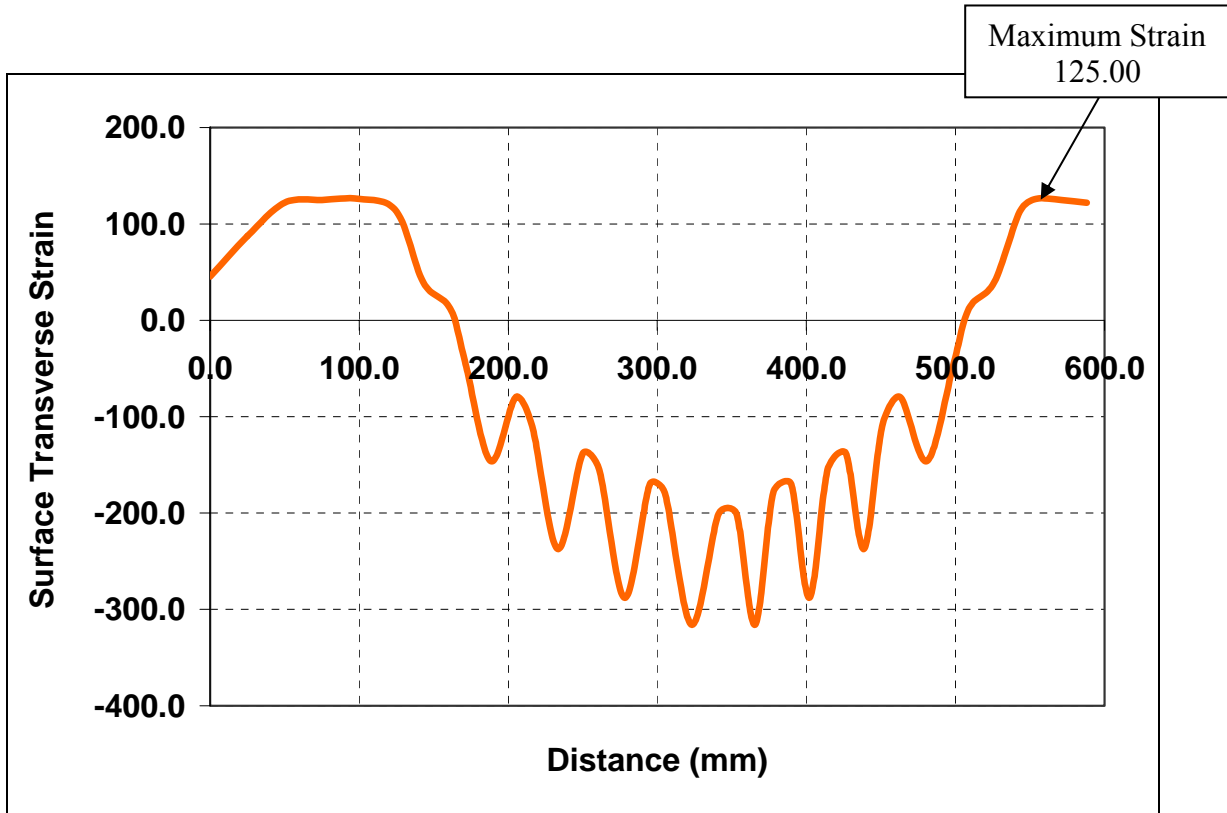
Based on these results, one may conclude that under the operating conditions, the 445/50R22.5 tire would cause less subgrade rutting and surface-initiated pavement cracking, approximately the same primary rutting damage, and more fatigue damage than the dual-tire configuration. On the other hand, results indicate that the 455/55R22.5 tire would cause less primary and secondary rutting and surface-initiated top-down cracking; but more fatigue damage than the conventional dual-tire assembly. Using the logarithmic damage distribution (see Equation 6.9), the combined damage ratio was estimated at 1.09 for the 445/50R22.5 tire and at 0.76 for the 455/55R22.5 tire. Therefore, to result in the same damage, the load reduction for the 445/50R22.5 tire should be 2.5%, and the load increase for the 455/55R22.5 tire could be 7%. This analysis did not consider the dynamic impacts of the different tires, which were reported about 17% lower for the wide-base than for the dual-tire assembly (COST 334 2001).



(a)



(b)



(c)

Figure 7-3. Comparison between Calculated Surface Strain at a Temperature of 25°C for (a) the Dual Tires and (b) the First New Generation of Wide-Base Tire (445/50R22.5) and (c) the Second Size New Generation of Wide-Base Tire (455/55R22.5) for the Laval Test Site

7.3. SUMMARY

Due to the lack of accurate models to predict pavement damage due to different axle configurations, load regulations in North America are still based on ill-posted design models that barely simulate real field conditions. Therefore, these design models may not appropriately differentiate between the conventional and the new generation of wide-base tires in terms of pavement damage. This has led pavement agencies to adopt an over-conservative approach resulting in erroneous load limitations. Current load regulations in Quebec limit the maximum allowable load on an axle with single tires to 8000kg, compared to 9000kg for a standard dual-tire axle. This represents a reduction of 11% during ten months of the year. For the two months of the spring thaw season, a 1000kg per axle load reduction is applied to all axle configurations.

Results of the Laval research study recommended that the maximum allowable load on an axle with single tires should be reduced by 16% in the summer and spring seasons. A load reduction of 20% is also recommended on all axle configurations during the spring thaw season. This implies that the 18% increase in tire width of the new generation over the first generation of wide-base tire, the reduction in tire pressure, and the increase of tire flatness, did not have any effect in pavement damage.

Based on the results of the FE analysis of the Laval test site, the recommended axle load reduction for the 445/50R22.5 tire is 2.5%, and the axle load may be increased by 7% when 455/55R22.5 tire is used. This analysis did not address the load reduction during the spring thaw season, which is expected to be the same for both tire configurations. Given the identified trend in the summer, the suggested spring load reduction by the Canadian study could be too high. Table 7-6 compares the different load regulations.

Table 7-6. Comparison of the Different Load Regulations

Source	10-Month Period			
	Section B		Laval Section	
	A [§]	B [§]	A	B
Current Load Limits [^]	9000	8000	9000	8000
Virginia Tech Analysis (445/50R22.5)	9000	8400	9000	8775
Virginia Tech Analysis (455/55R22.5)	9000	9500	9000	9600
Laval Study	----	----	9000	7560

[^] Load regulations in Quebec are not dependent on the pavement design.

[§] A: Axle with dual tires, and B: Axle equipped with the new generation of wide-base tires.

In summary, the research effort reported by the Laval study is a step in the right direction. This chapter made use of the available information to conduct further needed analysis using FE modeling. Results of the developed FE analysis indicated that current load regulations need to be revisited. Recognizing the effect of pavement system structure, it is recommended that an analytical research project be initiated to address the shortcomings of the research at the Virginia Smart Road and at the Laval test site, which only analyzed a single pavement design, and to evaluate the impact of the spring thaw season.

8. CONCLUSIONS

The primary objective of this study was to quantify pavement damage caused by dual tires and a newly-developed wide-base tire using three-dimensional FE analysis. The developed FE models were unique in different ways. First, geometry and dimensions of the developed theoretical models were selected to simulate the axle configurations typically used in North America. Second, the developed FE models simulate the actual contact between the pavement and the tire by considering actual tread sizes and applicable contact pressure for each tread. Third, these models incorporated laboratory-measured material properties. Finally, the developed FE models were calibrated and validated using pavement response collected at the Virginia Smart Road.

Four main failure mechanisms were considered in the pavement performance analysis: fatigue cracking, primary and secondary rutting, and top-down cracking. For pavement structure with a thick HMA layer, as the one considered in this study, the probability of fatigue and secondary rutting failure is usually low. Pavement damage was calculated at three pavement temperatures (5, 25, and 40°C) and at two vehicle speeds (8 and 105km/h). Both the first new generation of wide-base (445/50R22.5) tire and the second size new generation of wide-base (455/55R22.5) tire were evaluated in this study. Dynamic impacts of the different tire types were not considered in this study, however. The dynamic impact was reported to be about 17% lower for the wide-base tire than for the dual-tire assembly (COST 334 2001). In general, the (455/55R22.5) tire was always less damaging than the 445/50R22.5 tire. Based on the results of the FE analysis, the followings were found:

- The first and second size new generation of wide-base (445/50R22.5 and 455/55R22.5, respectively) tires would cause greater fatigue damage in the pavement structure than the conventional dual-tire assembly. The damage ratios between the two tire assemblies ranged between 1.13 and 2.58 depending on the vehicle speed and pavement temperature.
- The 445/50R22.5 tire would result in slightly greater subgrade rutting damage in the pavement structure than the conventional dual-tire assembly. The damage ratio between the two tire assemblies ranged between 1.05 and 1.40 depending on the vehicle speed and pavement temperature. On the other hand, the 455/55R22.5 tire was found to cause less subgrade rutting damage than the conventional dual-tire assembly at slow speed; while more damage at high speed.
- The 445/50R22.5 tire would result in slightly greater primary rutting damage in the pavement structure than the conventional dual-tire assembly. The damage ratios between the two tire assemblies ranged between 1.09 and 1.56 depending on the vehicle speed and pavement temperature. On the other hand, the 455/55R22.5 tire induced less primary rutting damage than the conventional dual-tire assembly at slow speed and was as damaging or slightly more damaging at high speed.
- The 445/50R22.5 and 455/55R22.5 tires would result in significantly less top-down cracking. The damage ratio when compared to the dual-tire assembly

ranged between 0.06 and 1.07, depending on the vehicle speed and pavement temperature.

Based on the calculated combined damage ratios, equivalent loads were determined to balance the damage induced by the new generations of wide-base tires with that of the dual-tire assembly. This was based on the concept of load equivalency assuming the validity of the fourth power law. Tables 8-1 and 8-2 summarize the results of this analysis. Results of this analysis indicated that the recommended load reduction on an axle equipped with the 445/50R22.5 tire should range between 4.0 to 6.0% at a speed of 8km/h and between 5.0 to 11.0% at a speed of 105km/h to maintain the same effect on flexible pavement as that of dual tires. However, using the wide-base tires would reduce the overall truck weight by approximately 450kg, and therefore, the gross vehicle weight may be increased by the difference in tire weights, without causing any increase in pavement damage. Therefore, the recommended effective load reductions may differ from the limits shown in Tables 8-1 and 8-2.

Finite element analysis was also used to determine the load that can be used with the 455/55R22.5 tire to cause an equitable damage to flexible pavements as that caused by the dual-tire assembly. Using the 455/55R22.5 tire would reduce pavement damage at slow speed and would increase it at high speed. It was found that the axle load could be increased by 5 to 10%, depending on the pavement temperature, when 455/55R22.5 tires are used at low speed and should be reduced by 2 to 5% at high speed. In summary, if the 455/55R22.5 tires are used, it is reasonable to uphold the current load limits that are applied to dual-tire assembly at this point of research.

Table 8-1. Recommended Load Limits at a Speed of 8km/h

Temperature (°C)	Tire	Dual (kg)	Wide-Base Tire	
			445/50R22.5 (kg)	455/55R22.5 (kg)
5		9000	8700	9900
25		9000	8400	9500
40		9000	8600	9500

Table 8-2. Recommended Load Limits at a Speed of 105km/h

Temperature (°C)	Tire	Dual (kg)	Wide-Base Tire	
			445/50R22.5 (kg)	455/55R22.5 (kg)
5		9000	8600	8900
25		9000	8200	8900
40		9000	8000	8500

8.1. RECOMMENDATIONS

Due to absence of accurate models to predict pavement damage, State and Province regulations are still based on ill-posted design models that barely simulate real field conditions. Transportation agencies in North America have adopted an over-conservative approach based on empirical design models to assess pavement damage due to different tire configurations. The availability of proper models would ensure an accurate determination of load regulations for the different axle configurations commonly used in North America. Although significant advancements have been achieved in this project in accurately defining pavement damage due to different tire configurations, there is an urgent need to provide State and pavement agencies in the United States and Canada with a simple-predictive tool that would allow them to accurately determine pavement damages due to different axle configurations including the new generation of wide-base tire. The identification and incorporation of the pavement damage controlling parameters would allow better assessment of pavement damage caused by different tire types. Such models would also allow to accurately establishing seasonal load restrictions for the different tire configurations. In addition, implementation of such models would ensure homogeneous load regulations throughout the different regions in North America, which would result in smooth and effective trucking operations.

9. REFERENCES

- American Association of State Highway and Transportation Officials (AASHTO). (2002). "Development of the 2002 guide for the design of new and rehabilitated pavements." Unofficial Presentation.
- ABAQUS. (2001). *Finite Element Computer Program, Theory Manual*. Version 6.3-1, Hibbit, Karlsson and Sorensen, Inc., Pawtucket, USA.
- Al-Qadi, I.L., Loulizi, A., Elseifi, M.A., and Lahouar, S. (2000). "Effect of tire type on flexible pavements response to truck loading." Final Report submitted to Michelin Americas Research and Development Corporation, 515 Michelin Road, South Carolina.
- Al-Qadi, I. L., Loulizi, A., Janajreh, I., and Freeman, T.E. "Pavement response to dual and new wide-base tires at the same tire pressure." *Transportation Research Record 1806*, Transportation Research Board, Washington, D.C., 38-47.
- Al-Qadi, I.L., Loulizi, A., Elseifi, M.A., and Lahouar, S. (2004). "The Virginia Smart Road: the impact of pavement instrumentation on understanding pavement performance." Paper accepted for publication by the Journal of the Association of Asphalt Pavement Technologists (In Press).
- American Society of Civil Engineers. (2001). "2001 report card for America's infrastructure." available at www.asce.org/reportcard, Washington D.C.
- Ang-Olson, J., and Schroerer, W. (2002). "Energy efficiency strategies for freight trucking: potential impact on fuel use and greenhouse gas emissions." *Transportation Research Record 1815*, Transportation Research Board, Washington, D.C., 11-18.
- Bathe, K. J. (1982). *Finite Element Procedures in Engineering Analysis*, Prentice-Hall, NJ.
- Bonaquist, R. (1992). "An assessment of the increased damage potential of wide bases single tires." *Proc., of the 7th International Conference on Asphalt Pavements*, Nottingham, UK, 1-16.
- COST 334. (2001). "Effects of wide single tyres and dual tyres." Final Report of the Action (Version 29), European Cooperation in the field of Scientific and Technical Research.
- De Jong, D.L., Peatz, M.G.F., and Korswagen, A.R. (1973). "Computer program Bisar layered systems under normal and tangential loads." Konin Klijke Shell-Laboratorium, Amsterdam, External Report AMSR.0006.73.
- Finn, F., Saraf, C. L., Kulkarni, R., Nair, K., Smith, W., and Abdullah, A. (1986). "Development of pavement structural subsystems." NCHRP Report 291, Transportation Research Board, Washington, D.C.
- Gillespie, T.D., Karamihas, S.M., Sayers, M.W. Nasim, M.A. Hansen, W. Ehsan, N. and Cebon, D. (1993). "Effect of heavy-vehicle characteristics on pavement response and performance." NCHRP Report 353, Transportation Research Board, Washington, D.C.

- Holzer, S. (1985). *Computer analysis of structures: matrix structural analysis structured programming*, Elsevier Science Ltd, NY.
- Hsu, T.W., and Tseng, K.H. (1996). "Effect of rest periods on fatigue response of asphalt concrete mixtures." *Journal of Transportation Engineering*, American Society of Civil Engineering, Vol. 122, No. 4, 316-322.
- Huang, Y. H. (1993). *Pavement analysis and design*, 1st ed., Prentice Hall, NJ.
- Hugo, F., and Schreuder, W. J. (1993). "Effect of sample length on indirect tensile test parameters." *Proc., Annual Meeting of the Association of Asphalt Paving Technologists*, Vol. 62, 422-449.
- Huhtala, M. (1986). "The effect of different trucks on road pavements." *Proc., the International Symposium on Heavy Vehicle Weights and Dimensions*, Kelowna, British Columbia.
- Huhtala, M., and Pihlajamaki, J. (1992). "Strain and stress measurements in pavements." *Proc., Conference Sponsored by the U.S. Army Cold Regions Research and Engineering Laboratory – Road and airport pavement response monitoring systems*, Federal Aviation Administration, West Lebanon, New Hampshire, American Society of Civil Engineers, 229-243.
- Y.R. Kim, Daniel, J.S. and Wen, H. (2002). "Fatigue performance evaluation of Westrack asphalt mixtures using viscoelastic continuum damage approach." Final Report, Report No. FHWA/NC/2002-004.
- Kraus, H. (1980). *Creep analysis*, 1st ed. New York. John Wiley & Sons.
- Kumara, M. W., Gunaratne, M., Lu, J. J., and Dietrich, B. (2002). "A probabilistic model for prediction of asphalt pavement crack depths." Paper presented at the 81st Transportation Research Board Annual Meeting, Washington, D. C.
- Loulizi, A., Al-Qadi, I.L., Elseifi, M.A. and Freeman, T. (2004). "Comparison between measured and calculated stresses and strains induced by truck loadings in flexible pavements." Paper No. 04-4033 presented at the Transportation Research Board 83rd Annual Meeting, Washington, D.C.
- Markastaller, M., Pearson, A., and Janajreh, I. (2000). "On vehicle testing of Michelin new wide base tire." Paper No. 01-3432. Presented at Annual ASE International Truck and Bus Conference, Portland, Ore.
- Myers, L. A. (2000). *Development and propagation of surface-initiated longitudinal wheel path cracks in flexible highway pavements*, PhD Thesis, Department of Civil Engineering, University of Florida, Gainesville, FL.
- Monismith, C.L., Sousa, J., and J. Lysmer. (1988). "Modern pavement design technology including dynamic load conditions." Truck and Bus Meeting and Exposition, 33-52.
- Nilsson, R.A. (1999). *Viscoelastic Approach to Flexible Pavement Design*, PhD thesis, Dept. of Infrastructure and Planning, Royal Institute of Technology, Sweden, 1999.

- Prophète, F. (2003). "Effets de différents types de pneu sur les chaussées." Project No. 5.2R456.1, Quebec Minister of Transportation, Direction Laboratoire des Chaussées (In French).
- Svasdisant, T., Schorsch, M., Baladi, G. Y., and Pinyosunun, S. (2002). "Mechanistic analysis of top-down cracks in asphalt pavements." Paper presented at the 81st Transportation Research Board Annual Meeting, Washington, D. C.
- Sebaaly, P.E. (1992). "Pavement damage as related to tires, pressures, axle loads, and configurations. Vehicle, tire, pavement interface." ASTM STP 1164, J.J. Henry and J.C. Wambold, Eds., American Society for Testing and Materials, Philadelphia, 54-68.
- Soon, S.C., Drescher, A., Stolarski, H. (2003). "Tire-induced surface stresses in flexible pavements." Paper No. 03-2887 presented at the Transportation Research Board 82nd Annual Meeting, Washington, D.C.